Wavelet Transform based Techniques for Evoked Potential Signal Estimation

A Thesis
Submitted for the Degree of
Doctor of Philosophy
in the Faculty of Engineering

G. Sita

Department of Electrical Engineering
Indian Institute of Science
Bangalore – 560 012

SEPTEMBER 2001

Abstract

Evoked potentials (EP) are electrical responses of the central nervous system to sensory stimuli applied in a controlled manner. The stimuli are applied in the form of auditory clicks, visual patterns or electrical pulses, depending upon the neural pathway being tested. The responses are essentially electrical potential differences and are picked up at different identified locations on the scalp using surface electrodes. The amplitudes, occurrence times and durations of the various characteristic components of the EP's convey diagnostically important information about the corresponding sensory neural pathway. Based on the analysis time segment chosen from the time of application of the stimulus, evoked responses are classified as short, middle and long latency responses. EP occurs as an additive process to the natural brain activity known as electroencephalogram (EEG) and other physiological noise. The major problem in the acquisition of evoked potentials lies in their unfavourable signal-to-noise ratio (SNR). Usually, stimulus-synchronous averaging of a few hundreds to few thousands of responses to identical stimuli is carried out to increase the SNR. This is effective, since the stimulus induced changes in the EEG are negligible. Various attempts have been made by different research groups either to reduce the number of sweeps to be averaged to obtain a meaningful signal in order to reduce the recording time or to recover the information lost by averaging.

In this thesis, we address the problem of estimation of brainstem and middle latency auditory evoked potentials, both of which are cortical responses of the brain. We propose methods for enhancing the averaged BSAEP signal, consequently reducing the number of sweeps required to obtain an acceptable signal to noise ratio. Although AEP can be considered stationary across an ensemble, it is non-stationary within a sweep, during which time, the frequency characteristics of the various temporal components vary. We use multiresolution techniques because wavelets provide a basis matched to a large class of non-stationary signals, and are by far superior to conventional approaches from the point of view of noise reduction. A wavelet basis

is localized in both time and frequency, and so can effectively track signal non-stationarities. The multiresolution structure of wavelets allows one to zoom in on local signal behaviour to analyze signal details, or zoom out to get a global view of the signal. The techniques are aimed at reducing the number of sweeps to be averaged to achieve a good SNR.

In the first approach, an attempt is made to improve the SNR of the ensemble average and enhance the significant components of the signal, namely, the peaks and valleys by using spatially selective Gaussian filtering in the wavelet domain. When the signal is corrupted by correlated noise that cannot be separated in either frequency or time domain, a signal based local filtering of the noisy signal in the transform domain is a promising solution for improving the balance between detail preservation and noise attenuation. We have used a nonlinear filtering method in the wavelet domain for enhancement of evoked potentials corrupted by stationary correlated noise. In the absence of knowledge about the noise statistics, a transform domain filtering, which takes local statistics into consideration rather than the global signal structure, is a better choice. It adapts the spatially selective filtering technique for EP signal enhancement. We decompose the signal employing an undecimated nonorthogonal discrete wavelet transform (UDWT), implemented using à trous algorithm. Inter-scale correlation information in the UDWT domain has been used for edge detection, since a sharp transition in the signal gives rise to maxima in several adjacent scales.

Edges are present at positions where there are maxima in the non-orthogonal wavelet transform at several adjacent scales. This property is used to identify and enhance significant component regions of the EP signal. Instead of retaining just the identified edges, and masking out the rest of the wavelet coefficients, a Gaussian shrinkage function is placed at each identified edge, scaling the wavelet coefficients around the edges. This ensures retention of not only the signal peak information, but also the surrounding information. To distinguish and remove transient and spurious noise, the variance of the wavelet coefficients in a window region around the identified transition region is made use of. This filter entails component enhancement, while avoiding visual artifacts around the edges. The filter may be viewed as a low-pass filter that passes selected high frequency data. Results are presented for both simulated and actual AEP signals.

In the second approach, we use a combination of two different wavelet methods for signal estimation, namely, a hierarchical Wiener filtering which is a parametric approach, and a

thresholding method such as hard/soft thresholding which is a non-parametric approach, both in the UDWT domain. Results obtained using all the proposed methods are compared using objective criteria, such as, mean square error, correlation coefficient, and the accuracy of the latencies measured from the estimated signals.

In yet another approach, a model based estimator is used. We use neural network filters, which possess built in nonlinear processing elements. A radial basis function neural network is utilised as a model for the EP signal to account for the nonlinear nature of the signal. Gaussian kernels are used to model the signal. Radial basis function (RBF) network can be considered as an amalgamation of data modeling in high-dimensional space and artificial neural networks. The input first undergoes a nonlinear transformation via the basis functions in the hidden layer; the responses of the basis functions are then linearly combined to give the network output. The choice of the number of basis functions in the hidden layer and their parameters is a key problem in designing an RBF network. Deriving the kernel parameters from the signal can improve both the effectiveness of the model and tracking property of the network. In the present work, the Gaussian RBF network parameters are deduced from the wavelet transform of the noisy signal to enable the network to learn the functional form of the underlying EP signal more effectively. Several computer simulations have been carried out to examine the performance of the proposed technique both for simulated and actual data. Results are presented which demonstrate the superiority of using signal knowledge in deciding the network parameters to a fixed parameter network. The latencies of the peak components are more consistent in the filtered responses than in the original ones.

Acknowledgements

I am extremely grateful to my advisor, Dr. A G Ramakrishnan, for giving me an opportunity to work with him and expressing confidence in my abilities. The support I recieved from him was not just limited to the technical part of this thesis. The way he comes out with positive and simple solutions for many seemingly difficult problems provided me with not only a guide, but also a real friend with whom I could share many of my problems.

I gratefully acknowledge the support extended to me by the authorities of Indian Institute of Science by giving me an opportunity to register for Ph.D. and providing me necessary facilities.

My sincere thanks to the chairman of the Department of Electrical Engineering, Prof. V. Ramanarayanan, for permitting me to register for Ph.D.

I am fortunate to have been surrounded by many very friendly and nice people all through. Mr. Bhanu Prakash is on top of the list. He has been a good friend, whose support I could always take for granted. I sincerely thank him for his help. I wish to express my sincere thanks to my other friends Susheela Devi, Rishikesh, JV, Vijaya Krishna and Murali Shankar who have helped me out many times during this period.

Words cannot truly express my deepest gratitude and appreciation to my mother, C. Hemalatha, and my husband, G. Udaya Bhaskar, for their understanding, and encouragement when it was most required. Without their support, I could not have seen this in a finished form. I am forever indebted to them. This section remains incomplete if I do not mention the support I received from my children, Pawan and Pujitha, by sacrificing some of the time, which is rightfully theirs and eagerly waiting for its completion. I express my sincere thanks to both of them.

Contents

Abstract i

1 Introduction 1
- 1.1 Evoked Potentials . . . 1
- 1.2 Introduction to auditory evoked potentials . . . 3
- 1.3 Issues in EP research . . . 5
- 1.4 Overview of EP estimation methods . . . 9
  - 1.4.1 Averaging methods . . . 9
  - 1.4.2 Linear filtering methods . . . 11
  - 1.4.3 Adaptive filtering methods . . . 13
  - 1.4.4 Model based approaches . . . 14
  - 1.4.5 Wavelet based methods . . . 16
  - 1.4.6 Other approaches . . . 16
- 1.5 Objective of the thesis . . . 16
- 1.6 Data used for the study . . . 17
  - 1.6.1 Simulated data . . . 18
  - 1.6.2 Real data . . . 18
- 1.7 Organization of the thesis . . . 19

2 Wavelet based spatially selective Gaussian filtering 21
- 2.1 Introduction . . . 21
- 2.2 Wavelet Transform . . . 23
- 2.3 DWT computation methods . . . 25
  - 2.3.1 Multiresolution wavelet decomposition - Pyramidal algorithm . . . 25
  - 2.3.2 Undecimated wavelet transform - à trous algorithm . . . 27
- 2.4 Filtering in the wavelet domain . . . 28
  - 2.4.1 Spatially selective filtering . . . 29
  - 2.4.2 Spatially selective Gaussian filtering . . . 30
- 2.5 Pseudo-code for spatially selective Gaussian filtering in the wavelet domain . . . 32
- 2.6 Performance evaluation . . . 34
- 2.7 Experimental Results . . . 35
  - 2.7.1 Simulated data . . . 35
  - 2.7.2 Real data . . . 44
- 2.8 Discussion . . . 46
- 2.9 Conclusion . . . 46

3 Spatially selective Wiener filtering in the wavelet domain **48**
3.1 Introduction . . . 48
3.2 Overview of wavelet domain estimation methods . . . 49
3.2.1 Thresholding methods . . . 49
3.2.2 Filtering methods in wavelet domain . . . 50
3.3 Spatially selective Wiener filtering . . . 52
3.4 Experimental Results . . . 54
3.4.1 Results for simulated data . . . 54
3.4.2 Results for real data . . . 64
3.5 Discussion . . . 66
3.6 Conclusion . . . 66

4 Gaussian radial basis function network for EP estimation **68**
4.1 Introduction . . . 68
4.2 Radial basis function networks . . . 69
4.2.1 EP estimation by Gaussian radial basis function network . . . 71
4.3 Determination of the kernel parameters . . . 72
4.4 Experimental results . . . 73
4.4.1 Results for simulated data . . . 75
4.4.2 Results for real data . . . 79
4.5 Conclusion . . . 84

5 Conclusion **85**
5.1 Significant contributions of the thesis . . . 87
5.2 Directions for future research . . . 87

Bibliography **89**

List of Figures

1.1 Recording setup for auditory evoked potentials 4
1.2 Typical auditory evoked potential signals (a) BSAEP (b) MLR 5
1.3 Ensemble averages for different lengths of the ensemble - BSAEP. (a) EA of 50 sweeps (b) EA of 100 sweeps (c) EA of 200 sweeps (d) EA of 300 sweeps (e) EA of 500 sweeps. x-axis: Time in ms; y-axis: amplitude in micro Volts 7
1.4 Ensemble averages for different lengths of the ensemble - MLR. (a) EA of 50 sweeps (b) EA of 100 sweeps (c) EA of 200 sweeps (d) EA of 300 sweeps (e) EA of 500 sweeps. x-axis: Time in ms; y-axis: amplitude in micro volts 8

2.1 Multiresolution orthogonal decomposition of a signal. 26
2.2 Undecimated discrete wavelet transform of a signal. 28
2.3 Filtering in wavelet domain 29
2.4 Block diagram of spatially selective Gaussian filtering in wavelet domain 31
2.5 Decomposition of BSAEP-Sim signal using UDWT. (a): BSAEP-Sim signal at SNR 1.75 dB. (b,c,d,e): Decomposition into scales 1, 2, 3, and 4, respectively. . . 36
2.6 Derivation of Gaussian masks for BSAEP-Sim signal. Row 1: Correlation between scales 1 - 2, 2 - 3, and 3 - 4, respectively. Row 2: Binary masks obtained using the principles of selective filtering. Row 3: Corresponding Gaussian masks. . . . 37
2.7 Output of spatially selective Gaussian filtering of BSAEP-Sim signal. Column (a): UDWT coefficients at scales 1, 2, 3 and 4, respectively. Column (b): Spatially selected scale data after Gaussian filtering. 38
2.8 Comparison of outputs estimated using binary and Gaussian masks for BSAEP-Sim signal with a SNR of 1.75 dB. (a) Noisy signal. (b) Filtered output obtained using binary masks. (c) Output obtained using Gaussian masks. 39
2.9 Performance evaluation of the estimator on BSAEP-Sim signal of different input SNRs (a) Correlation coefficinet Vs. input SNR (b) MSE Vs. input SNR 39
2.10 Decomposition of MLR-Sim signal using UDWT. (a) MLR-Sim signal with a SNR of 1.75 dB. (b,c,d,e): Decomposion into scales 1, 2, 3, and 4, respectively. 40
2.11 Derivation of Gaussian masks for MLR-Sim signal. Row 1: Correlation between scales 1 - 2, 2 - 3, and 3 - 4, respectively. Row 2: Binary masks obtained using spatially selective filtering. Row 3: Corresponding Gaussian masks. 41
2.12 SSG filtering of MLR-Sim signal. (a) Decomposition of MLR-Sim signal into scales 1, 2, 3 and 4 using UDWT. (b) Corresponding modified coefficients after Gaussian filtering. 42
2.13 Comparison of outputs obtained using binary and Gaussian masks for MLR-Sim signal. (a) Noisy signal. (b) Filtered output obtained using binary masks. (c) Output obtained using Gaussian masks. 43

2.14 Performance evaluation of the estimator on MLR-Sim signal of different SNR's. (a) Correlation coefficient Vs. input SNR. (b) MSE Vs. input SNR. 43
2.15 Estimation of real BSAEP signals for different ensemble lengths. Row (a): EA of 100, 200 and 300 sweeps. Row (b): Signals estimated using SS filtering. Row (c): Signals estimated using SSG filtering. 44
2.16 Estimation of real MLR signals for different ensemble lengths. Row (a): EA of 100, 200 and 300 sweeps, respectively. Row (b): Signals estimated using SS filtering. Row (c): Signals estimated using SSG filtering. 45

3.1 Block diagram of the spatially selective Wiener filtering in the wavelet domain. . 53
3.2 Signals estimated from BSAEP-Sim at different SNR's. Row (a): BSAEP-Sim signal with input SNRs of 1.75 dB, 3.0 dB and 5.0 dB, respectively. Row (b): Signals estimated using SS-W filtering. Row (c): Original signal. 55
3.3 Comparison of signals estimated from simulated BSAEP using two different techniques. (a) Ensemble averaged BSAEP-Sim signal at a SNR of 3 dB. (b) Output of hard thresholding. (c) Output of SS-W. 56
3.4 MSE of the estimated output for different input SNRs. Solid line: SSW filter. Dashed line: Hard thresholding. Dotted line: EA. Input: BSAEPSim. 57
3.5 Correlation Coefficient of the estimated output with the original signal - for different input SNR's. Signal Studied: BSAEPSim. Solid line: SSW filter. Dashed line: Hard thresholding. Dotted line: EA. 59
3.6 Signals estimated from MLR-Sim for different input SNR's. Row (a): Noisy observations at SNRs 2.5 dB, 4 dB, and 6 dB, respectively. Row (b): Signals estimated using SS-W filter. (c) Original EP signal for comparison. 60
3.7 Comparison of signals estimated from simulated MLR using two different techniques. (a) MLR-Sim simulated with a SNR of 5 dB. (b) Output of hard threshold estimator. (c) Signal estimated using SS-W filter. 61
3.8 Correlation Coefficients of the estimated outputs with the original signal - for different input SNR's. Signal Input: MLR-Sim. Solid line: SSW filter. Dashed line: Hard thresholding. Dotted line: EA. 62
3.9 MSE of the estimated outputs for inputs of different SNR's. Input: MLR-Sim. Solid line: SSW filter. Dashed line: Hard thresholding. Dotted line: EA. 63
3.10 Real BSAEP signals estimated using SS-W and hard threshold estimators for ensembles of different lengths. Column (a): EA of 200, 300 and 400 sweeps, respectively. Column (b): Signals estimated using hard thresholding. (c) Signals estimated using SS-W filter. 64
3.11 Comparison of real MLR signals estimated using SS-W filter and hard threshold estimators for ensembles of different lengths. Row (a): EA of 200, 300 and 400 sweeps. Row (b): Signals estimated using hard thresholding. Row (c): Signals estimated using SS-W filter. 65

4.1 Schematic of the RBF network 70
4.2 Schematic of the GRBF network for EP estimation 72
4.3 (a) and (f): Noisy BSAEP signal at SNR of 1.5 dB. (b), (c), (d), and (e): Its decomposition into scales 1, 2, 3, and 4, respectively. (g) and (h): 2nd order correlation between scales 2 - 3 and 3 - 4. (i) and (j): Binary and the corresponding Gaussian mask vectors. 74

4.4 Signal estimation using GRBF network. (a) Simulated BSAEP signal (EA of 100 sweeps). (b) Binary mask vector in the wavelet domain. (c) The corresponding Gaussian kernels. (d) Signals estimated using W-RBFN (solid line) and U-RBFN (dashed line). 76
4.5 Signals estimated from BSAEP simulated with different lengths of the ensemble. Row(a): Current ensemble averages of 50, 200 and 400 sweeps, respectively. Row (b): Signals estimated using U-RBFN. Row (c): Signals estimated using W-RBFN. (d) Original signal. 78
4.6 Comparison of performance of U-RBF and W-RBF estimators on BSAEP-Sim signal. (a) MSE Vs. No. of sweeps. (b) Correlation coefficient Vs. No. of sweeps. 79
4.7 Signals estimated from MLR simulated with different lengths of ensemble. Row (a): Current ensemble averages. Row (b): Signals estimated using U-RBFN. Row (c): Signals estimated using W-RBFN. Row (d): Original signal. 80
4.8 Comparison of performance of U-RBFN and W-RBFN on simulated MLR signals. (a) MSE Vs. No. of sweeps. (b) Correlation coefficient Vs. No. of sweeps. 81
4.9 BSAEP signal estimated from real data. (a) EA of 500 sweeps. (b) Signal estimated using W-RBFN. (c) Signal estimated using U-RBFN. 82
4.10 MLR signal estimated from real data. (a) EA of 200 sweeps. (b) Signal estimated using W-RBFN. (c) Signal estimated using U-RBFN. 83

Chapter 1

Introduction

1.1 Evoked Potentials

Ever since Hans Berger's discovery, that the electrical activity of the brain can be measured and recorded via surface electrodes mounted on the scalp, there has been major interest in the relationship between such recordings and brain fucntion. The first recordings conducted by Berger and his followers [7] were concerned with the spontaneous electrical activity of the brain, appearing in the form of rhythmic voltage oscillations and are termed electroencephalogram (EEG). Subsequent research observed brain activity time-locked to specific external stimuli applied to a subject. In the last thirty years, the study of the electrical activity of the brain related to a well defined sensory stimulus or to the accomplishment of a specific task has become more and more widespread, aiming at a better understanding of the functioning of the central and peripheral nervous system and the human behavior.

The application of a sensory stimulus to the peripheral nervous system results in changes in the on-going activity of the central nervous system, which appear as additive superposition to the background EEG activity. These responses are known as evoked potentials (EP) and are commonly used for the clinical examination of perception. These responses are related to the sensory processing of stimuli. The sensory stimuli are applied in the form of auditory clicks, visual patterns or electrical pulses depending on the neural pathway being tested. The responses which are essentially electrical potential differences, are picked at different identified locations on the scalp using surface electrodes. Analysis of these signals can provide information about the integrity of the neural pathways, especially those in the spinal cord and the brain.

They can indicate the presence of disease or degeneration, and can help determine the location of nerve lesions. The analysis of evoked potentials has had a major impact on neurophysiological research, clinical neurology and neurosuregery in the last few years. There are three major EP modalities, classified based on the stimulus applied, that are used in regular clinical practice:

- Visual evoked potentials (VEP) are used to diagnose visual losses due to optic nerve damage, to monitor multiple sclerosis and to localize the cause of a visual field defect not explained by lesions seen on CT or MRI.

- Auditory evoked potentials (AEP) are used to evaluate brainstem function,to detect lesions in the auditory pathway, and to determine the type and degree of hearing problems. They can distinguish pathology of the auditory nerve from that of the auditory pathways within the brainstem. They may also be used to monitor brainstem function during surgery and to determine brain death,

- Somatosensory evoked potentials (SEP) record transmission of nerve impulses from the limbs to the brain, and can be used to diagnose nerve damage or degeneration within the spinal cord or nerve roots from multiple sclerosis, trauma, or other degenerative diseases. When combined with results from a nerve conduction velocity test, which measures nerve function in the extremities, they can also be used to distinguish central from peripheral nerve disorders.

Based on the analysis time segment chosen from the time of application of stimulus, an evoked response can broadly be classified as early, middle or long latency response. Short latency responses originate in the subcortical region or in the brainstem, while the middle and long latency responses have well defined cortical origin. The peaks and troughs that appear in the EP waveform are called "components". The latency of a component is normally taken as the time, in milliseconds, from the time the stimulus is delivered, to a peak or trough of a component. The amplitudes of the various peaks in a response may be measured either with respect to the preceding peak of opposite polarity or a baseline. The characteristic response and the individual component morphology are different for responses of different modalities. EP components are recognized by their polarity and latency. The components occuring within the first 100 milliseconds after the stimulus can be attributed to activity in localized anatomical structures along known sensory pathways. The amplitudes and latencies of different components

occurring within this duration convey diagnostically important information on the sensory pathways. Later components arise from more dispersed cortical sources [11] and are analysed to understand higher cognitive processes such as attention, perception, memory and learning. They are commonly referred to as, event related potentials (ERP).

The EPs are of very small amplitude, in the range of micro volts. Like many biological signals, the measurement of EP is corrupted by noise from background activities. A main source of noise is the spontaneous electroencephalogram generated in the brain. The amplitude of this noise is much higher than that of the EP response. Thus, the signal-to-noise ratio (SNR) of evoked signals is very low. Hence, to obtain an estimate of the buried signal, the common approach is to obtain an ensemble of many EP responses time locked to identical stimuli and then compute an average of the ensemble, commonly known as ensemble average (EA). Normally, several hundreds or thousands of epochs/sweeps are averaged before a satisfactory waveform is obtained, on which measurements can be made. Our objective is to obtain a satisfactory signal estimate with reduced number of sweeps in an ensemble.

We restrict our attention to a subclass of EPs, namely, auditory evoked potentials, which include both short and middle latency responses. Short latency auditory responses have a number of both high and low frequency components in the analysis time length. These signals are the most complex with more components in comparison with the other modalities of EPs, have very low SNR and hence are better suited to study any filtering or estimation algorithm. Middle latency responses can also be seen as a more general evoked response model since they contain typical characteristics of many types of evoked potentials The performance of any estimation algorithm on these AEPs can give an indication of their potential to deal with other evoked signals. Henceforth, we will use the term EP to indicate both brain stem and middle latency auditory evoked potentials. In the following section, we briefly explain the instrumentation required to record these EPs and the different diagnostically important components in them.

1.2 Introduction to auditory evoked potentials

Auditory evoked potentials are very small (2-10 microvolts for cortical AEPs to much less than 1 microvolt for the deeper brainstem structures) electrical potentials originating from structures within the brain. AEP signals are picked up in the far field from the cortex by

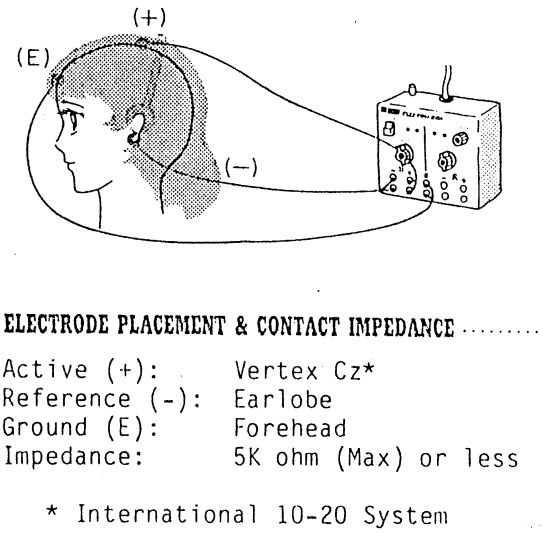

Figure 1.1: Recording setup for auditory evoked potentials

recording differentially with the active electrode placed on the vertex (Cz) and the reference electrode at the mastoid bone or ear lobe. Figure 1.1 shows the recording montage for AEP signals. They are recorded from the scalp in response to auditory stimuli, such as different tones and speech sounds. Both needle and surface electrodes can be used for recording AEPs. Both short and middle latency responses are used in assessing the auditory function. However, short latency responses, also called brainstem auditory evoked potentials (BSAEP), are more stable and are used to distinguish between conductive and sensory hearing loss.

A normal BSAEP signal and a typical middle latency response (MLR) are shown in Fig. 1.2 (a) and (b), respectively, with the significant components indicated. About seven peaks (designated as waves I - VII) are commonly identified in the BSAEP signals. Of these, the initial five peaks are of clinical interest. The succeeding peaks VI and VII are quite variable and therefore, are not used clinically. The troughs immediately following the peaks are designated by the same numeral followed by a prime mark, e.g. the trough of wave I is designated as I'. Each peak is considered to reflect a different portion of the auditory pathway [62]. It is the

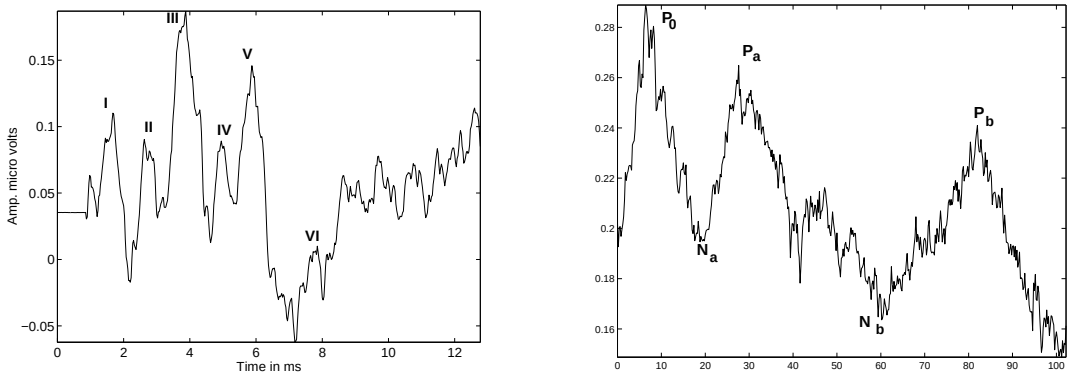

(a) (b)

Figure 1.2: Typical auditory evoked potential signals (a) BSAEP (b) MLR

fifth positive potential or wave V occurring at about 5.7 ms and the following negative going deflection, that provide the best means of estimating the auditory threshold. Typical latency values of the components of a normal BSAEP are given in Table 1.1. Waves $I - V$ are seen in most normal individuals. Occasionally, wave IV may form a IV-V wave complex in normal subjects. In such a case, wave IV does not indicate an abnomality. Wave II can be difficult to distinguish in some normal subjects. By changing the stimulus intensity, rate and phase, wave II can be identified in most normal subjects. It is abnormal to have only the wave I present and not the succeeding ones. Similarly, presence of waves I and III with waves IV and V absent, is also abnormal. The BSAEP abnormalities include absence of wave III and V and prolonged I-III inter-peak latency. Since the normal range of distribution of peak amplitudes and latencies is well specified, and since different diseases of the auditory pathway introduce predictable distortions in these parameters [13], the BSAEP has considerable utility in clinical diagnosis.

The individual components of MLR have been labelled N_0, P_0, N_a, P_a and P_b. The N_0, P_0 and N_a components overlap in latency. The N_a/P_a complex provides the most stable waveform, which is used in general to estimate the response threshold.

1.3 Issues in EP research

The major problem in the analysis of EP signals lies in the unfavourable signal-to-noise ratio (SNR), which characterises the stimulus evoked signal that is superimposed on the background EEG activity and other physiological noise. Moreover, neither the EP signal nor the

Table 1.1: Typical latency values of the components of normal BSAEP and MLR

Component Wave	Latency (ms)
I	1.7 ± 0.15
II	2.8 ± 0.17
III	3.9 ± 0.19
IV	5.1 ± 0.24
V	5.7 ± 0.25
VI	7.3 ± 0.29

Component Wave	Latency (ms)
N_0	8 - 10
P_0	10 - 13
N_a	16 - 30
P_a	30 - 45
N_b	40 - 60
P_b	55 - 80

background noise is limited to narrow frequency ranges. Rather, they overlap extensively. Specially, component latencies are harder to measure if the SNR is low. This necessitates the use of some type of averaging or filtering to increase the SNR. Hence, averaging of few hundreds or thousands of responses to identical stimuli is required in order to obtain a reasonable signal estimate on which measurements can be made. In commercially available equipment, the instantaneous average up to the current response is displayed in real time. Figure 1.3 presents the ensemble average for different ensemble lengths for the case of a real BSAEP signal.

Similarly, in Fig. 1.4, the ensemble averages of different number of MLR sweeps are shown. It can be observed from these figures, that the characteristic components that are not visible in shorter ensemble lengths become visible with longer ensemble lengths and also the amount of noise comes down facilitating mesaurements to be made on the signal. Generally, two to three repetitions of the entire recording are done and the estimated signals are superimposed to check for reproducibility. This can often take up to several minutes. However, it is highly desirable to have an evoked potential system with significantly reduced acquisition times and also resulting in a smoother signal with fewer number of sweeps. The following are the reasons:

- Longer recording times lasting few minutes may result in undue motion artifact, especially in infant patients.
- In critical-care or operating room applications, short measurement times are requisite.
- The assumption of stationarity of both evoked response and the noise is more accurate when a small number of sweeps is averaged i.e. the statistics of the observations are unchanged only in short durations.
- To avoid habituation and refractoriness.

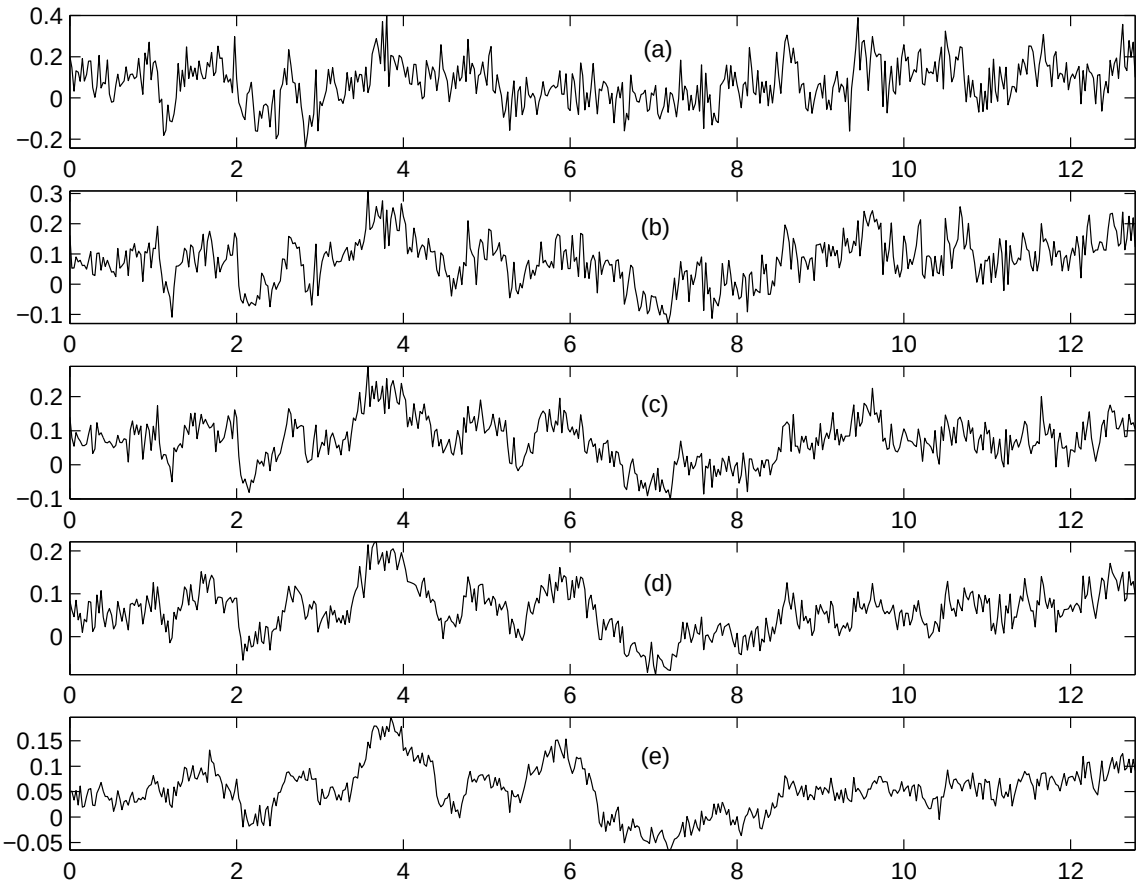

Figure 1.3: Ensemble averages for different lengths of the ensemble - BSAEP. (a) EA of 50 sweeps (b) EA of 100 sweeps (c) EA of 200 sweeps (d) EA of 300 sweeps (e) EA of 500 sweeps. x-axis: Time in ms; y-axis: amplitude in micro Volts

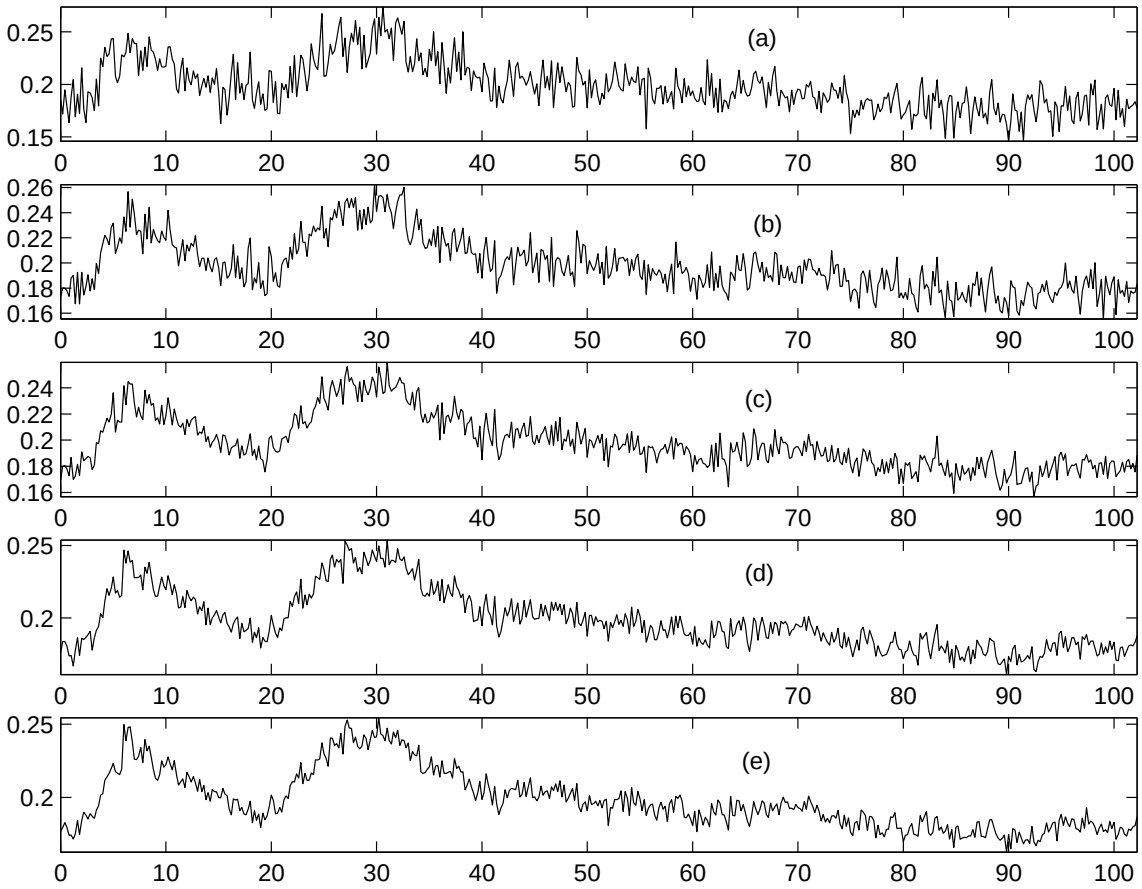

Figure 1.4: Ensemble averages for different lengths of the ensemble - MLR. (a) EA of 50 sweeps (b) EA of 100 sweeps (c) EA of 200 sweeps (d) EA of 300 sweeps (e) EA of 500 sweeps. x-axis: Time in ms; y-axis: amplitude in micro volts

Hence, with progress in advanced signal processing methods, the focus of evoked potential research has been on improving the SNR of ensemble averages with fewer number of EP sweeps, resulting in reduction in experimental time. The work presented in this thesis primarily deals with this issue.

Development of processing and analysis methods which look at each single response separately, has become another major area of work in EP research. In studies related to higher cognitive processes, components occurring later than 200 ms after the stimulus application are investigated. There is evidence that such processes could change from trial to trial [55]. A review of methods for single trial analysis may be found in [4]. In the following section, we present a brief overview of the methods used for EP estimation.

1.4 Overview of EP estimation methods

Dawson was the first to introduce methods of estimating evoked potentials from the background EEG, initially by means of photographic superimposition [19], and later by the technique of averaging [20]. Due to the development of advanced methods of signal processing that allow one to enhance information in a classical case of low SNR values, many researchers have been working on improving the SNR of either individual EP sweeps or the average of fewer sweeps to speed up the measurement time. The estimation methods may broadly be classified as averaging methods, filtering methods, model based approaches and wavelet based approaches. These are explained in the following subsections.

1.4.1 Averaging methods

One very widely used technique for EP recording is signal averaging, which suppresses brain activity unrelated to the stimulus. Signal averaging is based on the assumption that EP is a deterministic signal embedded in spontaneous brain activity, which is the additive noise in this case. The 'noise' is assumed to be zero-mean, uncorrelated with the signal and also uncorrelated from sweep to sweep. The additive signal model for the i-th EP sweep may be written as follows:

$$x_i(n) = s(n) + v_i(n) \qquad i = 1, 2, \cdots, P; \quad 0 \leq n < N \tag{1.1}$$

where $x_i(n)$ is the i^{th} observed sweep, $s(n)$ the underlying signal, $v_i(n)$ the noise associated with the ith sweep, and n is the time index. The average over a set of P observations is called

the ensemble average (EA) of P sweeps and is used to estimate the underlying signal $\hat{s}(n)$, decreasing the noise power proportional to $1/P$ [4]. Ensemble averaging may be represented as,

$$\hat{s}(n) = \frac{1}{P}\sum_{i=1}^{P} x_i(n) \tag{1.2}$$

One serious problem with the ensemble average is the inordinately large number of sweeps required to obtain a suitable EP estimate. For example, in the case of brainstem auditory EP measurements, several thousands of sweeps must be averaged. This measurement takes a few minutes during which time, there may be undue motion artifact. Although a large P would be desirable for adequate noise suppression, P needs to be kept small to keep experimental conditions roughly constant. It is therefore highly desirable to have an evoked potential system that can significantly reduce the acquisition time. Such a system could be especially useful in critical-care or operating room applications where short measurement times are requisite. Moreover, conventional ensemble averaging is typically used when the noise variance remains the same during the entire recording.

A few variants of ensemble averaging have been attempted to account for variations in signal or noise power in a session. One of them is weighted averaging, in which the weighting of each waveform is performed in relation to its noise content. To track dynamic changes in the signal component, moving window averaging (MWA) is performed, where a constant number of the most recent sweeps / observations are averaged [38]. In certain situations, the noise variance may vary considerably from one sweep to another. The method of weighted averaging proposed by [50] et al. assumes that the statistical properties of the noise change from sweep to sweep, while the evoked signal remains unchanged in each sweep. If the variance of the noise changes as a function of time, then they showed that a weighted averaging can improve the SNR to a large extent. This scheme can be represented as,

$$\hat{s}(n) = \sum_{i=1}^{P} w_i x_i(n) \tag{1.3}$$

where w_i is chosen such that the sweeps with low noise activity are weighted more heavily than the sweeps with high noise activity. The noise activity is estimated from the variance of individual sweeps. Exponentially weighted averager (EWA) is another averager with a forgetting factor, in which the most recent sweep is weighted the highest. The MWA may be considered as a special case of EWA in which the forgetting factor is a constant. Selective averaging involves the monitoring of the noise level of each sweep to eliminate the outliers [67]. The observations

with a noise level exceeding a pre-determined threshold are excluded from ensemble averaging. This approach is feasible as long as the noise level remains almost constant in all the observations except a few. The exclusion approach will not perform satisfactorily when large variations occur in the noise level.

A way to handle such non-stationary noise situations is to assume that the noise variance remains constant within each sweep, although it changes from sweep to sweep. A few non-parametric approaches have been attempted in such cases. In a few other methods, the weights are determined by optimizing a certain criterion for SNR improvement in the case of non-stationary noise. For example, maximum likelihood estimation of the signal results in weights that are inversely proportional to the noise variance [2]. In this approach, the noise variance is a parameter which is estimated prior to averaging. In another technique proposed by [10], the weights are determined such that the SNR of the resulting ensemble average is maximized. The weights are determined by the first eigenvector corresponding to a correlation coefficient, which is obtained by correlating the individual waveforms to the conventional average. For the case when the SNR is low, it has been suggested by [44] that the noise variance can be approximated by the variance of the observed data. In the weighted averaging approach proposed by Davila [18], an initial ensemble average is formed and the correlation coefficient of the incoming sweeps with the computed EA is used to fix the weights of the sweeps used in updating the ensemble average.

1.4.2 Linear filtering methods

The most common signal processing task is noise filtration. This is an essential part of any signal processing system, especially when the final product is used for visual inspection or for human interpretation. In most cases, filtering is the process of estimating a signal degraded by additive noise. A number of filtering and smoothing procedures have been proposed for estimating EP signals. Among them are linear processing techniques, whose mathematical simplicity and the existence of a unifying theory make their design and implementation easy. They exploit the signal's time structure which is not used in averaging techniques. Their common goal is to reduce noise further than possible with averaging. In all filtering or estimation methods, either explicit or implicit assumptions about the underlying signals are employed. The most

common assumptions are about the second order statistics of the evoked potential and the on-going EEG. The difference between the various algorithms is in the techniques used to design the optimal filter: either off-line from all the measurements or iteratively from a subgroup of measurements.

The filter most widely applied in EP processing is the Wiener filter, also known as minimum mean square error filter. It is a powerful tool for solving such problems. The idea of applying Wiener theory of optimal filtering to the estimation of evoked potentials was first reported by Walter [69] and later by Doyle [26]. Thereafter, it has been widely studied in the literature. If the signal is stationary and *a priori* knowledge about signal and noise can be obtained, then this technique will obtain a good estimation of the signal. The spectral properties of the band-limited signal are used in designing the filter. This information is obtained *a posteriori* from the averaged waveform. The design involves the computation of the spectrum for the averaged data to estimate the signal power spectrum and the average of the spectra from individual realizations [22] to estimate the noise power spectrum. The filter transfer function uses both of these estimated spectra and hence is called *a posteriori* Wiener filtering (APWF).

There has been a controversy over APWF with its rather unrealistic model of the EP as a stationary random process [4]. To overcome this limitation, time-varying filter was developed in which the spectral estimation is performed for successive intervals of the observed data. de Weerd [21] was the first to use time-varying filters for EP estimation. He divided the overall frequency band into many subbands, and designed a Wiener like filter in every subband. In doing so, the filter becomes better suited for processing of non-stationary data. The application of time varying *a posteriori* Wiener filtering to averaged data with low SNR has been found to reduce the variance of the signal estimate at the expense of an increased bias. However, a close look at this method will reveal a defect in that the narrower the width of the subband, the longer the filter response lasts, resulting in waveform overlap in the time-domain to a great extent. A similar phenomenon will happen in the frequency domain if we design the filters segment-by-segment in the time-domain.

McGillem and his group have extensively studied the Wiener filtering approaches in the time domain [4, 55, 73]. They have proposed both time invariant and time varying versions of the filters for EP estimation. The time invariant filter [55] is viewed as a linear operator, which projects the observations into the signal space. Their method involves estimation of

autocorrelation matrices of both the signal and the noise from several independent measurements of EP's which are then used in the optimal filter design. The time-varying filter model assumes the signal to be random and to consist of several components, the amplitudes and latencies of which are assumed to be random variables that may change within certain limits from one repetition of the experiment to the next. The design of the optimum filter is based on the covariance matrices of the signal and the measured data. The covariance matrix of the data is estimated from the measured observations. They report that the time-varying filter performs better than the time-invariant one, since the filter adjusts to the non-stationary nature of the signal and the noise. Although this filter is designed to be applied on single sweeps, it requires *a priori* knowledge of the signal and the noise. It provides a more powerful filtering than does the time-invariant filter. Improvement of the SNR of averaged data has been achieved by [29] et al by exploiting the fact that adjacent samples in the average are correlated. They have proposed an optimal filter which is applied on the averaged response to enhance its SNR and does not require *a priori* knowledge of the signal. The linear filtering approaches require stationarity of both noise and signal. Moreover, these methods implicitly assume the shape of the EP.

1.4.3 Adaptive filtering methods

While the above mentioned techniques rely on some sort of *a priori* knowledge of signal and noise, adaptive filters can automatically adjust their parameters based on the input signal without invoking any assumptions or *a priori* spectral information. Adaptive filters are self- designing filters which allow the filter to learn the initial input statistics and to track them if they are time varying. Adaptive filtering techniques are considered to be most appropriate to establish a functional relation between input and output, which is unknown due to incomplete knowledge of the signal and noise processes, and to account for the eventual dynamic variations of the signal shape during a recording session. The use of adaptive filtering in the analysis of EPs has been studied extensively during the last ten years.

A lot of attention has been paid to the use of the LMS algorithm in the filtering of single evoked responses. Usually, the measured single sweep is selected as the primary input and various other choices are proposed for the reference input. The LMS algorithm updates the parameters in the direction of the reference input. If the reference input is fixed, the iterative method can serve at most as a regularization method, i.e the mean squared error diminishes in

the direction that is determined by the reference input vector. In some cases, when the reference input changes during the iteration, true adaptation can also be achieved.

Laguna et al. [45] designed an adaptive impulse-correlated filter for the enhancement of somatosensory evoked potentials. The filter has two inputs; the primary input is the incoming recurrence of the EP signal, and the reference input is a unit impulse sequence synchronized with the beginning of each recurrence. If the variability of the signal is small and the SNR of recurrence is not too low, this method can obtain a satisfactory signal estimation. When the SNR of a recurrence is small, as is usually the case in EP measurements, it will take much longer to converge. Thakor [65] proposed a method of adaptive filtering using one sweep as primary input and the following sweep as the reference input. As the SNR of individual sweeps is very small, a very poor reference signal is being used for the adaptive filter. Therefore, the SNR at the output of the filter will hardly be improved, and the distortion of the signal will also be significant. Chan [12] et al. have presented a method using adaptive line enhancement technique to detect and track BSAEP signals. In order to make an optimal and rapid estimation of the signal corrupted with noise, they used the ensemble average of the first few sweeps as the reference input.

Adaptive implementation of the optimal time-varying filter is reported by Yu [74]. For each data point, they used a bank of filters whose weights are adaptively changed. They proposed a reduced order filter structure using which the computational complexity of the time- varying filter is reduced even while accounting for the non-stationary structure of the EP signal. Their data-adaptive scheme is shown to be asymptotically converging to the optimal time varying filter solution. The method is computationally intensive. A multireference adaptive noise cancellation technique is applied in [57] to improve the SNR of somatosensory evoked potential signals by eliminating predominant myoelectric interference in those signals. The model has multiple reference channels to model all the active sources contributing to the myoelectric interference in the observed signal. The model parameters are estimated adaptively using the adaptive noise cancellation principles.

1.4.4 Model based approaches

Another approach to extract EP from back ground noise is to obtain parametric models for the EP and noise and use this information to enhance the EP. Many of the linear models model the

EP as an autoregressive (AR) or autoregressive moving average (ARMA) process [37] [73]. The spontaneous EEG is modeled as an AR process, on which the evoked potential is superimposed [44]. The AR coefficients are calculated from the prestimulus EEG and are assumed to remain constant throughout the post-stimulus epoch. The characteristics of the EP are derived from the average waveform. This way, the *a priori* information about the stimulus time-point, the average EP response and the ongoing EEG activity are all incorporated in the model. Spreckelsen and Bromm [61] have proposed a method of estimating single evoked potentials using parametric modeling and Kalman filtering, They model the background EEG and the EP using the pre-stimulus information and ensemble average, respectively. Using this model information as the input to a Kalman filter, they have achieved significant SNR gains. The key to the successful operation of this technique is the initial qualitative estimate of the EP. In another work [51], the estimated AR coefficients are adaptively modified for every sweep to account for the non-stationary noise. Their method utilizes the pre-stimulus data and employs modern adaptive filter algorithms to produce significant reduction in noise variance in BSAEP signals.

Thakor et al. [68] have used function approximation methods. Their model takes into account both the periodic nature of the response as well as its band-limited nature. They assume the noise free evoked response as a quasi-periodic signal and represented it as a discrete dynamic Fourier Series where the Fourier coefficients are time-varying. An adaptive LMS algorithm is used to est1imate the coefficients. The estimator is designed to track spectral variation across trials. However, in the case of real data where both EP signal and EEG noise have overlapped frequency bands, the method has limited application. This is because, one of the assumptions for proposing the estimator is that the noise is uncorrelated with the signal as well as with every component of the Fourier series. In [36], event related potentials (ERP) are estimated using Prony's method. In their approach, they assumed the ERP as a sum of weighted damped sinusoid basis functions. The noise spectrum to be used for the parameter estimation is derived from the pre-stimulus data. The method has been tested to estimate the event related signal, which does not have many components to be detected. More recently, radial basis functions are used as a model for the EP signal to account for the nonlinear nature of the signal by Fung et al [28]. They used a fixed parameter Gaussian kernel to model the EP.

1.4.5 Wavelet based methods

A few wavelet transform based methods have been used basically to analyze the time varying structure of EP signals [5, 6, 66]. Thakor et al. [68] used multiresolution wavelet analysis of the EP signals using orthogonal wavelets to characterize complex changes in their shape during neurological injury. They were able to deduce components of diagnostic value from the decomposed signals. Bertrand et al. [8] have used filtering in the wavelet domain for EP signal estimation. They translated the time varying Wiener filtering formulation suggested by de Weerd et al. [22] into the wavelet domain with good results. The decomposition of frequency domain into overlapping frequency bands using analogue filters in [22] is made simpler by using the invertible wavelet transform. In their method, assuming the frequency characteristics of EP, they set the wavelet coefficients outside a specific time-frequency region to zero and retain the coefficients within the specified region. The wavelet coefficients are manually selected in order to eliminate high-frequency components before and after the occurrence of fast brain response. They used the magnitude of spectrograms in the wavelet domain to compute a level dependent Wiener filter transfer function which is used to scale the individual coefficients in the transform domain. By inverting the modified coefficients, a filtered signal is obtained.

1.4.6 Other approaches

Some of the other techniques are based on EEG cluster analysis [3, 31, 32] and segmentation procedures [41]. These methods basically analyze EP's on a single trial basis and therefore, take into account the dynamical processes involved in EP generation. In these approaches, a clustering algorithm is employed to identify a subset of sweeps that contain consistent responses and then these sweeps are used to obtain an enhanced EP estimate [14]. More recently, fuzzy clustering approach is used [76] for an improved EP estimate. This employs selective averaging, wherein fuzzy algorithm is employed to group individual sweeps according to their shape similarity; this is followed by averaging all the sweeps in the same group.

1.5 Objective of the thesis

The present work suggests methods to improve the SNR of ensemble averaged AEP's by reducing the residual noise. The objective is to obtain a smoother and improved estimate,

which facilitates component measurement. The AEP's consist of low-frequency components of relatively long duration and higher frequncy components of shorter duration. For a correct description of the signal power, we must take into account not only its spectral distribution, but also its temporal distribution. In other words, although EP is considered stationary across an ensemble, it can be considered as non-stationary within a sweep, during which the frequency characteristics of the various temporal components vary. Hence, time-invariant descriptors such as Fourier spectrum cannot provide an adequate representation of these transient responses. An important drawback of frequency domain models is that the Fourier transform may not parsimoniously represent the transient nature of EP components and may introduce Gibbs phenomenon in the estimates of the component waveforms. Hence, the analysis of EPs requires filters possessing time-varying characteristics.

Wavelets have become increasingly popular tools to efficiently deal with nonstationary signals. We propose novel estimator algorithms that use the inter-scale correlation information in the wavelet domain to differentiate the signal and the noise dominant regions. This facilitates the design of spatially selective filters in the wavelet domain to suit the application under consideration. The proposed techniques are based on the clustering property and the persistence property of the wavelet coefficients. The clustering property means that if a particular wavelet coefficient is large/small, then adjacent coefficients are also likely to be large /small. The persistence property of the wavelet coefficients is that large/small wavelet coefficients tend to propagate across scales. This property is also the foundation of the well-known embedded zerotree wavelet algorithm [59] proposed for image coding. We use these properties to design different estimators to denoise the EP signals. All the proposed estimators implicitly assume homogeneous responses across sweeps and colored noise corrupting the signal.

1.6 Data used for the study

All the estimators are tested extensively on simulated BSAEP and MLR data. They are then tested on real data. The details about the simulations and the acqusisition details of real data are presented in the following subsections.

1.6.1 Simulated data

A BSAEP which was obtained with the traditional techniques of averaging 512 sweeps of actual human responses sampled at 40 KHz, is used as the original signal, $s(n)$. To this, simulated EEG is added to generate an ensemble of noisy EP sweeps. The additive model to simulate a noisy EP sweep, $x(n)$ may be written as follows:

$$x(n) = s(n) + v(n) \tag{1.4}$$

where $v(n)$ is the simulated EEG signal and $s(n)$ is the evoked single sweep. The background EEG superimposed on the evoked signal was simulated as an autoregressive process [74] as follows:

$$v(k) = 1.5084v(k-1) - 0.1587v(k-2) - 0.3109v(k-3) - 0.0510v(k-4) + \theta(k) \tag{1.5}$$

where $\theta(k)$ is white Gaussian noise. The power spectrum of the simulated EEG noise is comparable to actual EEG. This is termed as BSAEP-Sim signal. In our experiments, ensembles of different SNR's are simulated by adding different amounts of noise to $s(n)$.

The middle latency responses are also generated in a similar fashion by choosing an EA of 512 actual MLR sweeps as the signal $s(n)$. To this, simulated EEG is added to generate 512 noisy sweeps. This ensemble is termed as MLR-Sim. To simulate MLR with different SNR's, the EEG is added to $s(n)$ with different scale factors.

1.6.2 Real data

Beckman silver-silver chloride electrodes are applied with conductive paste to sites C_z, P_z, O_z and I_n according to the 10-20 system. All the electrodes are referenced to linked mastoids; the forehead is used as ground. The responses are recorded by repetitive sound stimuli applied as auditory clicks to the ear. In the case of BSAEP signals, the stimulus pulse of 0.1 ms duration is applied with an intensity of 60 dB above normal hearing level. Stimulus click rate is 17 Hz. The low voltage of AEP signals combined with relatively high background noise requires the use of highly sensitive amplifiers and computer averaging equipment. The data is first amplified, then sampled at 40 KHz and quantized to 12 bits. For each stimulus, the first 512 points (or equivalently 12.5 msec) of the response is recorded. The low filter is set to 100 Hz and the high filter to 3000 Hz. The instrumentation required to record the BSAEP and the MLR are different as their bandwidths are different. The passband of the recording system for middle

latency responses is 25 to 175 Hz and the usual stimulus repetition rate is 10 per sec. The signal is sampled at 10 KHz frequency. We obtained BSAEP data for 4 subjects and MLR data for 9 normal subjects. An ensemble of 512 response trials for each subject is obtained in both the cases. The data is all post-stimulus. We evaluated the performance of all the proposed estimators with data simulated at different SNR's. In the case of real data, since there is very little difference between the results obtained on the different normal data, we present the results for one typical case each of BSAEP and MLR signals.

1.7 Organization of the thesis

In chapter 2, we propose a spatially selective filter in the wavelet domain to improve the SNR of the EA and enhance the components of the EP signals. It adapts the spatially selective filter (SSF) suggested for images by Xu et al [27], to account for the case of EPs corrupted by colored noise. The proposed filter does not require prior knowledge of the signal or noise and derives this knowledge from the noisy observation itself. It is based on the space-scale correlation of the subband decompositions of a noisy signal, obtained through an undecimated nonorthogonal discrete wavelet transform (UDWT) using à trous algorithm. Since a sharp transition in the signal gives rise to a maximum in several adjacent scales, the correlation between scales is used to identify the signal transition regions. Gaussian functions are placed at the identified edges, scaling wavelet coefficients around the edges. This ensures retention of not only the signal peak information but also the surrounding information. To distinguish transient noise, the variance of the wavelet coefficients in a window around the identified transition region is made use of. This filter may be viewed as a low-pass filter that passes selected high frequency data. Results obtained are compared with the ones obtained using SSF technique, in terms of correlation coefficient, mean square error and also individual component latencies. The method proves to be superior to the SSF method.

A spatially selective Wiener (SSW) filter is proposed in chapter 3. This uses inter-scale correlation in the wavelet domain to identify signal and noise regions. The signal and noise strengths are used to compute the Wiener filter transfer function that operates in a spatially selective fashion. We combine both the thresholding and filtering approaches in the wavelet domain using a feature sensitive selectivity that can effectively filter noisy data.

Chapter 4 presents a model-based estimation approach which employs built-in nonlinear processing elements. The powerful modeling capability of RBF networks is used to model the non-stationary characteristics of evoked potentials. A Gaussian radial basis function neural network is utilised as a model for the EP signal to account for the nonlinear nature of the signal. The choice of the number of the basis functions in the hidden layer and their parameters is a key problem in designing an RBF network. In our work, the GRBF network parameters are deduced from the wavelet transform of the noisy signal to enable the network to learn the functional form of the underlying EP signal more effectively. Deriving the kernel parameters from the signal improves both the effectiveness of the model and tracking property of the network. We show that this yields better results in terms of reduction in the order of the network and a more accurate signal model even in presence of noise. Results obtained are compared with the network whose kernel parameters are evenly distributed over the entire length of the signal with equal spreads. Results are presented which demonstrate the superiority of using signal knowledge in deciding the network parameters to a fixed parameter network. Chapter 5 concludes the thesis with a mention of certain directions for further work.

Chapter 2

Wavelet based spatially selective Gaussian filtering

2.1 Introduction

The wavelet transform (WT) has rapidly become an indispensable signal processing tool for a variety of applications, including estimation, classification and compression. One of the reasons for the success of wavelets is that they form *unconditional bases* for a wide variety of signal classes. In the wavelet domain, noise attenuation can be optimized locally with negligible distortion of the signal details. Wavelets, being well localized in time and scale, are useful tools in handling noisy data sets where signal and noise have overlapping frequency bands. The BSAEP is characterized by few high frequency component peaks of various short durations followed by 1 or 2 low-frequency components. If one wants to preserve both the high and low frequency components occurring at distinct times, a time-varying filter adapted to the local frequency characteristics of the signal is required. To take into account the non-stationary nature of evoked potential signals, de Weerd and Kap [22] have proposed a time varying filter based on the Wiener approach. They translate the original Wiener filter formulation from the frequency domain into time-frequency domain and use a set of zero phase-shift real digital filters having a bandwidth proportional to their center frequency. The filter applies time-varying attenuation functions to the outputs of the bank of filters, which are then summed to form the filtered EP.

Bertrand et al. [8] have translated this concept into wavelet domain using the invertible orthogonal wavelet transform. In their method, assuming the frequency characteristics

of EP, they set the wavelet coefficients outside a specific time-frequency region to zero and retain the coefficients within the specified region. The wavelet coefficients are manually selected in order to eliminate high-frequency components before and after the occurrence of fast brain response. The method is signal specific and also assumes prior knowledge of signal characteristics and hence is not a general one. Thakor et al. [68] have performed multiresolution analysis of the EP signal using orthogonal wavelets to characterize complex changes in their shape during neurological injury. They are able to deduce components of diagnostic value from the decomposed signals. Samar and Raghuveer [58] have described the application of wavelets to event-related potentials and examined their ability to represent the signal using fewer parameters. Bartnik et al. [5] have determined the wavelet coefficients that best discriminate EPs from spontaneous EEG, and used them to estimate single trial EPs. The need for better estimation methods for EP is growing with increased use of EP in clinical environments, either for diagnosis or for surgical monitoring. It is felt that an improved estimation of the buried signal is possible by using statistical knowledge of its wavelet decomposition. In this chapter, we propose a spatially selective Gaussian (SSG) filter that operates at specific identified locations in the wavelet domain.

Wavelet domain filtering is well suited for EP signals for the following reasons:

- Wavelets provide a basis matched to a large class of non-stationary signals. The significant constituents of a EP signal are the nonstationary components that appear along with the stationary EEG noise. Wavelet basis efficiently captures these signal features.

- Some local portions of the signal have important and significant components while considerable noise is also present in the same band. Unlike the purely frequency localization of the Fourier basis, a wavelet basis localizes in both time and frequency, and so can effectively track signal non-stationarities when the signal and noise frequency bands overlap.

- Wavelet transform has the property that large/small wavelet coefficients tend to propagate across scales. This persistence property can be advantageously used to identify signal dominant regions by studying the correlation of the coefficients across the scales.

- Temporally varying thresholding with local estimation of noise variance in different scales is possible in wavelet domain.

- The content and the accuracy of the diagnostic information can be improved by using scale-dependent spatially selective filtering.

In this chapter, we propose a WT based algorithm to account for the non-stationary components in the EP's. This technique is an adaptation of the spatially selective (SS) filter algorithm proposed for images by Xu et al. [27]. It is simple, efficient and can be implemented in real time. The proposed filter does not require prior knowledge of the signal or noise and derives this knowledge from the noisy observation itself. Before explaining the details of this algorithm, we briefly explain the basics of WT in section 2.2. Section 2.3 presents the orthogonal and nonorthogonal wavelet decomposition using the two popular algorithms, namely, Mallat's pyramidal algorithm and the à trous algorithm. Further organisation of the chapter is as follows: The general concept of filtering in the wavelet domain, the spatially selective filtering based on the direct spatial correlation of wavelet coefficients across the scales, and the proposed modification leading to spatially selective Gaussian filtering are all explained in section 2.4. A pseudo-code illustrating the entire procedure is outlined in section 2.5. In section 2.6, we describe the different measures used to evalauate the performance of the estimator. The results obtained using evoked potential data are presented in section 2.7. We discuss the results in section 2.8 and the conclusion follows in section 2.9.

2.2 Wavelet Transform

The continuous wavelet transform (CWT) representation $\gamma(s,\tau)$ of a function $f(t)$ may be defined as,

$$\gamma(s,\tau) = \int_{-\infty}^{+\infty} f(t)\psi^*_{s,\tau}(t)dt \tag{2.1}$$

where $\psi_{s,\tau}(t)$ belongs to a set of basis functions called the wavelets. s and τ are the two continuous real variables representing the wavelet scale and translation respectively and $*$ denotes complex conjugation. The basis function set is generated from a single basic wavelet $\psi(t)$, the so-called *mother wavelet* or *analyzing wavelet*:

$$\psi_{s,\tau}(t) = \frac{1}{\sqrt{|s|}}\psi\left(\frac{t-\tau}{s}\right) \tag{2.2}$$

In the above equation, the set of basis functions is generated by varying s and τ. For any given value of s, the function $\psi_{s,\tau}(t)$ is a shift of the wavelet $\psi_{s,0}(t)$ by an amount τ along the time axis. The result of applying eqn.(2.1) on the signal will be a collection of time-frequency representations of the signal, each with different resolution. The definition of the wavelets as

dilations of the function $\psi_{s,\tau}(t)$ means that high frequency wavelets correspond to $s < 1$ or wide bandwidth and possess good time resolution, while low frequency wavelets have $s > 1$ or narrow bandwidth and possess good frequency resolution. The factor $\sqrt{s}$ normalizes the energy across different scales. The inverse CWT is given by,

$$f(t) = \int_{s=-\infty}^{\infty} \int_{\tau=-\infty}^{\infty} \frac{1}{|s|^2} \gamma(s,\tau) \psi_{s,\tau}(t) d\tau ds \tag{2.3}$$

Some of the problems associated with CWT are that it has an infinite number of transform coefficients and is also computationally complex. The obtained coefficients are highly redundant. Furthermore, it is not necessary to use the entire support of $\gamma(s,\tau)$ to reconstruct $f(t)$.

Discrete wavelets are not continuously scalable and translatable; they can only be scaled and translated in discrete steps. This is achieved by modifying the representation as,

$$W(i,j) = \int_t f(t) \psi^*_{i,j}(t) dt \tag{2.4}$$

where $\psi(t)$ is defined as,

$$\psi_{i,j}(t) = \frac{1}{\sqrt{s_0^i}} \psi \left(\frac{t - j\tau_0 s_0^i}{s_0^i} \right) \tag{2.5}$$

Although it is called a discrete wavelet, it normally is a (piecewise) continuous function. In the above eqn. i and j are integers and $s_0 > 1$ is a fixed dilation step. The translation factor τ_0 depends on the dilation step. When discrete wavelets are used to transform a continuous signal, the result will be a series of wavelet coefficients, and it is referred to as the wavelet series decomposition. The inverse wavelet transform for discrete wavelets is given by,

$$f(t) = \sum_{i \in \mathbf{Z}} \sum_{j \in \mathbf{Z}} W(i,j) \psi_{i,j}(t) \tag{2.6}$$

To reconstruct a signal from its wavelet decomposition, the necessary and sufficient condition is that the energy of the wavelet coefficients must lie between two positive bounds. The discrete wavelets can be made orthogonal to their own dilations and translations by special choices of the mother wavelet. An arbitrary signal can be reconstructed by summing the orthogonal wavelet basis functions, weighted by the wavelet transform coefficients. By using orthogonal basis functions, all the redundancy in a DWT can be removed. However, orthogonality is not essential for the representation of signals.

Mallat's multiresolution decomposition [53] and the à trous algorithm [60] are two separate implementations of the discrete wavelet transform. Mallat's method is based on the principle of reducing the redundancy of the information in the transformed data. Moreover, the transform is shift variant. It means that the wavelet transforms of a signal and its time-shifted version are not simply shifted versions of each other. The à trous algorithm results in a non-orthogonal and redundant data set. Depending on the application, each of these models can be advantageously used. Both the algorithms are observed to be special cases of a single filter bank structure [60]. A good improvement is possible in the case of denoising applications by giving up orthogonality and using a redundant and shift invariant discrete wavelet transform. We briefly explain the difference between these two popular decomposition methods in the following subsections. For an in depth study of DWT and related subjects, one may refer to [39, 53, 63].

2.3 DWT computation methods

2.3.1 Multiresolution wavelet decomposition - Pyramidal algorithm

The idea of consecutive approximations at finer and finer frequency resolutions is formalized by the concept of multiresolution approximation (or multiresolution analysis). Mallat has explained the relationship between multiresolution analysis and wavelet transform in [53]. A function $f(x) \in V_j$ is projected, at each scale j, onto the subset V_{j-1}. This projection, $s_{j,k}$ is defined as the scalar product of $f(x)$ with a scaling function, $\phi_{j,k}(x)$.

$$s_{j,k} =< f(x), 2^{-j}\phi(2^{-j}x - k) > \tag{2.7}$$

where k is the translation parameter and j is the dilation parameter. Integer translations and dyadic dilations are used. $\phi(x)$ has the following property:

$$\phi(x) = \sum_{n=-\infty}^{\infty} h(n)\phi(2x - n) \tag{2.8}$$

This is referred to as dilation equation since $\phi(x)$ is expressed in terms of its own dyadic dilations and translations. The dilation equation results in a decreasing sequence of closed subspaces, $V_j \in Z$ which approximate $L^2(\Re)$. Each of the successive approximation spaces, $\cdots \subset V_2 \subset V_1 \subset V_0 \subset V_{-1} \subset V_{-2} \cdots$, have a resolution 2^j and form a nested sequence, i.e

$$V_j \subset V_{j-1} \tag{2.9}$$

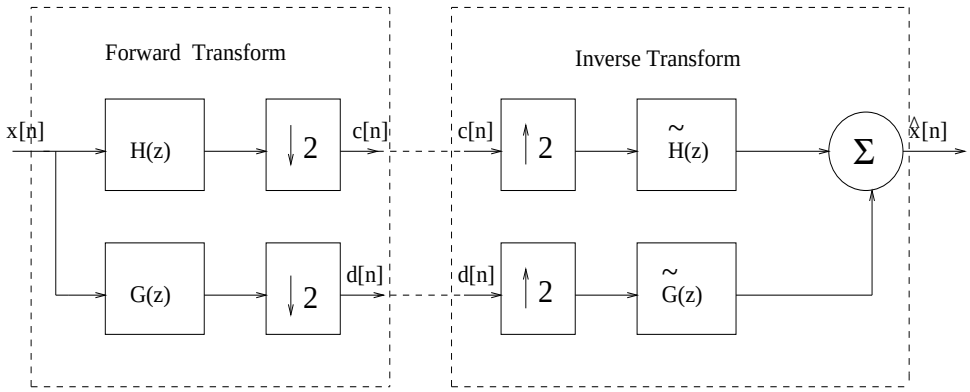

Figure 2.1: Multiresolution orthogonal decomposition of a signal.

The sequence $\{h(n), n \in Z\} \in l^2$ is the impulse response of a low-pass filter. The principle of multiresolution decomposition is shown in Fig. 2.1. The information lost in V_{j+1} can be restored using the complementary subspace U_{j+1} of V_j. Subspaces U_j are generated by a wavelet function $\psi_{j,k}(x)$ which is derived from the scaling function to analyze finer details of the signal. The projection $d_{j,k}$ of $f(x)$ on U_j is defined as

$$d_{j,k} =< f(x), 2^{-j}\psi(2^{-j}x - k) > \tag{2.10}$$

The scaling functions and the wavelet functions are related as,

$$\frac{1}{2}\psi(\frac{x}{2}) = \sum_n g(n)\phi(x - n) \tag{2.11}$$

The sequence $\{g(n), n \in Z\} \in l^2$ is the impulse response of a high pass filter. Using $h(n)$ and $g(n)$, the wavelet analysis is defined as,

$$\begin{aligned} s_{j,k} &= \frac{1}{2}\sum_n h(n - 2k)s_{j-1,k} \\ d_{j,k} &= \frac{1}{2}\sum_n g(n - 2k)s_{j-1,k} \end{aligned} \tag{2.12}$$

For orthogonal wavelets, the reconstruction is performed by

$$s_{j,k} = 2\sum_n h(k - 2n)s_{j+1,n} + 2\sum_n g(k - 2n)d_{j+1,n} \tag{2.13}$$

The behavior of the computed discrete wavelet transform is governed by the choice of the filters. One disadvantage of the classical decimated DWT is the lack of shift invariance. As shown in [46], the wavelet decomposition of a signal can differ enormously when the input signal is shifted by even one sampling interval. However, it is a non-redundant representation and is very useful for coding applications since it removes redundant information.

2.3.2 Undecimated wavelet transform - à trous algorithm

The undecimated wavelet transform (UDWT) has been independently discovered several times, for different purposes and under different names, e.g. shift/translation invariant wavelet transform, stationary wavelet transform, or redundant wavelet transform [9, 52, 60]. In signal analysis, unlike compression applications, a redundant expansion of the signal is often desired. It is a closer approximation to the continuous wavelet transform. It is a nonorthogonal variant of the classical wavelet transform and plays an important role in denoising algorithms. It is translation-invariant, which means that it is independent of the position of the input signal. Several redundant decompositions exist in the literature [23, 48]. One such scheme, the à trous (means 'with holes') algorithm is well known for its computational efficiency. A discussion of the algorithm and its history can be found in [47]. We briefly present this method in this section.

In this algorithm, the filters are dilated at each projection, but the decomposition is not decimated. Therefore, each scale has N points corresponding to the N data points. For the scale j, these points correspond to 2^j different decompositions obtained with the decimated transform using all the circulant shifts of the signal. These decompositions, each one composed of $N/2^j$ points, are intertwined. This overcomes the dependence of the transform on the position of the input signal. Hence it is translation invariant unlike the decimated wavelet transform. This is a WT defined as the difference between the scaling functions of two successive scales. The sampled data is assumed to correspond to zeroth scale and is denoted as $\{c(0,k)\}$. The subsequent smoothed sequences are given by,

$$c(j,k) = \sum_l h(l)c(j-1, k+2^{j-1}l) \tag{2.14}$$

and the wavelet coefficients are the difference between two successive smoothed sequences:

$$w(j+1,k) = c(j+1,k) - c(j,k) \tag{2.15}$$

The coefficients {h(l)} are derived from the scaling function $\phi(t)$:

$$\frac{1}{2}\phi(\frac{t}{2}) = \sum_l h(l)\phi(t-l) \tag{2.16}$$

The reconstruction is the sum of all the scales and the smoothed signal at the coarsest scale:

$$c(0,k) = \sum_{j=1}^{J} w(j,k) + c(j,k) \tag{2.17}$$

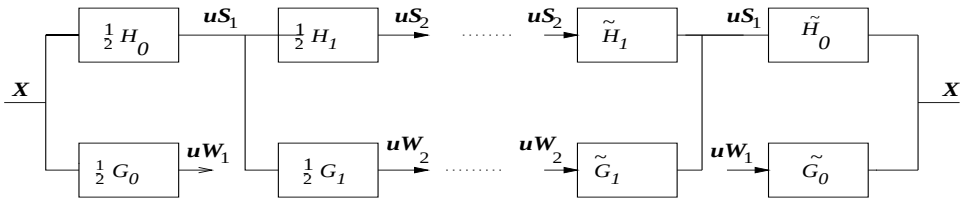

Figure 2.2: Undecimated discrete wavelet transform of a signal.

J being the number of decomposition scales. Fig. 2.2 shows the computation of the UDWT of a signal as a block diagram. This can be viewed as the scalar product of a function $f(x)$ with a scaling function that corresponds to a low pass filter. The transform is typically iterated on the output of the low-pass band $c(j,k)$ to create a series of detail coefficients at different scales.

In a recent work [60], Shensa has shown that à trous algorithm bears an intimate relationship to Mallat's decomposition. Both schemes are shown to be different instances of a single filter bank structure, the DWT. The Mallat's scheme is simply the decimated output of the DWT which is characterized by octaves obtained by alternating the low-pass filter H with decimation and tapped by a band-pass filter G. Since the coefficients are not downsampled, the conditions necessary for perfect reconstruction in the case of decimated wavelet transform need not be met in the case of UDWT.

2.4 Filtering in the wavelet domain

Consider the classical problem of estimating an unknown deterministic signal $\mathbf{s} = \{s(n)\}, n = 1, \cdots, N$, from a set of noise-corrupted samples, $\mathbf{x} = \{x(n)\}, n = 1, \cdots, N$, which may be denoted as,

$$\mathbf{x} = \mathbf{s} + \mathbf{v} \tag{2.18}$$

where $\mathbf{v} = \{v(n)\}, n = 1, \cdots, N$ is a zero-mean white Gaussian noise of variance σ^2. By taking the DWT of eqn. (2.18),

$$\mathcal{W}\mathbf{x} = \mathcal{W}\mathbf{s} + \mathcal{W}\mathbf{v} \tag{2.19}$$

or equivalently,

$$\mathbf{y} = \theta + \mathbf{z} \tag{2.20}$$

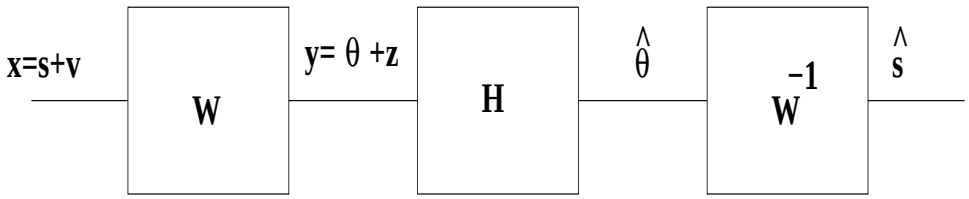

Figure 2.3: Filtering in wavelet domain

where $\mathcal{W}\mathbf{x} = \mathbf{y}, \mathcal{W}\mathbf{s} = \theta$ and $\mathcal{W}\mathbf{v} = \mathbf{z}$, respectively. After applying the WT, the resulting sequence, $\mathbf{y}$ is again the sum of the transformations of the signal (θ) and the noise (z). This is a consequence of the linearity of $\mathcal{W}$. In general, the wavelet coefficients of a function are large in regions where the function is irregular and small in smooth regions.

If a function is corrupted by additive noise, the noise dominates the wavelet coefficients at small scales. Thus, most of those coefficients contain the noisy part of the signal and only a few large coefficinets are related to strong singularities in the underlying function. An orthogonal wavelet transformation will map $\mathbf{v}$ to $\mathbf{z}$, which is again a zero-mean white Gaussian with variance σ^2, while compacting the signal $\mathbf{s}$ into a small number of large wavelet coefficients. A reasonable approach to wavelet-based signal estimation is to zero out the small entries of $\mathbf{y}$, which are most likely due to the noise (where there is no signal), while retaining the large entries that are most likely due to the signal; such an approach is known as wavelet denoising. An operator H may be so defined as to modify the transform coefficients to obtain the signal estiamte $\hat{\mathbf{s}}$. This may be represented as,

$$\hat{\mathbf{s}} = \mathcal{W}^{-1}\mathbf{H}\mathcal{W}\mathbf{x} \tag{2.21}$$

The block diagram for the above filtering operation in wavelet-domain is given in Fig. 2.3. The nature of H determines the effectiveness of the filter. Thresholding filters, and other statistical filters are different approaches for denoising a given observation. In the following subsection, we explain the spatially selective filtering of Xu et al. [27] proposed for noise filtration in images. Then we propose an extension to this work using a Gaussian filter in a spatially selective manner for estimating EP's.

2.4.1 Spatially selective filtering

Mallat et al. [52] introduced the concept of complete signal representation by WT domain maxima. They were able to distinguish signal maxima from noise maxima by analyzing the

singularity properties of WT domain maxima of a signal across various scales [54]. Witkin [71] first introduced the idea of using space-scale correlation of the subband decompositions of a signal to filter noise from the signal. Using direct multiplication of the coefficients across subband decompositions, he was able to distinguish major edges from noise. Xu et al. [27] studied spatial filters in the wavelet domain as an alternative to Fourier domain filters. They proposed a spatially selective filter (SSF) based on the space-scale correlations of the subband decompositions of a noisy signal. The major transitions in the signal are tracked from coarse scales to fine scales, thereby distinguishing major signal edges from the background noise. The method relies on the persistence property of the wavelet transform to accomplish the task of filtering noise from signals. A large spatial correlation between the scales is considered to indicate a signal edge. Direct l^{th} order spatial correlation across scales, $corr_l(m,n)$ is defined to be

$$corr_l(m,n) = \Pi_{i=0}^{l-n} w(m+i,n), \qquad n = 1,2,\cdots,N \tag{2.22}$$

where l is the number of scales involved in the direct multiplication and $m < M - l + 1$, where M is the total number of scales. An edge is identified at any position n for which

$$|corr_l(m,n) > |w(m,n)| \tag{2.23}$$

This algorithm, which iteratively identifies the important wavelet coefficients in each scale, is well explained in [27]. A binary mask is used to retain the identified significant wavelet coefficients and discard others. The absence of edges or significant features in a localized region of the signal allows the noisy background to be removed there. We propose modifications to this filter by introducing an additional measure to discriminate between the signal and noise edges and smoothing the regions surrounding the identified edges. The proposed method is explained in the following subsection.

2.4.2 Spatially selective Gaussian filtering

We adapt the edge identification algorithm proposed by Xu et al [27] to suit the case of EP estimation. Our experiments showed that the use of binary masks for selecting wavelet coefficients in each scale at the identified edges leads to oscillations or artifacts at the end points of the masks. Hence we use Gaussian masks rather than binary masks. This optimizes noise attenuation locally, with negligible distortion of the signal details at the identified edge points.

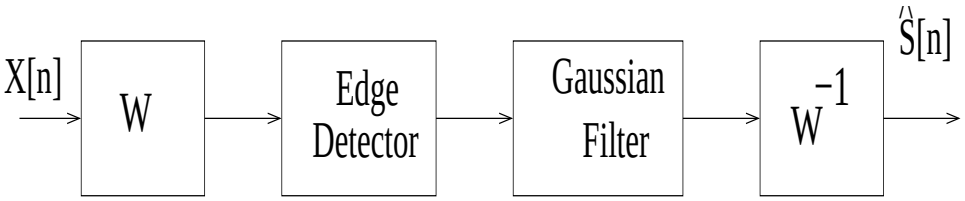

Figure 2.4: Block diagram of spatially selective Gaussian filtering in wavelet domain

It smooths and scales not only the significant edge information, but also the surrounding information. This helps in avoiding Gibb's oscillations or artifacts around the identified significant features.

By using the spatially selective filtering algorithm suggested in [27], binary masks are obtained, that are to be applied on the different wavelet scales. To avoid detection of spurious noise as significant features, the variance in the wavelet domain in a small window of length k before the identified edge, is compared with the variance in a window after the edge. Since the noise is assumed to be a stationary process, this measure eliminates the false detection of transient noise edges as signal features. Figure 2.4 shows the block diagram of the proposed spatially selective Gaussian (SSG) filter. The inter-scale correlation, coupled with the changes in variance around the identified point, are thus used to differentiate between noise and signal dominant coefficients.

To differentiate a signal edge from a noise edge, we consider small regions in each scale, before and after the identified edge location, n, and compare the variances of the regions. Employing windows of width k, we define, for scale m, $\sigma_1^2(n) = var(win1 = w(m, n-k : n-1))$, and $\sigma_2^2(n) = var(win2 = w(m, n+1 : n+k))$,

if $abs(\sigma_1(n) - \sigma_2(n)) < \epsilon$

discard the edge (indicates noise edge)

else

retain the edge (indicates signal edge)

end

where $\epsilon \in R$ is fixed as a small fraction of $\sigma_1(n)$ and is positive. The absence of edges or other significant features in a localized region of the signal allows the wavelet coefficients in that region to be made zero thereby removing the background noise. The Gaussian shrinkage function $\eta(w(m,n))$ centered at the identified edge n, with a standard deviation $p_n = 0.1\sigma_1(n)$

is defined as

$$\eta_n(k) = \frac{1}{p_n\sqrt{2\pi}} e^{-\left(\frac{(n-k)^2}{2p_n^2}\right)} \tag{2.24}$$

In summary, the proposed algorithm works in three stages. Initially, it identifies the locations, where the correlation between adjacent wavelet scales is high. Then, it uses the change in variance in the neighborhood of identified edges to exclude correlated noise edges. Finally, a Gaussian shrinkage function centered at the edge point scales the wavelet coefficients to enhance the non-stationary signal components. The number of levels of decomposition $M(\geq 1)$ is dependent on the structure of the signal. For the signals under consideration, $M = 4$ is found to give satisfactory results in all the cases. The B_3-spline scaling function is used as the basic wavelet in our work. The associated filter $H(z)$ is given by,

$$H(z) = \frac{1}{16}z^{-2} + \frac{1}{4}z^{-1} + \frac{3}{8} + \frac{1}{4}z + \frac{1}{16}z^2 \tag{2.25}$$

We compare our results with those of the space-scale filter, wherein binary masks are used at the identified edges instead of Gaussian masks.

The detecion of significant signal regions is a fundamental step for all the different techniques proposed in this thesis for EP estimation. Accordingly, the algorithm for detecting the component regions in the wavelet domain is given as a pseudo code in the section that follows.

2.5 Pseudo-code for spatially selective Gaussian filtering in the wavelet domain

Loop for each wavelet scale m

{

Loop for the iteration process

{

% Compute the Power of $Corr_2(m,n)$ and $W(m,n)$:

$$\begin{aligned} PCorr(m) &= \Sigma_n Corr_2(m,n)^2 \\ PW(m) &= \Sigma_n W(m,n)^2 \end{aligned}$$

Re-scale the power of $Corr_2(m,n)$ to that of $W(m,n)$:

% Loop for each point n

{

new $Corr_2(m,n) = Corr_2(m,n) * \sqrt{\frac{PW(m)}{PCorr(m)}}$

} end loop n

% Loop for each point n

{

if $|Corr_2(m,n)| > |W(m,n)|$

{ % Identify significant features using $W(m,n)$ and $Corr_2(m,n)$

$Corr_2(m,n) = 0.0$

$W(m,n) = 0.0$

$mask(m,n) = 1$

} end if

} end loop n

} iterate until $PW(m) \leq$ the noise threshold at scale m

% At the identified points, check for change in variance to rule out noise edges

% Loop for all $mask(m,n) = 1$

{

$\sigma_1(n) = var(win1 = W(m, n-k : n-1))$

$\sigma_2(n) = var(win2 = W(m, n+1 : n+k))$

if $abs(\sigma_1(n) - \sigma_2(n)) < \epsilon$

Discard the detected point as noise

else

Retain the detected point as a signal feature

end

}

% Compute Gaussian shrinkage function $\eta(W(m,n))$ centered at the identified point n,

% with a standard deviation $p(n) = 0.1\sigma_1(n)$ defined as

$$Gmask(m,k) = \eta(W(m,k)) = \frac{1}{p(n)\sqrt{2\pi}} e^{-\left(\frac{(n-k)^2}{p^2(n)}\right)}$$

Loop for each point n

{

$Wnew(m,n) = Gmask(m,n) * W(m,n)$

} end loop n

} end loop m

2.6 Performance evaluation

In order to compare the performance of different estimation methods, we need to define criteria that measures how well the estimator approximates the true signal. We have used mean square error (MSE) and correlation coefficient (CC) to evaluate the performance of the proposed estimators. We compute these quantities for different SNR's of the input noisy signal. If s is the required actual signal and $\hat{s}$ is the estimator's output, the MSE is defined as,

$$MSE = E[(s - \hat{s})^2] \tag{2.26}$$

The correlation coefficient is defined by,

$$\rho_{s\hat{s}} = \frac{cov(s,\hat{s})}{\sigma_s \sigma_{\hat{s}}} \tag{2.27}$$

where $cov(s,\hat{s})$ is the covariance obtained from,

$$cov(s,\hat{s}) = E\{[s - E(s)][\hat{s} - E(\hat{s})]\} \tag{2.28}$$

and variance σ_s^2 is given by,

$$\sigma_s^2 = E(s^2) - [E(s)]^2 \tag{2.29}$$

The input/output SNR is calculated as,

$$inputSNR = 10\log\left[\frac{\sum_{n=1}^{N} s^2(n)}{\sum_{n=1}^{N} v^2(n)}\right] \tag{2.30}$$

$$outputSNR = 10\log\left[\frac{\sum_{n=1}^{N} \hat{s}^2(n)}{\sum_{n=1}^{N} v^2(n)}\right] \tag{2.31}$$

In addition to the above quantifiers, the latencies of all the components in the estimated signals are compared with the latencies obtained from a simple EA of all the sweeps in a given data file. It is to be mentioned that the performance metrics defined here are used to evaluate not only the spatially selective Gaussian filter, but also the other techniques proposed in this thesis in other chapters.

2.7 Experimental Results

To begin with, we present the experimental results obtained with simulated brainstem auditory evoked potentials and middle latency auditory responses. Subsequently, we illustrate the performance of the proposed SSG filter on clinically recorded BSAEP and MLR responses.

2.7.1 Simulated data

The BSAEP-Sim signal, simulated at different SNR's starting from 1 dB, is used as input to the SSG filter. Fig. 2.5 shows the BSAEP-Sim signal at 1.75 dB and also its decomposition into 4 scales with a B_3-spline scaling function using non-orthogonal UDWT as per à trous algorithm. The simulated signal has all the first five components although they are not visible because of the low SNR. The estimator's performance is found to be poor in terms of visual perception, at SNR's less than 0 dB. Consequently, we present the results obtained with inputs of SNR greater than 0 dB. In all the implementations, we decomposed the signal into 4 scales and computed the spatial correlation between two adjacent scales ($l = 2$).

The correlations between adjacent scales for three different sets of scales, namely, $corr_2(1,2)$, $corr_2(2,3)$ and $corr_2(3,4)$ are displayed in Fig. 2.6 in three columns. The wavelet coefficients corresponding to significant features in the original signal such as sharp peaks and valleys appear stronger in the correlation domain than in the wavelet domain. The binary masks obtained using the principles of SSF technique are shown in the second row of the same figure. The corresponding Gaussian masks obtained after the variance check are shown in the third row of the figure. This filtering technique preserves the finest scale information corresponding to high frequency edges. In other denoising techniques, either the finest scale information is removed altogether or a homogeneous smoothing operator is applied on the complete length of a scale. Using the information from the neighbourhood of the identified important coefficients, spurious noise edges are eliminated.

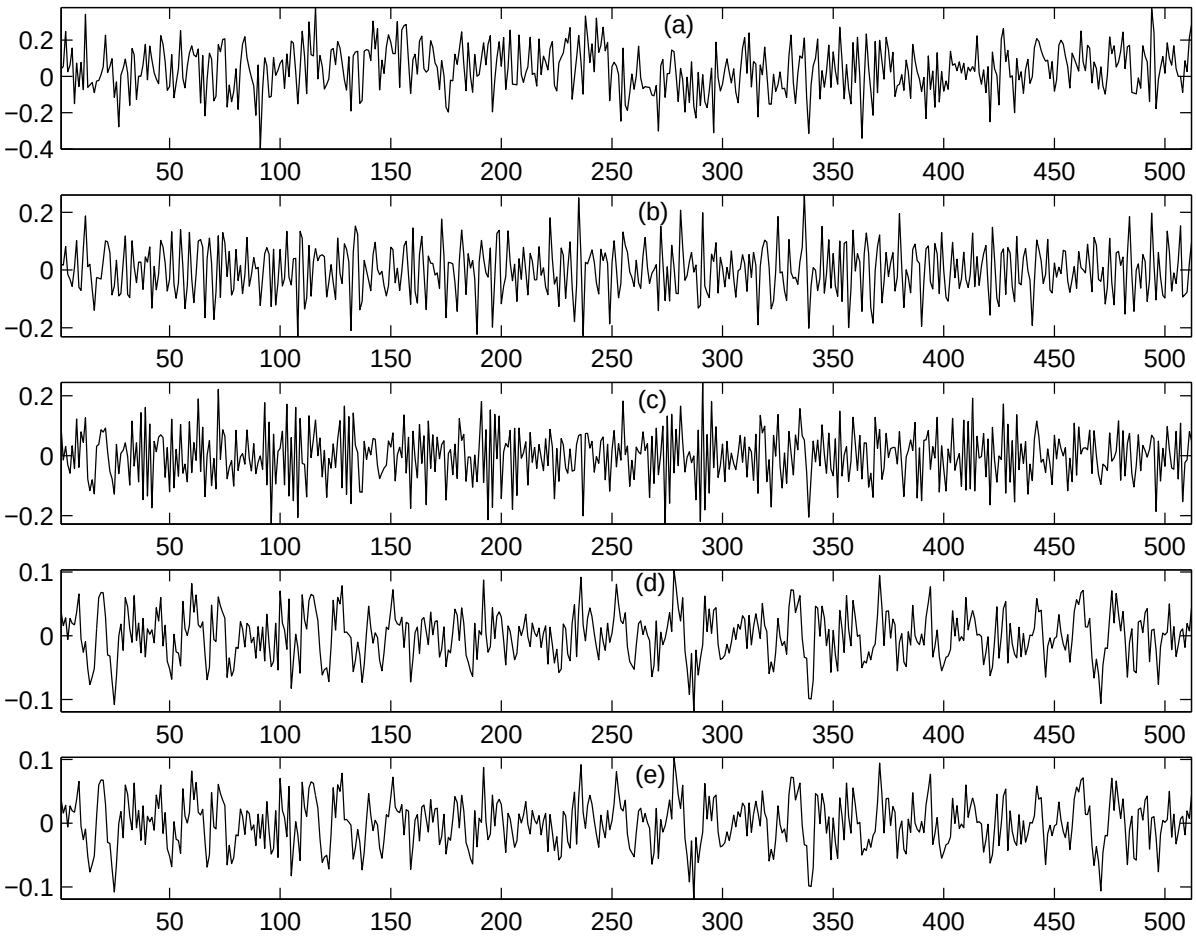

Figure 2.5: Decomposition of BSAEP-Sim signal using UDWT. (a): BSAEP-Sim signal at SNR 1.75 dB. (b,c,d,e): Decomposition into scales 1, 2, 3, and 4, respectively.

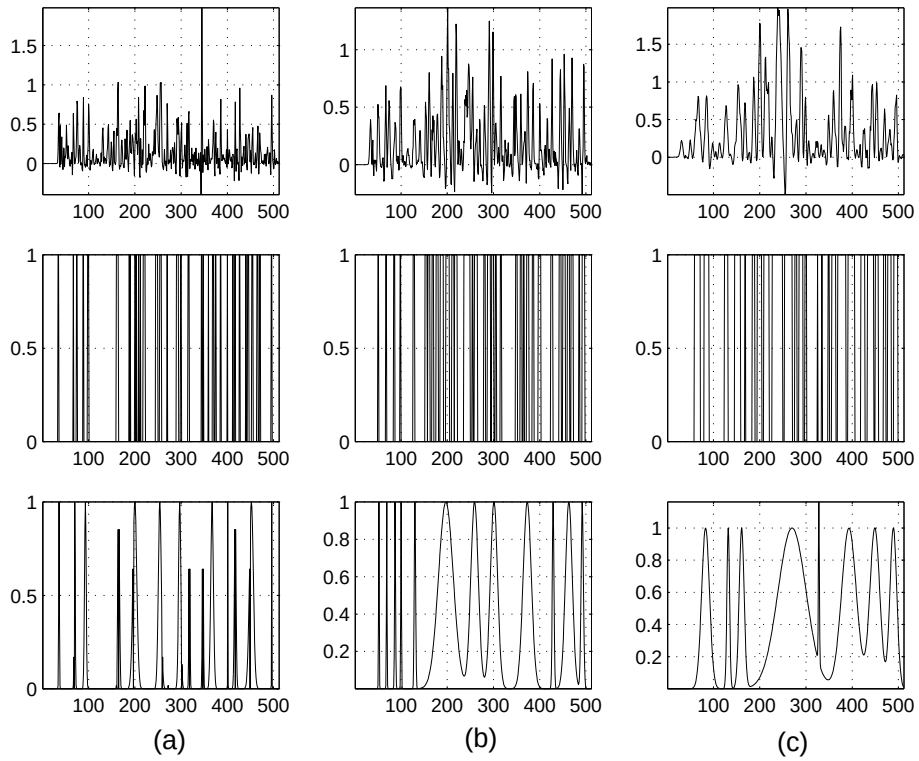

Figure 2.6: Derivation of Gaussian masks for BSAEP-Sim signal. Row 1: Correlation between scales 1 - 2, 2 - 3, and 3 - 4, respectively. Row 2: Binary masks obtained using the principles of selective filtering. Row 3: Corresponding Gaussian masks.

It may be observed from Figs. 2.6 (b) and (c), that the number of significant wavelet coefficients detected in each scale comes down after the variance check. The wavelet coefficients in each scale are shown in Fig. 2.7, before and after being modified by the Gaussian masks. The coarsest scale (which in this case is the fourth one) coefficients are unaltered since we get only $M-1$ correlation vectors by using second order spatial correlation when the signal is decomposed into M scales. The retension of the coarsest scale data preserves the shape information of the signal. Coefficients with higher values persisting across scales are retained and the remaining are discarded as seen from the second column of Fig. 2.7.

Figure 2.8 compares a signal obtained by the proposed method with the one obtained using binary masks. The input signal has a SNR of 1.75 dB. It can be seen that the small noisy variations present in the output of binary mask filtering are removed by the proposed technique. This is due to the fact that we study the variance around the identified edge region in order to retain or suppress the wavelet coefficients. The performance of the estimator for different input SNR's is investigated in terms of correlation coefficient and MSE. The estimator output for each

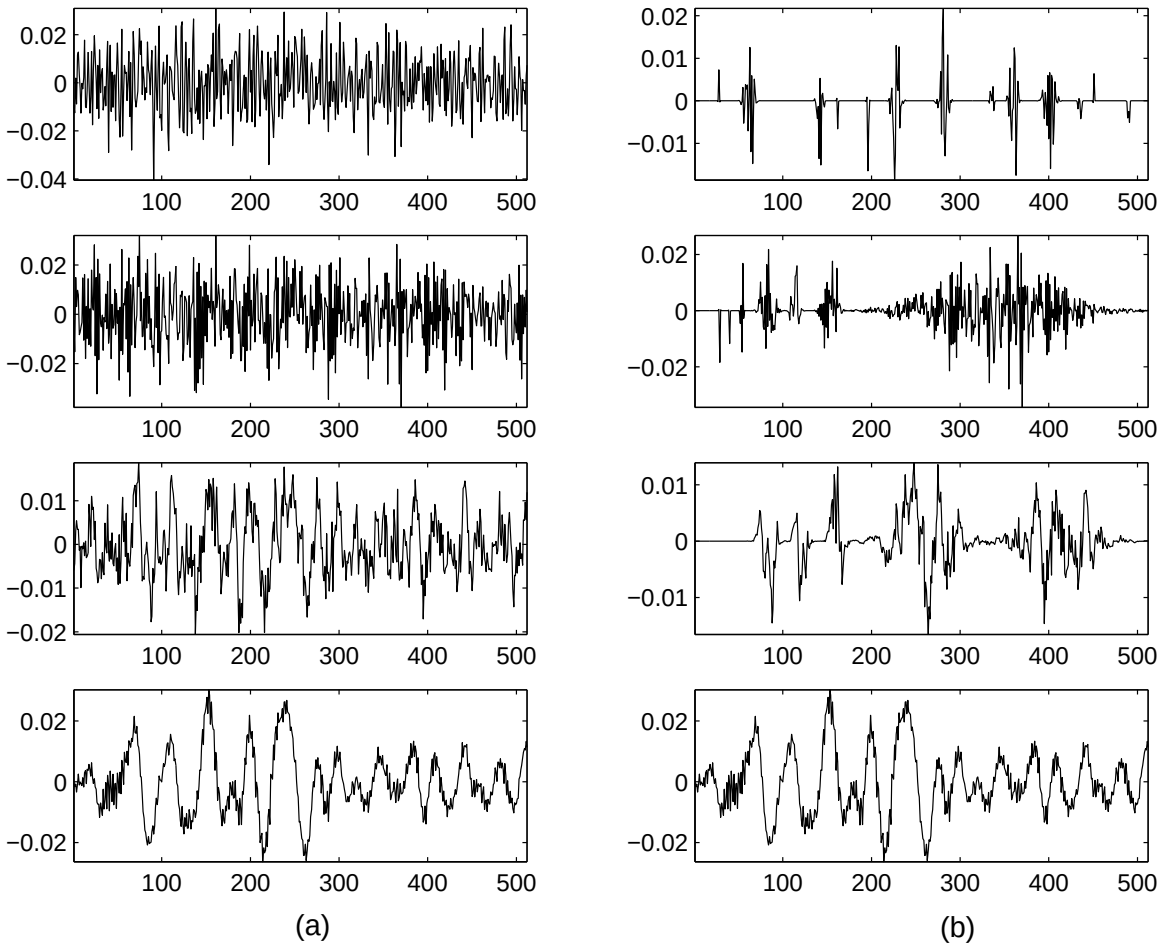

Figure 2.7: Output of spatially selective Gaussian filtering of BSAEP-Sim signal. Column (a): UDWT coefficients at scales 1, 2, 3 and 4, respectively. Column (b): Spatially selected scale data after Gaussian filtering.

input SNR is correlated with the original signal and is plotted in Fig. 2.9(a). The performance of the estimator is found to be unsatisfactory for input SNR's less than zero. Hence, the outputs of the estimator are computed and plotted for SNR's of the input signal ranging from 1.75 dB to about 10 dB. Similarly, the MSE of the estimated outputs is plotted in Fig. 2.9(b) for different SNRs of the input signal. It can be observed that the MSE achieved by the proposed filter is less for any input SNR compared to the space-scale filtered (SSF) output.

Similarly, the proposed filtering is tested on the simulated middle latency response, MLR-Sim. In Fig. 2.10, we show the decomposition of the MLR-Sim signal into 4 scales. The inter-scale correlations between scales 1-2, 2-3, and 3-4 are shown in the first row of Fig. 2.11. The significant regions, detected for different scales using SSF method, are presented as binary

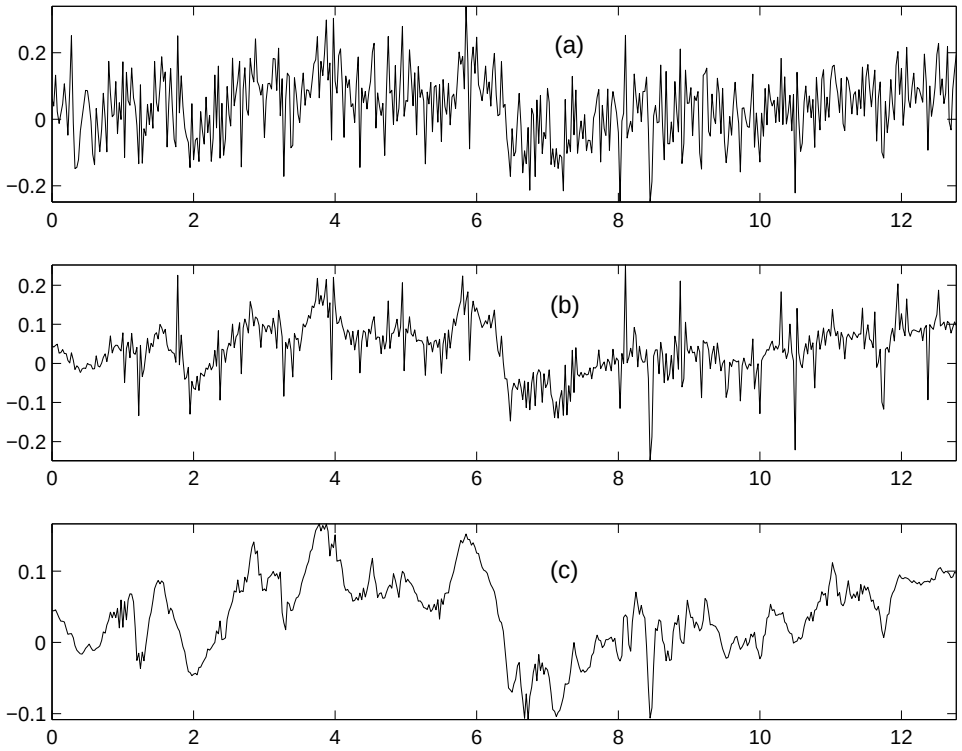

Figure 2.8: Comparison of outputs estimated using binary and Gaussian masks for BSAEP-Sim signal with a SNR of 1.75 dB. (a) Noisy signal. (b) Filtered output obtained using binary masks. (c) Output obtained using Gaussian masks.

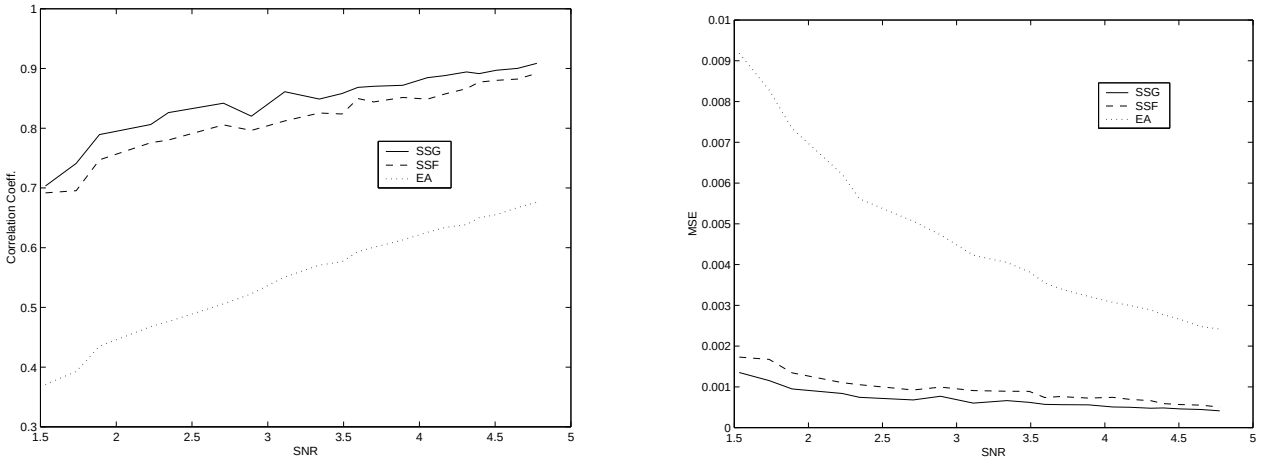

(a) (b)

Figure 2.9: Performance evaluation of the estimator on BSAEP-Sim signal of different input SNRs (a) Correlation coefficinet Vs. input SNR (b) MSE Vs. input SNR

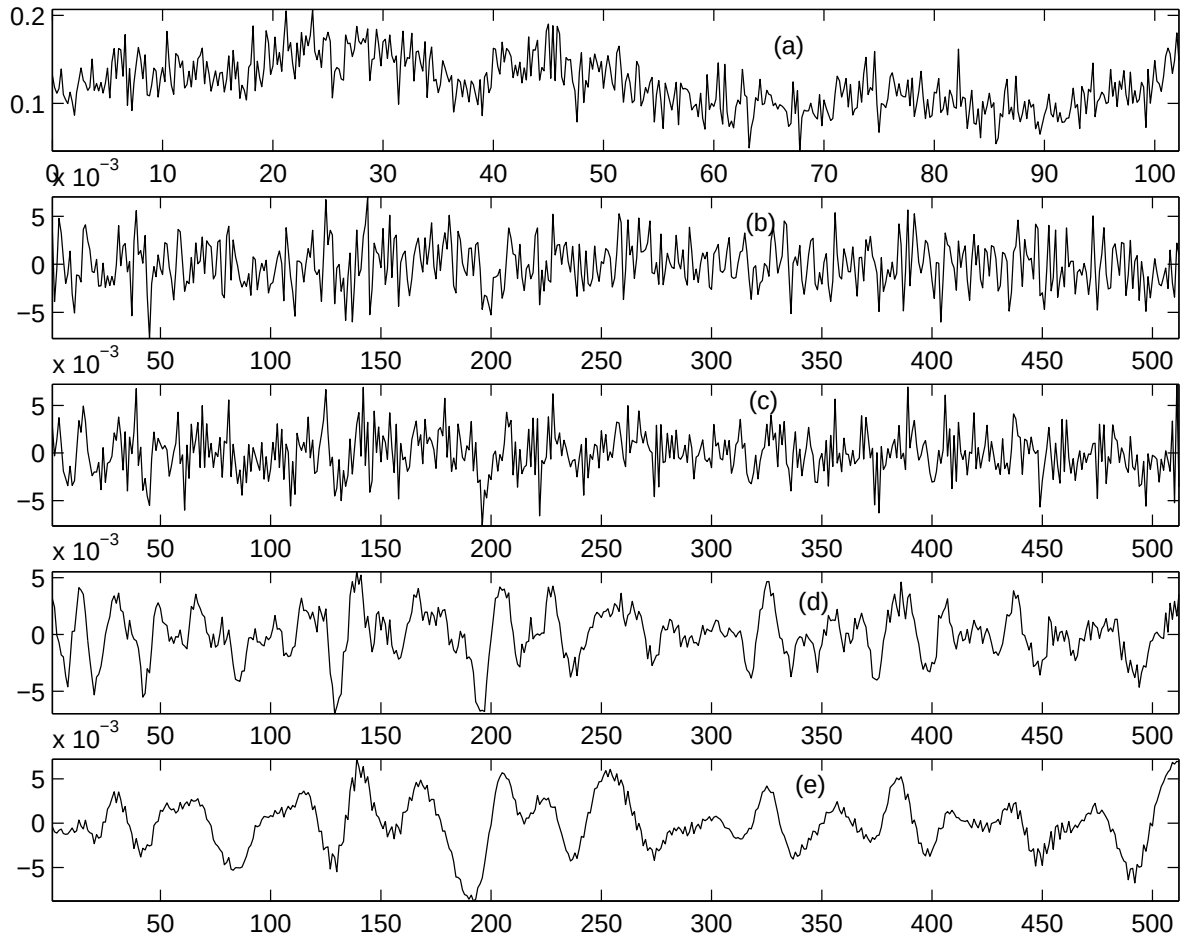

Figure 2.10: Decomposition of MLR-Sim signal using UDWT. (a) MLR-Sim signal with a SNR of 1.75 dB. (b,c,d,e): Decomposion into scales 1, 2, 3, and 4, respectively.

masks in the second row of Fig. 2.11. The coarsest scale data is retained without modification, since it generally has less noise and contains the shape information of the signal. The Gaussian masks for different scales, determined using our method, are shown in the third row. The retained wavelet coefficients, after multiplication by the Gaussian masks, are shown in Fig. 2.12, along with the original decompositions. The signals estimated using both SS filtering and SSG filtering are shown in Figs. 2.13 (b) and (c), respectively. In this figure too, it can be observed that the Gaussian filtering around the identified edges helps in retaining the edge information and smoothing the small variations around the edges. The performance of the estimator, in terms of correlation coefficient and MSE, is investigated for different input SNR's. The results obtained are plotted in Fig. 2.14.

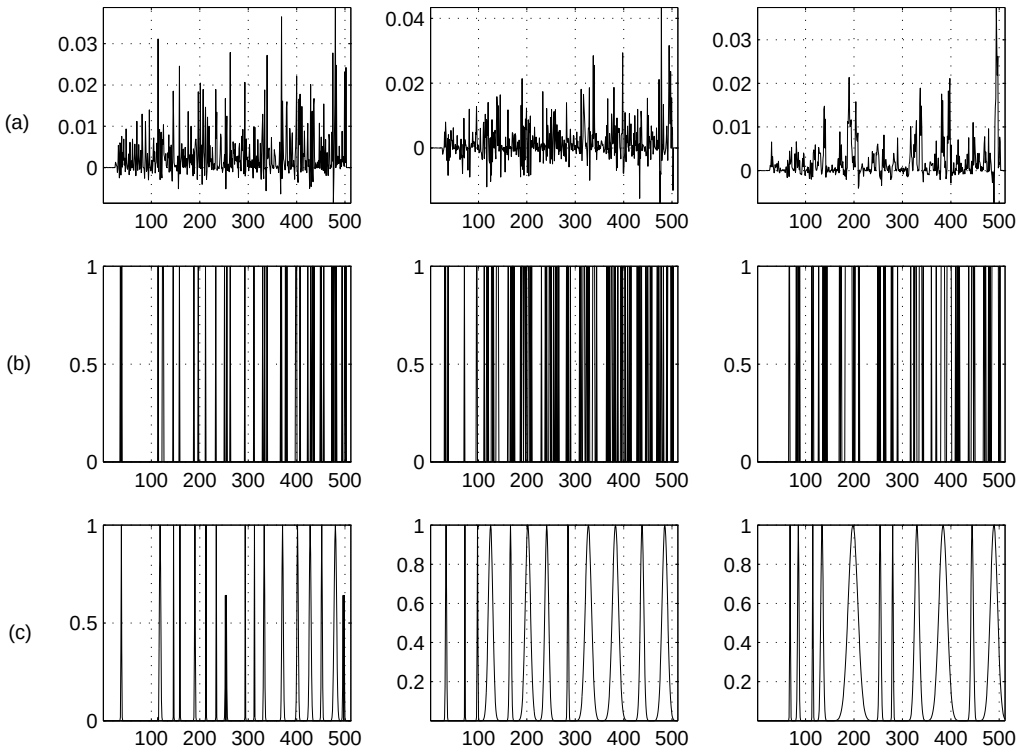

Figure 2.11: Derivation of Gaussian masks for MLR-Sim signal. Row 1: Correlation between scales 1 - 2, 2 - 3, and 3 - 4, respectively. Row 2: Binary masks obtained using spatially selective filtering. Row 3: Corresponding Gaussian masks.

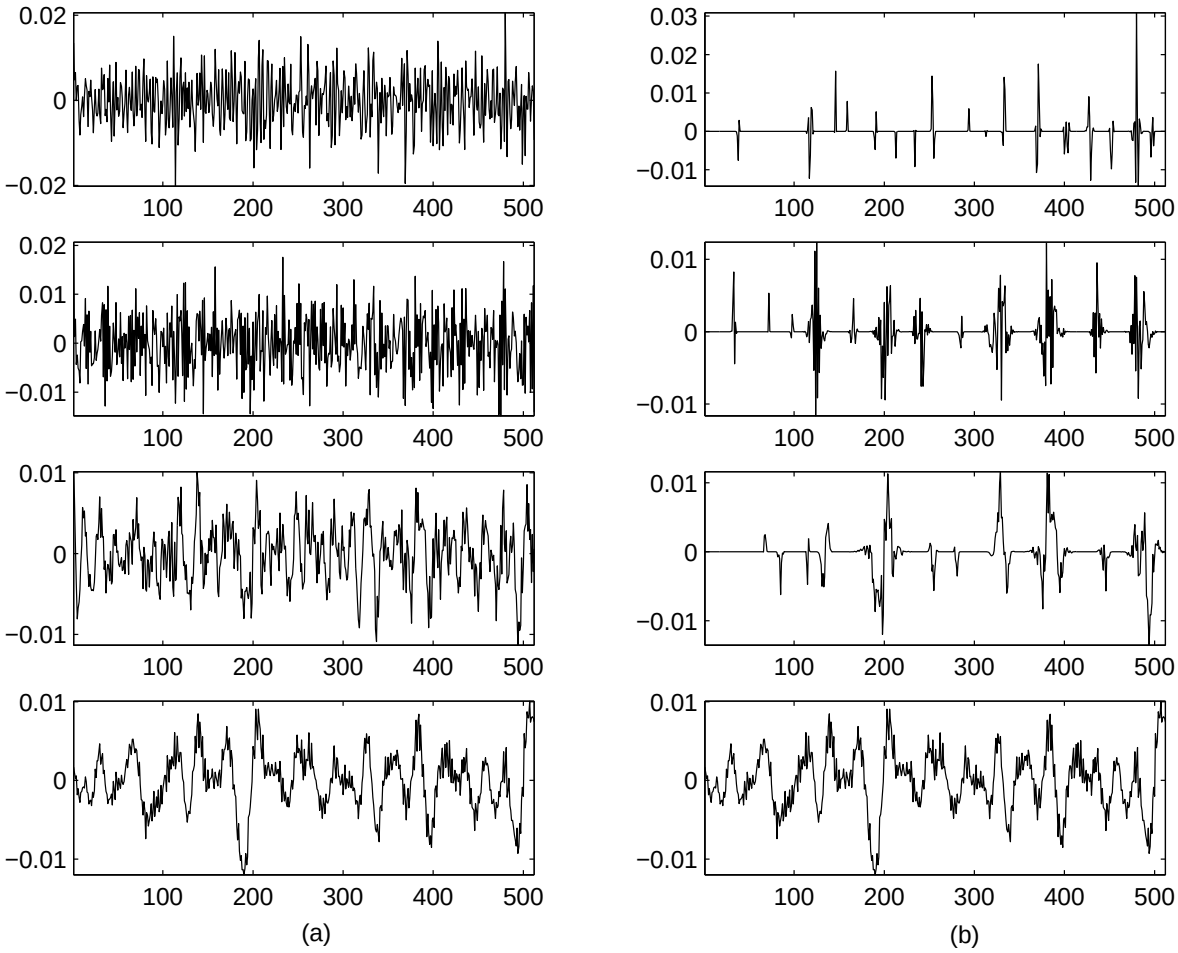

Figure 2.12: SSG filtering of MLR-Sim signal. (a) Decomposition of MLR-Sim signal into scales 1, 2, 3 and 4 using UDWT. (b) Corresponding modified coefficients after Gaussian filtering.

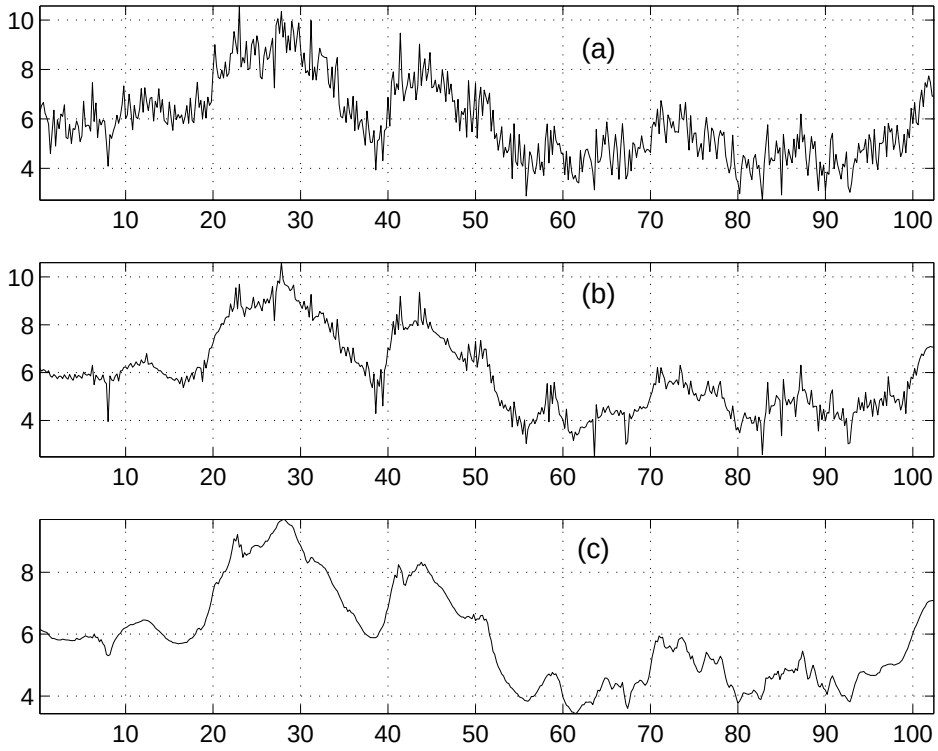

Figure 2.13: Comparison of outputs obtained using binary and Gaussian masks for MLR-Sim signal. (a) Noisy signal. (b) Filtered output obtained using binary masks. (c) Output obtained using Gaussian masks.

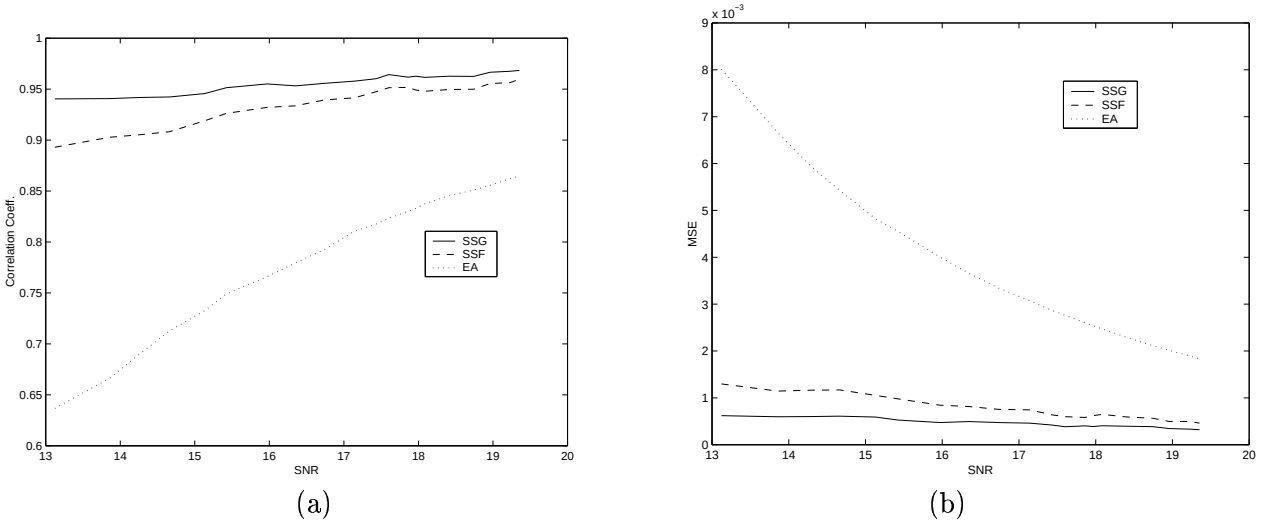

(a) (b)

Figure 2.14: Performance evaluation of the estimator on MLR-Sim signal of different SNR's. (a) Correlation coefficient Vs. input SNR. (b) MSE Vs. input SNR.

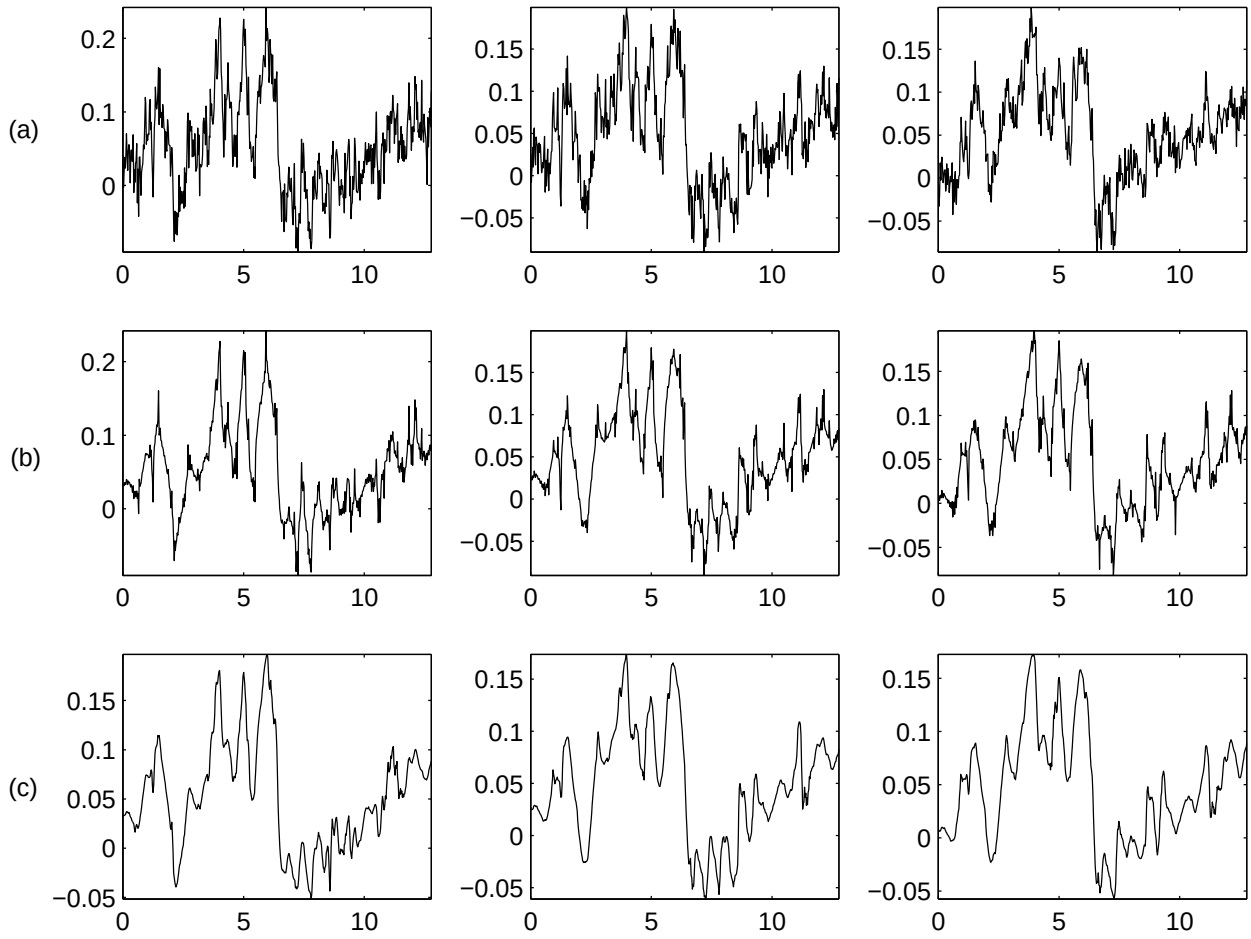

Figure 2.15: Estimation of real BSAEP signals for different ensemble lengths. Row (a): EA of 100, 200 and 300 sweeps. Row (b): Signals estimated using SS filtering. Row (c): Signals estimated using SSG filtering.

2.7.2 Real data

We tested the technique on 4 different ensembles of BSAEP signals of four different subjects. In Fig. 2.15, ensemble averaged BSAEP signals are shown along with the processed signals for different lengths of the ensemble. It can be noticed that for any ensemble length that is considered, the filtered signal results in an improved estimate suppressing the wriggles in the component peaks, thereby facilitating accurate measurement of the diagnostically important latencies and amplitudes. It may be observed from both Figs. 2.15 and 2.16, that changes in the morphology of the EA are always reflected in the processed outputs.

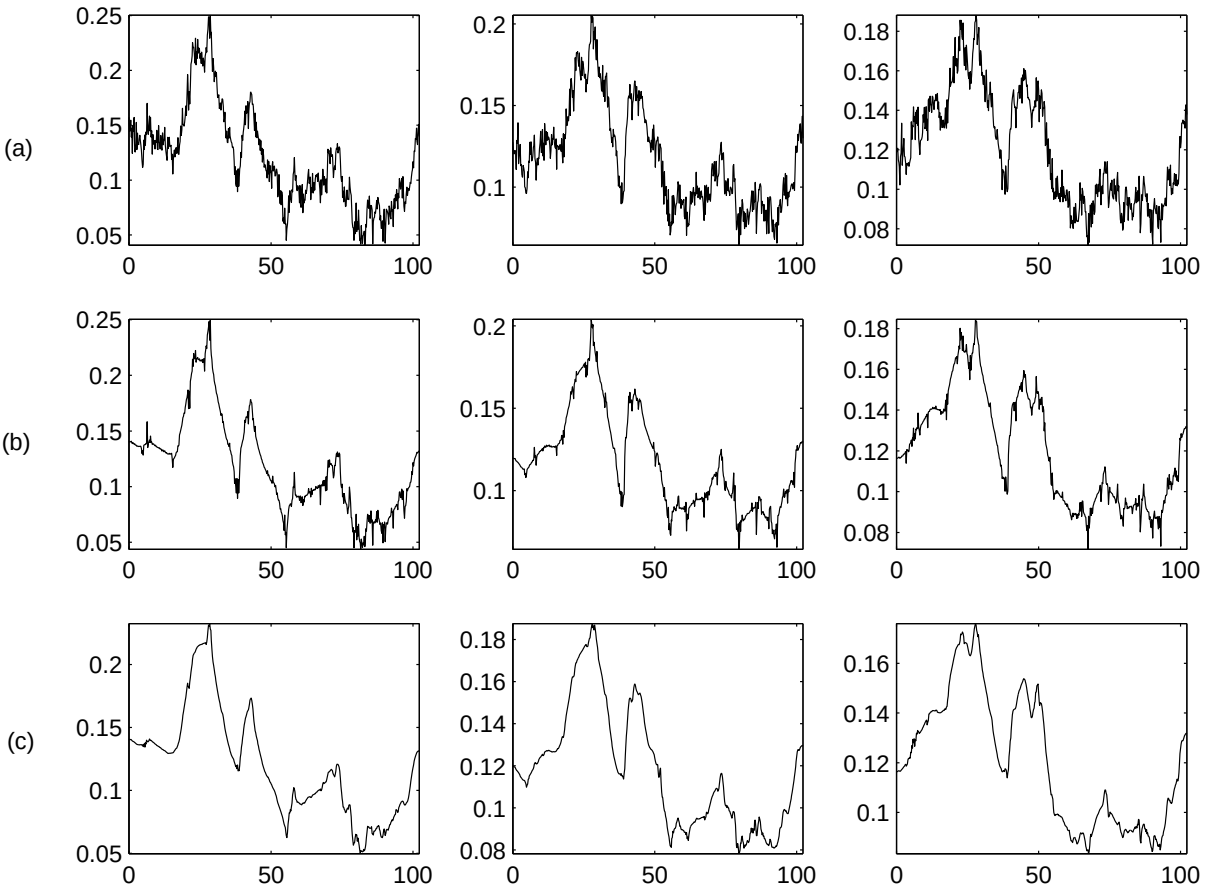

Figure 2.16: Estimation of real MLR signals for different ensemble lengths. Row (a): EA of 100, 200 and 300 sweeps, respectively. Row (b): Signals estimated using SS filtering. Row (c): Signals estimated using SSG filtering.

2.8 Discussion

The proposed spatially selective Gaussian filter has feature sensitive selectivity in passing high frequency data at low SNR. Methods based only on the magnitudes of wavelet coefficients are suitable when the noise is white; the signal information is packed into few large coefficients and the noise is distributed into smaller magnitude coefficients. Spatially selective filtering is required in cases where the noise is colored. Since SSG filter uses the statistical distribution of wavelet coefficients across the scales and also in localised regions within a scale, it better estimates signals corrupted with correlated noise. As far as the precision of the predicted latencies are concerned, binary mask performs as good as Gaussian filtering. However, our method results in a lower MSE than binary mask based SSF.

Since the wavelet transform merely involves a multistage filtering operation, it is neither computationally complex nor expensive. The inter-stimulus interval is shortest for the BSAEP, which is roughly 58 msec. Of this, 45 msec is available for computation, after the acquisition of individual sweep of 12.5 msec. Execution of our algorithm takes only 0.853 msec using a Pentium 300 MHz processor under Windows NT Operating System in MATLAB environment. With the inclusion of ensemble averaging, total computation time is around 1 msec, out of the available 58 msec. Thus the algorithm can be integrated into any existing EP system.

2.9 Conclusion

Unlike images, EP signals do not have very sharp edges. This calls for an approach different from the simple hard thresholding of wavelet coefficients at edge locations. The wavelet domain Gaussian filter is superior because of its edge and feature-sensitive selectivity in passing and scaling the wavelet coefficients. The filtering around the identified edge is smooth, thus enhancing the signal component regions, without introducing any distortions like in the case of binary masks. Temporally varying the threshold using local estimation of noise variance can account for slow transition regions better. The features with the same strength as the noise are distinguished by using the change in variance around the identified edge. By using this additional measure, false detection of sharp noisy edges is avoided. The proposed filtering algorithm is based on a non-orthogonal undecimated DWT, since the latter offers better edge detection and leads to signal that is correlated across scales. In contrast, the orthogonal wavelet

transforms have fewer coefficients at coarse scales, which prevents computation of correlation across scales. Although the proposed SSG filter does not possess any optimality property, it is simple and efficient and well suited for the case of EP's.

When the signal is corrupted by correlated noise that cannot be separated in either frequency or time domain, a signal based local filtering of the noisy signal in the transform domain is a promising solution. It improves the balance between detail preservation and noise attenuation. We have used Gaussian filtering in wavelet domain for enhancing evoked potentials corrupted by stationary correlated noise. Hard thresholding the regions, where correlation is high between adjacent scales of nonorthogonal wavelet tranform, causes artifacts and Gibbs oscillations around the boundaries of the thresholding masks. A Gaussian function at the transition region is found to be better suited for signals whose nonstationary regions are not too sharp. The proposed method can be used when the signal is non-stationary and a proper noise model is not available, and is effective as a post-processing tool in EP estimation.

Chapter 3

Spatially selective Wiener filtering in the wavelet domain

3.1 Introduction

Signal denoising approaches in the wavelet domain may broadly be classified as thresholding approaches and filtering approaches. Thresholding algorithms are based on the energy compaction property of the wavelet transform and assume noise to be white with Gaussian distribution. Due to this, small coefficients are more likely to be due to noise, while the large coefficients are due to important signal features. The essence of a threshold is that it should be large enough to eliminate noise, but small enough to keep the signal features. However, if the noise is coloured, then the noise coefficients could to be larger than signal coefficients in some bands, and it may not be possible to accomplish both of the above goals with just one threshold.

In filtering approaches, the fundamental philosophy is to consider the set of wavelet coefficients as a stationary random process and use statistical estimation techniques for denoising the signal. These schemes tend to manipulate individual wavelet coefficients in order to denoise the observed signals. Wiener filtering has been the most popular among the filtering approaches in the wavelet domain. However, the drawback of Wiener filter is that while it suppresses the high frequency noise, it also removes the high frequency components that represent the signal edge features.

We combine both the thresholding and the filtering approaches using a feature sensitive selectivity in the wavelet domain that can effectively filter noisy data. In this chapter, we

propose a spatially selective Wiener (SSW) filtering scheme that uses inter-scale correlation in the wavelet domain to identify signal and noise regions and use their strengths to compute the Wiener filter transfer function. This computed function is used in a spatially selective fashion to filter the noisy signal. We first present an overview of the various denoising approaches in the wavelet domain and then explain in detail the proposed method. We then provide the results obtained for both simulated and real signals.

3.2 Overview of wavelet domain estimation methods

3.2.1 Thresholding methods

The ability of wavelets to pack most of the signal energy in relatively few large coefficients makes wavelet based processing particularly attractive for signal denoising and estimation. Wavelet thresholding procedures exploit this energy compaction property for effective signal denoising, and are optimal in a minimax mean-square-error (MSE) sense for a variety of signal classes [25]. The thresholding schemes generally assume identically and independently distributed white Gaussian noise with unit variance corrupting the signal of interest.

In the most basic form of *wavelet thresholding* for denoising, if the coefficient is smaller than the threshold, it is set to zero; otherwise, it is kept or modified. The process of thresholding wavelet coefficients can be divided into two steps. The first step is the choice of the nature of the thresholding scheme. Two standard choices are: **hard** and **soft** thresholds [24]. The second step is the choice of the threshold, λ. Hard-thresholding zeroes every coefficient that falls below a defined threshold, while in soft-thresholding, a smooth and continuous non-linear function is applied to the transform coefficients. The most straightforward approach is to additionally shrink all the surviving coefficients by the value of the threshold. The thresholding function is given by:

- "Hard thresholding:"

$$T_{\lambda}^{HARD}(d_{j,k}) = d_{j,k}, [|d_{j,k}| \geq \lambda] +$$

- "Soft thresholding:"

$$T_{\lambda}^{SOFT}(d_{j,k}) = sgn(d_{j,k})(|d_{j,k}| - \lambda) +$$

A variety of methods have been proposed for the estimation of λ [34]. The earliest method proposed by Donoho and Johnstone [24] is a universal threshold, which is a function of the noise variance and the length of decomposition. It is defined as,

$$\lambda = \sigma\sqrt{2log(n)}, \qquad where, \sigma = MAD/0.6745,$$

MAD is the median absolute deviation of the coefficients of the finest scale and n is the number of data samples. The factor 0.6745 is chosen after a calibration with Gaussian distribution. Often, the initial noise variance is estimated from the wavelet coefficients at the finest transform level, and a normalization by the MAD is applied. This method assumes the noise to be white with Gaussian distribution and the underlying signal of interest to be sufficiently smooth such that only noise is present at high frequencies. A level dependent thresholding of wavelet coefficients is more appropriate for correlated noise. Threshold selection is determined by the manner in which the denoising procedure is optimized: in a mean squared error, minimax, or visually appealing (Visu-shrink) [24] sense. The success of these methods depends entirely on the noise variance used to fix the threshold. The noise variance is estimated in the wavelet domain.

Bayesian approaches to thresholding were recently explored by Chipman [15], Abramovich [1], Clyde [17] and Johnstone [42]. Bayesian shrinkage does a heavy shrinking of small arguments instead of thresholding. It does not separate the signal and noise sharply into two parts, but obtains the best signal and noise estimates based on a particular prior distribution structure of the space of wavelet coefficients. A prior distribution is imposed on the wavelet coefficients of the unknown function. A relation between the parameters of the prior model and those of the spaces within which realizations from the prior will fall, is established. This relation makes it possible to incorporate knowledge about the function's regularity properties into the prior model of its wavelet coefficients. Gaussian mixture model for the wavelet coefficients is a popular prior model in which each coefficient is assumed to arise from a mixture of two Gaussian distributions. The prior parameters are determined *a posteriori*.

3.2.2 Filtering methods in wavelet domain

Empirically designed wavelet-domain filters have a performance superior to those of other denoising algorithms using wavelet thresholding. The two important filtering approaches that are widely investigated in wavelet domain are Wiener filtering and spatially selective filtering, both of which exploit the statistics of the wavelet coefficients. Spatially selective filtering methods

use either the propagation of wavelet domain modulus maxima of a signal across scales [52] or analyze the correlation across scales [27, 72] to identify signal and noise edges. The filtering approaches adopted after characterizing the signal edges vary slightly in different methods. [27, 49, 56, 75].

The design of the Wiener filter requires the knowledge of the strength of signal coefficients. By using estimated values for signal strength, we obtain an approximate form of Wiener filtering in the wavelet domain which may be written as,

$$\tilde{\theta}(i,j) = \frac{\hat{\theta}(i,j)}{\hat{\theta}(i,j) + \sigma(i)^2} y(i,j) \tag{3.1}$$

where $\hat{\theta}(i,j)$ is the estimated energy density of the signal component at resolution level i and time j, $\sigma(i)^2$ is the variance of $\mathbf{z}$ in scale i. Filtering by (3.1) preserves time-frequency regions where the signal power is stronger than that of the noise, and attenuates regions where the noise predominates. Mallat [52] has used a signal estimate obtained by hard thresholding in the wavelet domain as a signal model to design a Wiener filter. This approach depends on the statistics of the wavelet coefficients. In [64], statistical properties of the wavelet coefficients are analyzed to design a block Wiener filter for denoising images.

Ghael et al. [33] have proposed empirical Wiener filtering of wavelet coefficients for denoising based on two wavelet bases. In their *Wienerchop* algorithm, the signal is initially estimated using a hard threshold in one transform domain and this estimate is subsequently used to design the Wiener filter to be applied in another transform domain. Large coefficients representing important signal features are estimated via wavelet thresholding. The thresholded signal is then transformed into a new basis. This is required to implicitly provide an estimate of the smaller coefficients via the smearing produced by the mismatch between the two bases. An analysis of this filter is given by Choi et al. [16]. Although the analysis shows that this results in an improvement in estimation error when compared to an estimate obtained by simple hard thresholding, the difficulty is in the choice of the pair of wavelet bases used. *Wienerchop* technique has been extended by Gallaire [30] by generating the second basis function via a unitary transform to a class of multiple bases. A similar idea is pursued by Ishwar et al. [40].

As pointed out in [30], the most critical part in designing Wiener filter in wavelet domain is the estimation of smaller signal coefficients. Our goal is to design an empirical Wiener filter in which the signal model is obtained using the correlation between adjacent scales, instead of using the magnitudes of individual coefficients. By taking into account the

statistical distribution of the wavelet coefficients, an improved signal model is achieved which leads to better filter performance. The design of the filter is explained in the following section.

3.3 Spatially selective Wiener filtering

The original optimal Wiener filter transfer function in frequency domain was modified by Walter [69] by using estimated power spectral densities from *a posteriori* data in computing the filter tranfer function. In this case, a suboptimal Wiener filter transfer function in the frequency domain is formulated as,

$$H(\omega) = \frac{P_s(\omega)}{P_s(\omega) + P_v(\omega)} \tag{3.2}$$

where $P_s(\omega)$ and $P_v(\omega)$ are the estimated power spectra of the signal and the noise, respectively. As originally proposed by Walter [69] and Doyle [26], this filter is estimated *a posteriori* from an ensemble of R single responses, by

$$H(\omega) = \frac{R}{R-1}\left(1 - \frac{1}{R}\right)\frac{\bar{P}_x(\omega)}{P_{\bar{x}}(\omega)} \tag{3.3}$$

where $P_{\bar{x}}(\omega)$ and $\bar{P}_x(\omega)$ and are the power spectrum of the average of individual responses embedded in noise and the average of the power spectra of the individual sweeps, respectively. This *a posteriori* Wiener filter is a zero phase-shift digital filter. To take into account the non-stationary nature of the individual evoked responses, de Weerd and Kap [22] proposed a time-varying filter derived from the above approach. The filter applies time-varying attenuation functions to the outputs of the bank of filters, which are then summed to form the filtered EP. Bertrand et al. [8] have extended the DFT based time varying *a posteriori* Wiener filtering technique to the wavelet domain by weighting each wavelet coefficient to get the time-frequency Wiener filtered average response.

The design of the Wiener filter in the wavelet domain requires the knowledge of noise-free signal coefficients which necessitates a data adaptive or empirical approach that infers the filter directly from the noisy observations. The challenging part is the estimation of smaller signal coefficients. A spatially selective filtering strategy is needed because a uniform threshold may not be good enough if the noise is correlated. If we can use additional information, extracted from the noisy observations, to distinguish between the signal and noise coefficients, then spatially adaptive thresholds can be used to reap the benefits of keeping the important signal features

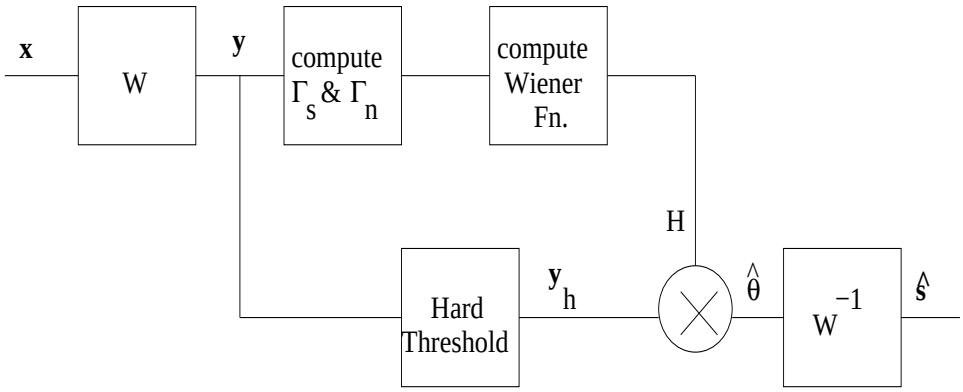

Figure 3.1: Block diagram of the spatially selective Wiener filtering in the wavelet domain.

while removing most of the noise. The proposed method adapts the thresholds of the individual coefficients to the spatially changing statistics of the EP signals.

In our earlier work [35], we used a Wiener filter formulation in the wavelet domain. In that work, the signal scalogram is obtained from the ensemble average of a subset of observations; the noise scalogram is obtained by alternate averaging the observations, which process minimises the signal contribution. This is an adaptation to the wavelet domain, of the work carried out by de Weerd [22]. We now approach the signal estimation problem from the perspective of spatially adapting the Wiener filter in the wavelet domain. For the Wiener filter formulation, we use the signal model obtained by exploiting the correlation properties in the wavelet domain. The inter-scale correlation is used as an index to group the wavelet coefficients in each scale into signal and noise coefficients. The powers of signal and noise in each of these groups in each scale are used in (3.1) to compute a real, scale-dependent Wiener transfer function, in addition to discarding the noise dominant coefficients. The block diagram of the proposed scheme is presented in Fig. 3.1. The procedure is simple and easy to implement:

- *step 1:* Transform the data into the wavelet domain via the DWT: $\mathbf{y} = \mathbf{W}.\mathbf{x}$
- *step 2:* At each resolution level j, group the empirical wavelet coefficients into disjoint blocks $\{S^j = w(i,j), |w(i,j)| > corr_2(i,j)\}$ and $\{V^j = w(i,j), |w(i,j)| < corr_2(i,j)\}$.
- *step 3:* Compute the signal power from $\{S^j\}$ and the noise power from $\{V^j\}$ to be used in the transfer function in (3.2).
- *step 4:* Hard threshold the scale coeffcients obtained in *step 2* to eliminate the noise dominant coefficients and retain significant coefficients.

- *step 5:* Use the computed scale-dependent weighting factor in the significant signal regions to attenuate the noise.

It is observed that such a two level filtering results in an improved response. The algorithm is simpler than the one proposed in [30], which is based on multiple orthogonal bases. We present the results obtained using the proposed SSW filter in the next section.

3.4 Experimental Results

The proposed algorithm has been tested on both synthesised and real BSAEP signals and middle latency responses. Experimental results show that this spatially varying wavelet thresholding yields significantly superior estimation of the signal.

3.4.1 Results for simulated data

The BSAEP-Sim signal estimated using the proposed technique for different input SNRs is illustrated in Fig. 3.2. The SNR's of the input noisy signals shown in the first row of Fig. 3.2 are 1.75 dB, 3.0 dB and 5.0 dB, respectively. The corresponding signals, estimated using SS-W filter, are shown in the second row. The third row displays the original signal for comparison. The significant components of the BSAEP are clearly visible in the estimated output, and facilitate measurement even at a low input SNR of 1.75 dB, although it shows a small amount of residual noise. The residual noise in the estimated signal reduces with increase in the SNR of the input. Figure 3.3 compares the results obtained by our technique on BSAEP-Sim signal simulated at a SNR of 3 dB to the results achieved by simple hard thresholding. Fig. 3.3(a) presents the noisy input signal; the corresponding signals estimated using hard thresholding and the SS-W filter are shown in Figs. 3.3 (b) and (c), respectively. The output of the hard threshold estimator has a large amount of impulse noise and spurious fluctuations at the boundaries of the thresholding masks. This phenomenon is observed for input SNRs less than 3 dB. However, this noise is not present in the signals estimated using our technique.

The performance of the two estimators is also studied in terms of the MSE of the estimated output for different input SNRs. The results of comparison are presented in Fig. 3.4, along with the MSE of the simple ensemble average. At any instant, the input to the SS-W filter is the ensemble average up to the current sweep, which may also be termed as current ensemble

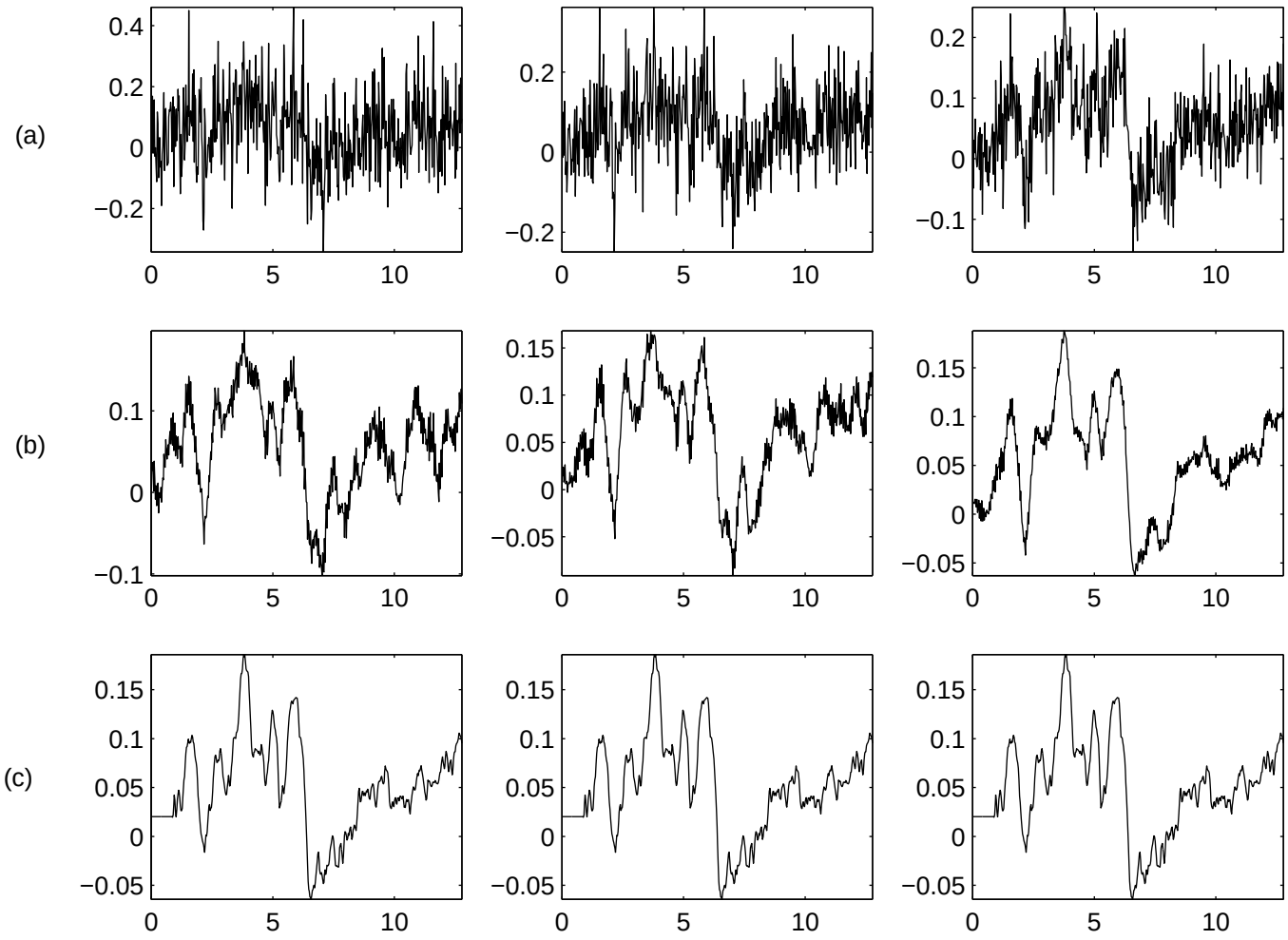

Figure 3.2: Signals estimated from BSAEP-Sim at different SNR's. Row (a): BSAEP-Sim signal with input SNRs of 1.75 dB, 3.0 dB and 5.0 dB, respectively. Row (b): Signals estimated using SS-W filtering. Row (c): Original signal.

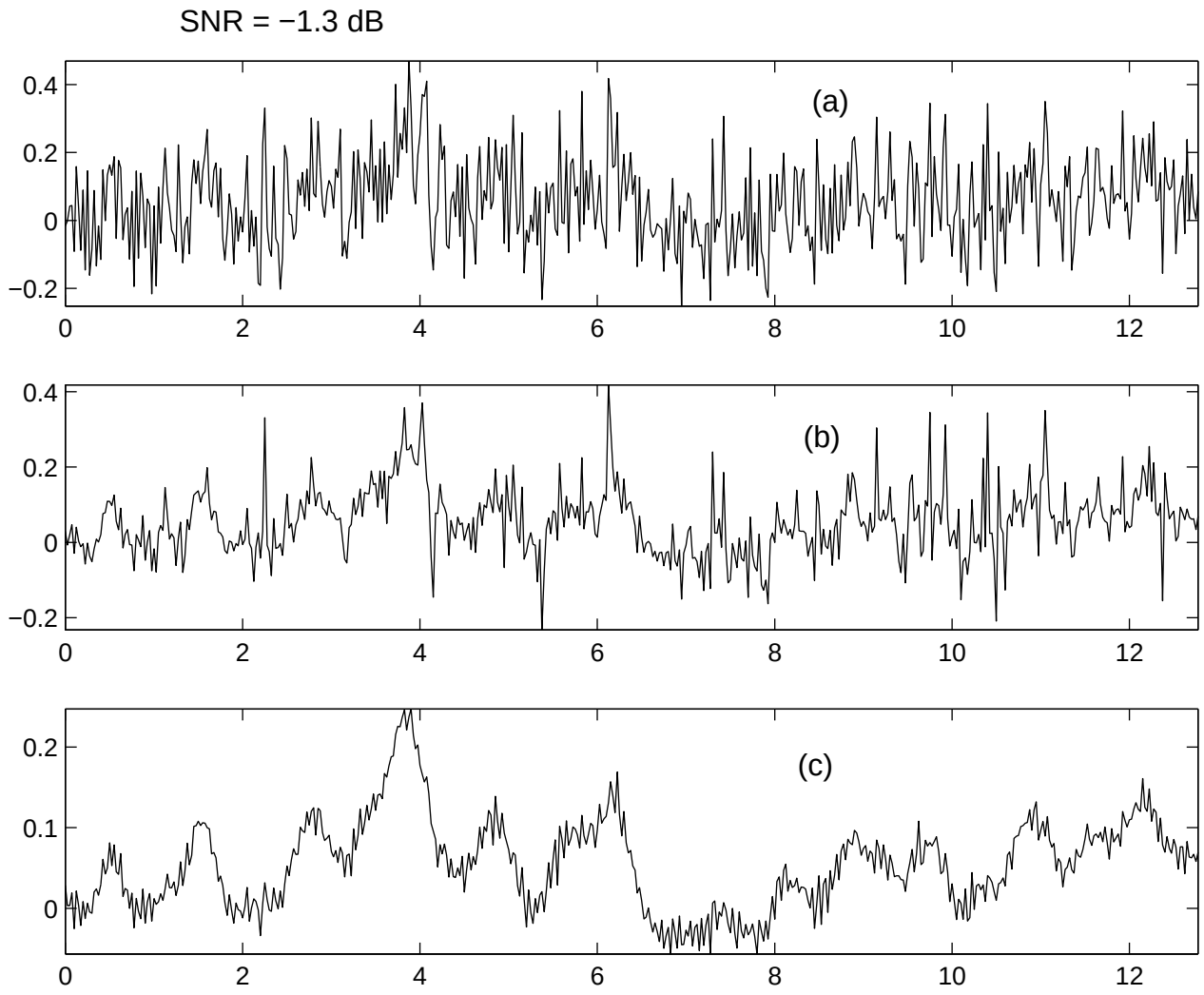

Figure 3.3: Comparison of signals estimated from simulated BSAEP using two different techniques. (a) Ensemble averaged BSAEP-Sim signal at a SNR of 3 dB. (b) Output of hard thresholding. (c) Output of SS-W.

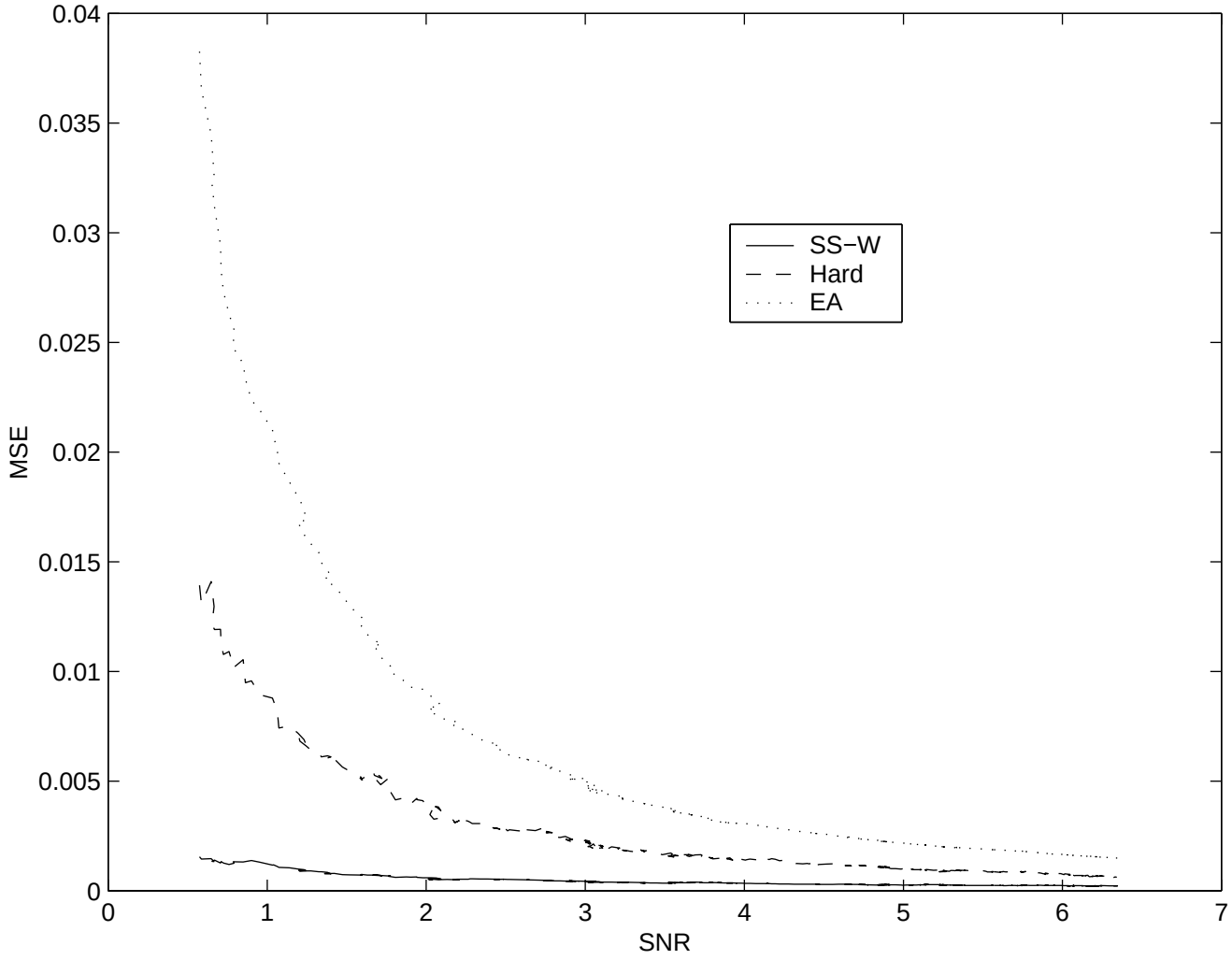

Figure 3.4: MSE of the estimated output for different input SNRs. Solid line: SSW filter. Dashed line: Hard thresholding. Dotted line: EA. Input: BSAEPSim.

average (CEA). The SNR for the CEA increases with larger ensemble length. In Fig. 3.4, the x-axis shows the different input SNR's studied and the y-axis shows the corresponding MSE obtained. It can be seen that for any given CEA or SNR, the MSE of the signal estimated using SS-W is smaller than that obtained using the hard threshold estimator. The comparison of the three techniques in terms of correlation coefficient is shown in Fig. 3.5. This comparison too reveals superior performance of the SS-W filter method compared to both hard thresholding and simple EA.

Similar study is carried out for the simulated MLR signals too. MLR-Sim signals estimated using the proposed technique for different input SNR's are shown in Fig. 3.6. The first row shows the input signal at SNRs of 2.5 dB, 4 dB and 6 dB, respectively. The corresponding estimated signals are shown in the second row and the original signal is shown in the third row for comparison. At low SNRs also, the signal estimated using SS-W filter shows distinct component peaks. The performance of the estimator is compared to that of the hard threshold estimator in Fig. 3.7 for an input SNR of 5 dB. The impulse noise in the signal estimated using hard threshold is due to the rectangular thresholding (windowing) performed in this case. Although the signal estimated using SS-W filter has some residual noise, measurements can still be made from it. Comparison with the hard threshold estimator and ensemble averaging is carried out using the performance metrics of correlation coefficient and MSE. The correlation coefficients of the outputs obtained for diferent input SNRs are presented in Fig. 3.8 for all the three estimators. Figure 3.9 presents the MSE of the estimators for different input SNRs. Both the figures show a superior performance of the proposed SS-W filter compared to the other two estimators.

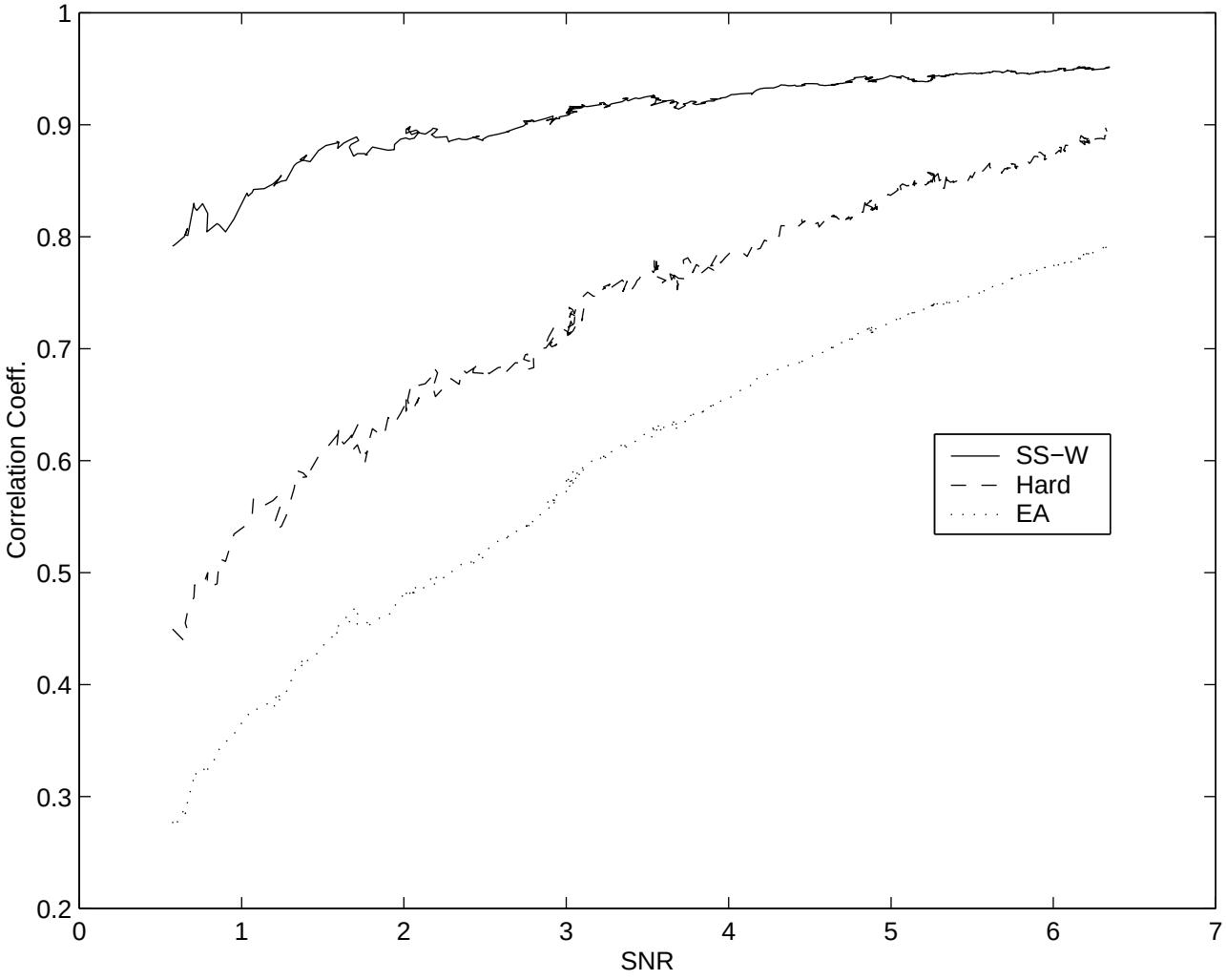

Figure 3.5: Correlation Coefficient of the estimated output with the original signal - for different input SNR's. Signal Studied: BSAEPSim. Solid line: SSW filter. Dashed line: Hard thresholding. Dotted line: EA.

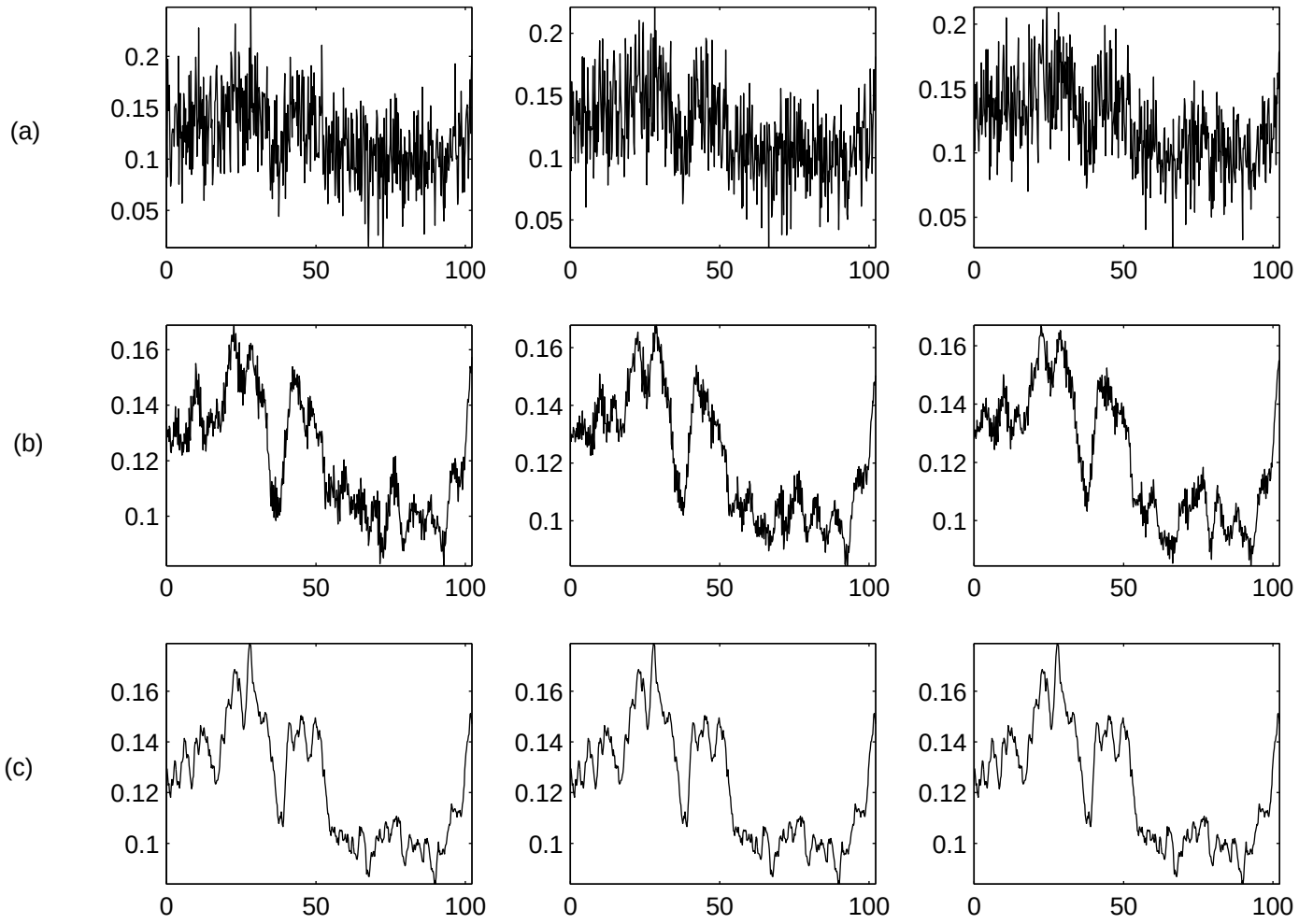

Figure 3.6: Signals estimated from MLR-Sim for different input SNR's. Row (a): Noisy observations at SNRs 2.5 dB, 4 dB, and 6 dB, respectively. Row (b): Signals estimated using SS-W filter. (c) Original EP signal for comparison.

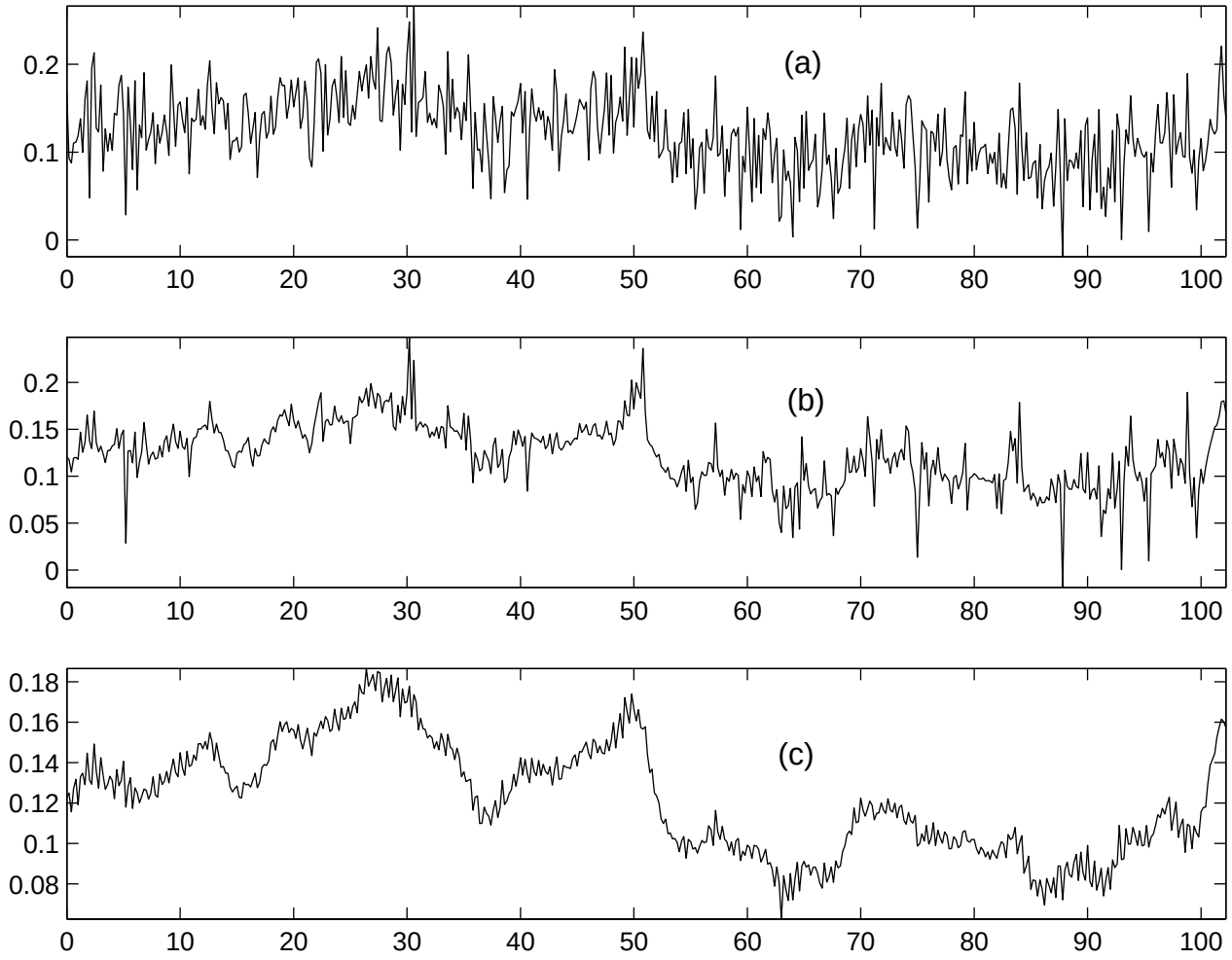

Figure 3.7: Comparison of signals estimated from simulated MLR using two different techniques. (a) MLR-Sim simulated with a SNR of 5 dB. (b) Output of hard threshold estimator. (c) Signal estimated using SS-W filter.

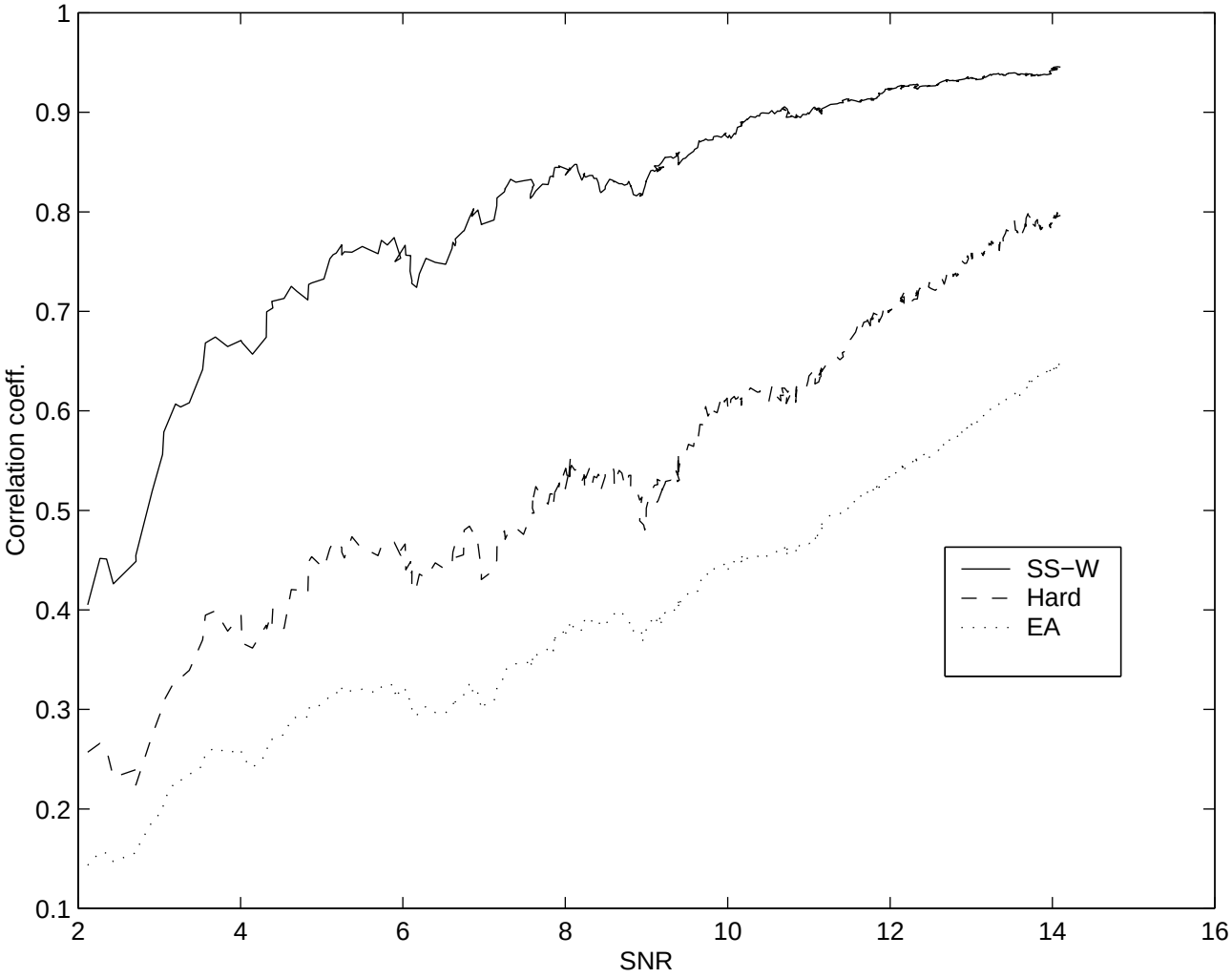

Figure 3.8: Correlation Coefficients of the estimated outputs with the original signal - for different input SNR's. Signal Input: MLR-Sim. Solid line: SSW filter. Dashed line: Hard thresholding. Dotted line: EA.

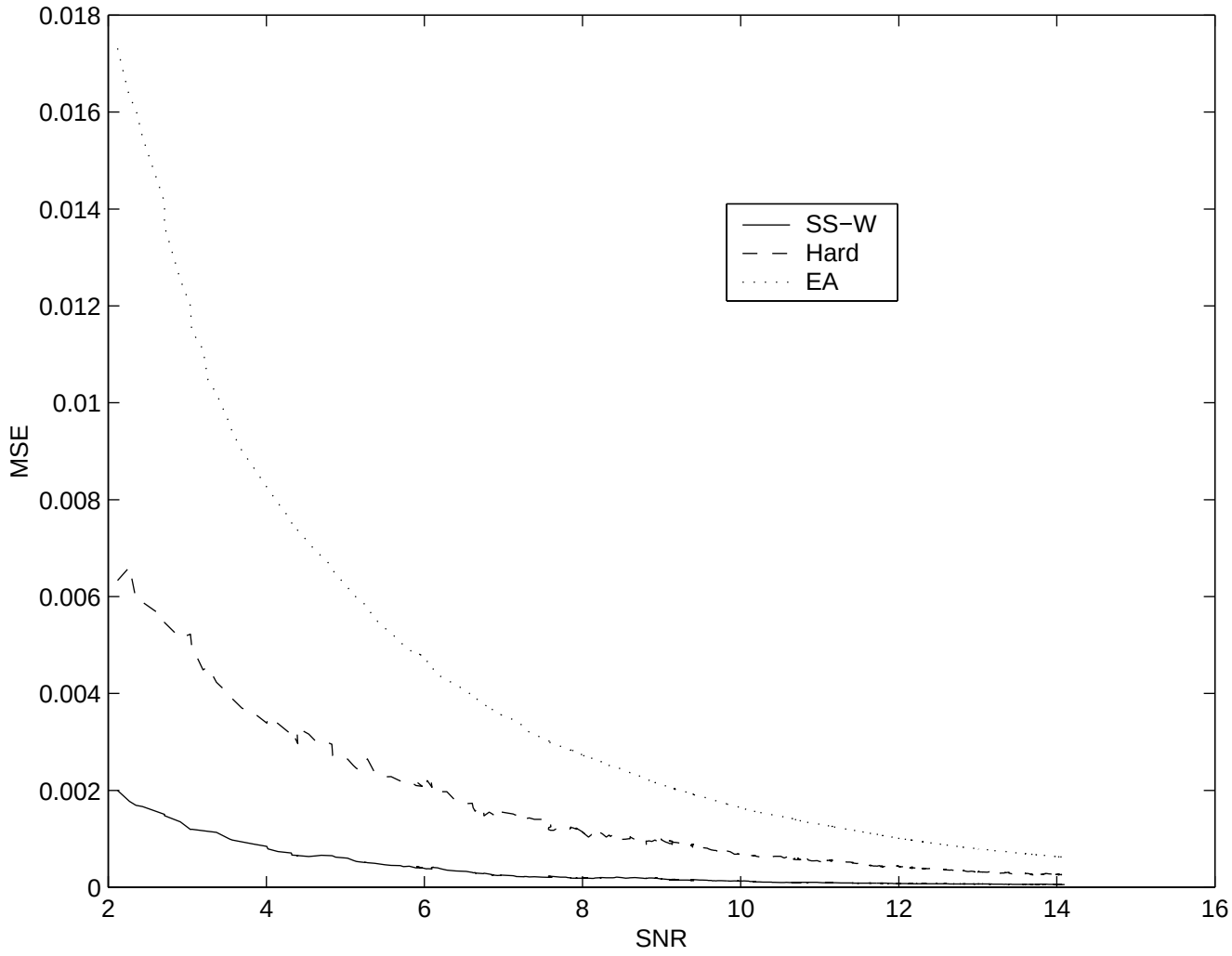

Figure 3.9: MSE of the estimated outputs for inputs of different SNR's. Input: MLR-Sim. Solid line: SSW filter. Dashed line: Hard thresholding. Dotted line: EA.

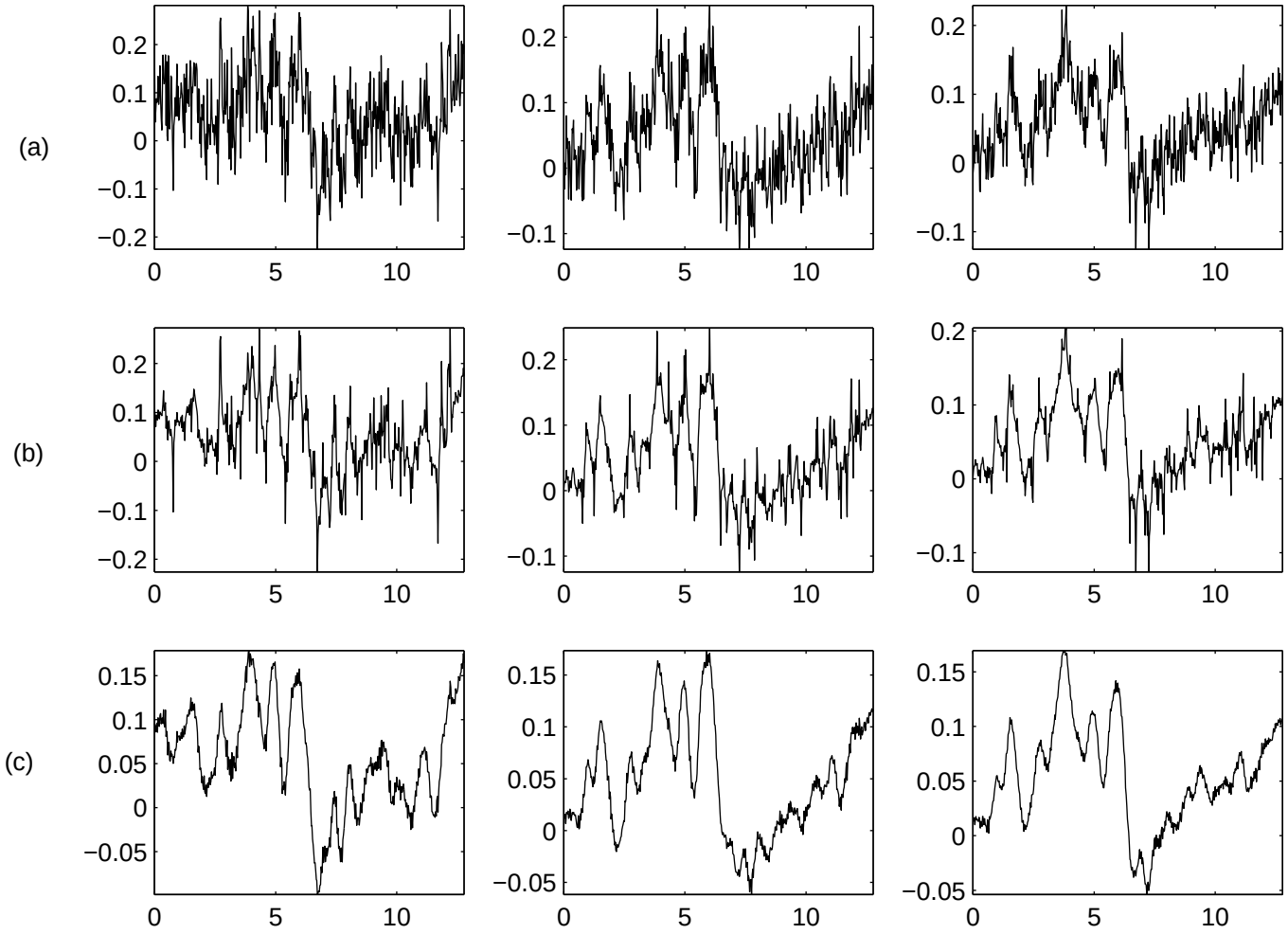

Figure 3.10: Real BSAEP signals estimated using SS-W and hard threshold estimators for ensembles of different lengths. Column (a): EA of 200, 300 and 400 sweeps, respectively. Column (b): Signals estimated using hard thresholding. (c) Signals estimated using SS-W filter.

3.4.2 Results for real data

The proposed technique has been tested on a set of real brainstem AEP and middle latency responses. The results obtained are presented in Fig. 3.10, along with those of hard thresholding. Good and well defined components have been estimated from the noisy observations with the proposed technique. As seen from the figure, the SS-W is clearly superior in estimating the signal. Similar results for real MLR data are presented in Fig. 3.11.

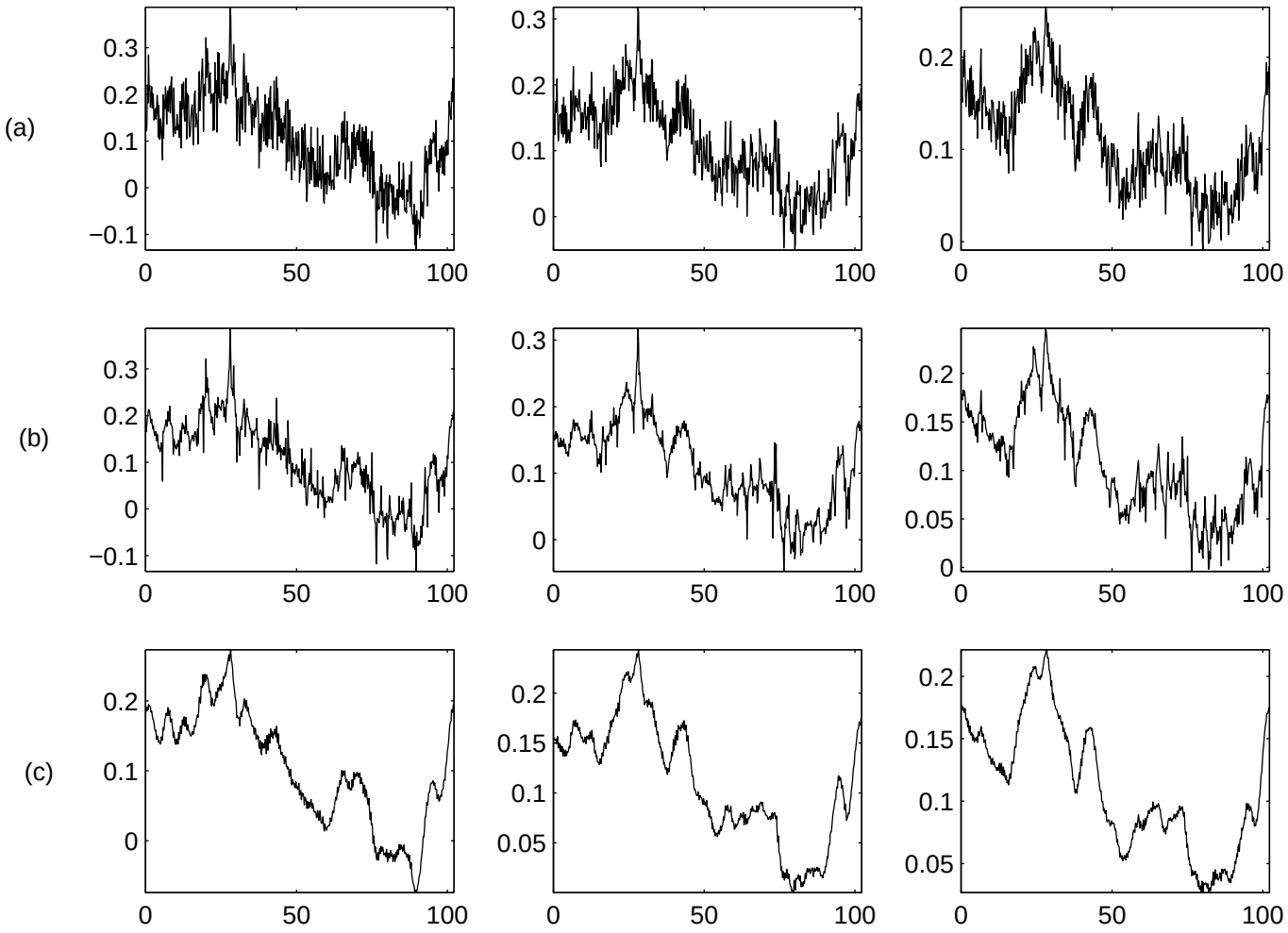

Figure 3.11: Comparison of real MLR signals estimated using SS-W filter and hard threshold estimators for ensembles of different lengths. Row (a): EA of 200, 300 and 400 sweeps. Row (b): Signals estimated using hard thresholding. Row (c): Signals estimated using SS-W filter.

3.5 Discussion

Thresholding in a shift-invariant or translation-invariant (TI) expansion eliminates some of the unpleasant artifacts introduced by modifying the coefficients of the orthogonal wavelet expansion. Hence denoising in a shift-invariant, redundant representation outperforms that by the orthogonal basis [46]. The wavelet transform based Wiener filter as described above improves the EP data from repeated trials. A substantial reduction in noise has been observed. This reduction is expected to improve subsequent quantitative analysis for extracting characteristics such as amplitude, width and onset time of individual responses. Spatially selective Wiener filtering is found to be giving better results both visually and in terms of mean square error in comparison with hard thresholding.

Fig. 3.10 clearly illustrates the effectiveness of the proposed technique. For example, the first column shows that the filtering scheme is able to recover all the signal maxima and minima even from a highly noisy average of an ensemble of just 200 sweeps. Compared to the normal case of a BSAEP which requires a minimum of 2000 sweeps, this is a reduction by a factor of 10. Further, as seen from Fig. 3.3, hard thresholding introduces unwanted sharp spikes in the resultant waveform, because of which the principal peaks and valleys of the response are not always unambiguously identified. This is because of the phenomenon akin to the Gibbs oscillations. Hard thresholding is equivalent to applying a rectangular window in the wavelet domain, which entails the oscillations seen in the signal (time) domain. On the other hand, the proposed spatially selective Wiener filter results in smooth, clear peaks and valleys, from which measurements can be made easily. For the same input SNR, the MSE of the SSW estimate is always less than that obtained with hard thresholing by a factor of at least 5. This is a significant improvement in performance. In fact, as seen from Fig. 3.4, at low input SNR's of the order of 0.5 dB, SS-W filter gives rise to a very low MSE, which is comparable to that given by the hard threshold estimator at SNR's of around 4 dB. Results shown in Figs. 3.10 and 3.11 confirm that the technique produces equally valid results for real data too.

3.6 Conclusion

In this chapter, we have proposed a two level filtering method for estimating AEP signals. A Wiener filter is formulated exploiting the inter-scale correlation in the wavelet domain. The

wavelet transform data at a given scale is compared to its correlation with the data at larger scales. Signal features are identified and retained because they are strongly correlated across scales in the wavelet domain; noise is removed since it is poorly correlated across scales. The signal features remain relatively undistorted because they are very well localized in space in the wavelet domain. The spurious fluctuations normally caused near the end points of the thresholding window in the hard thresholding scheme, and the smearing of the high frequency data due to Wiener filtering are both nullified by using a combination of the two approaches, resulting in an estimated signal far superior to that obtainable by either of them invidually.

Chapter 4

Gaussian radial basis function network for EP estimation

4.1 Introduction

In the case of evoked potentials, the exact functional relation between the noisy observation and the evoked signal is unknown due to incomplete knowledge of the signal and noise processes. Most of the efforts that have been made so far in EP estimation have used linear parametric models. They include both time domain [73] and frequency domain [22] models. Thakor et al. [68] have modeled EP as a dynamic Fourier series and the Fourier coefficients are estimated adaptively using least mean squares (LMS) algorithm. Another relatively new model-based estimation approach uses neural network filters, which possess built-in nonlinear processing elements. Neural networks are used to effectively represent nonlinear mappings and they can provide models that embody a much broader class of functions than linear models do. Recently, a Gaussian radial basis function neural network (GRBFNN) has been used by Fung et al [28] as a model for EP to account for the nonlinear nature of the signal. They assume that EP responses can be modelled by a finite number of Gaussian radial basis functions (GRBF) with their centers evenly distributed over the sweep time. Their weights are adaptively determined using LMS algorithm.

The choice of the number of basis functions in the hidden layer and their parameters is a key problem in designing a radial basis function (RBF) network. In the absence of *a priori* knowledge about the latencies of individual component peaks of the signal, a uniform parameter

radial basis function network (U-RBFN), with its centers uniformly placed over the length of signal and with equal variances, may not be able to model the signal components efficiently. Deriving the kernel parameters from the signal itself can improve both the effectiveness of the model and the tracking property of the network. Hence, we propose a method, using which the GRBF network parameters are deduced from the wavelet transform of the noisy signal to enable the network to learn the functional form of the underlying EP signal more effectively. We use the correlation in the wavelet domain for significant edge detection as explained in chapter 3, and use the latter information to determine the GRBF network. We show that this yields better results in terms of reduction in the order of the network and a more accurate signal model even in the presence of noise. The results are compared with a network, whose kernels have centers evenly distributed over the entire length of the signal and have equal spreads.

This chapter is organised as follows. A brief description is presented in section 4.2 on generalised RBF networks and a network with Gaussian kernel functions for EP estimation. The method adopted for determining the network parameters is explained in section 4.3. The results obtained for both simulated and actual data are discussed in section 4.4. This is followed by conclusions in section 4.5.

4.2 Radial basis function networks

A RBF network approximates an unknown mapping function by using a two-layer data processing structure. First, the input data undergoes a nonlinear transformation via the basis functions in the network hidden layer. Then the responses of the basis functions are linearly combined to give the network output. In particular, RBF networks have been proven to possess the 'best approximation property'; that is, they can represent a continuous function arbitrarily well. They perform the nonlinear mapping $f : \mathbf{R}^M \rightarrow \mathbf{R}$ according to the formula

$$y(\mathbf{X}) = \sum_{k=1}^{M} w_k \phi(\| \mathbf{X} - \mathbf{C}_k \|) \tag{4.1}$$

where $\mathbf{X} \in \mathbf{R}^N$ is an N-dimensional input vector, $\phi(.)$ is the given nonlinear radial basis function, also known as kernel function, $\| \ . \ \|$ denotes the Euclidean norm, $w_k, (k = 1, 2, ..., M)$ are the weights, $\mathbf{C}_k \in \mathbf{R}^N$ are the RBF centers, and M is the number of hidden units. A block schematic of the RBF network is shown in Fig. 4.1. In place of the sigmoidal functions used in multilayer perceptrons, radial basis functions are employed as the nonlinear activation functions of the

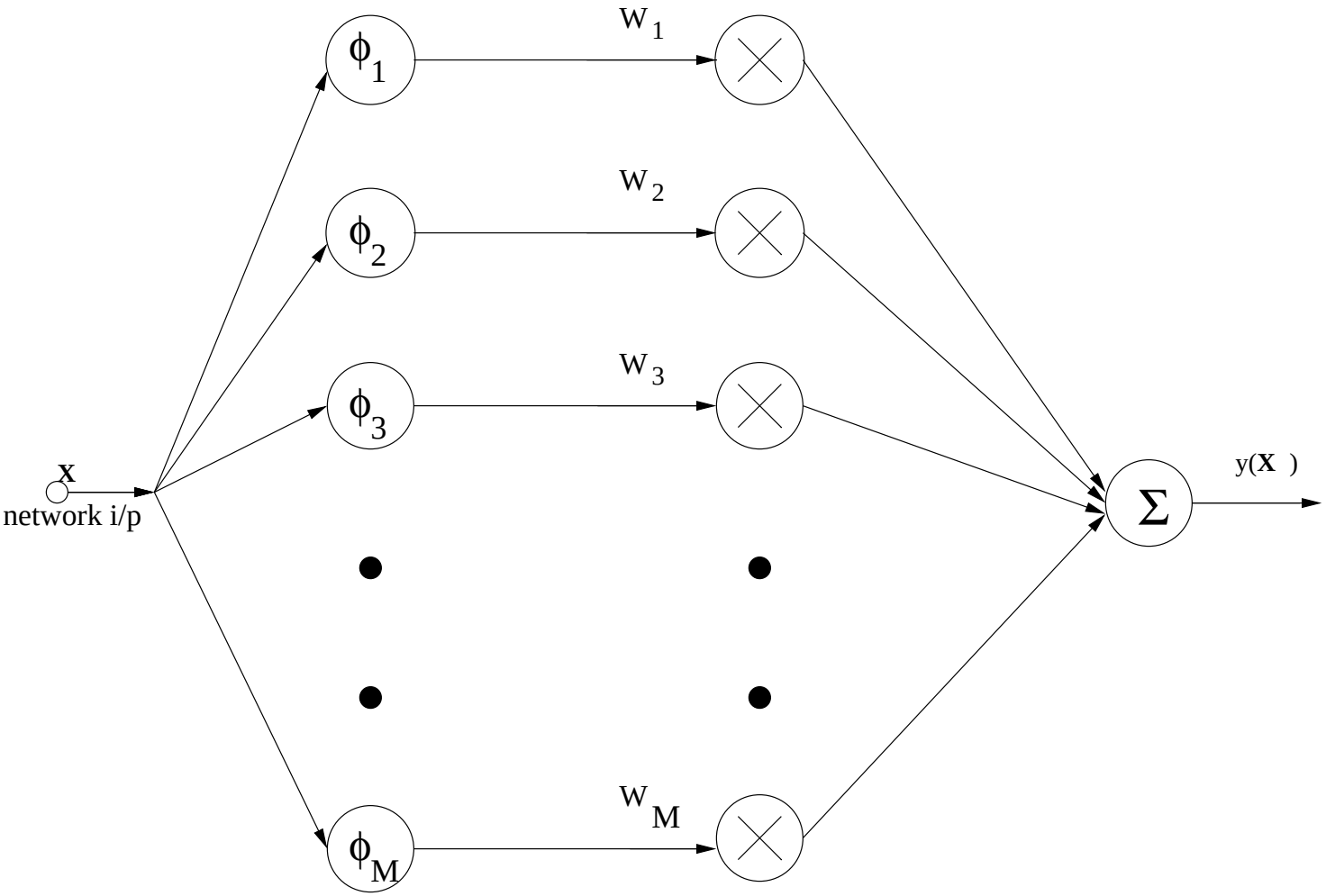
W 1
W 2
W 3
W M
x
network i/p
y(X)
Σ

hidden nodes. A radial basis function produces a localised response to an input. The response is a function of the Euclidean distance between the input and the centroid associated with the basis function. The nonlinearity within a RBF network can be chosen from a few typical nonlinear functions. A general concensus is that the choice of the nonlinearity is not crucial for the good performance of the RBF network. However, the performance critically depends on the chosen centers and their widths.

The design of the network involves the selection of the basis functions, their number, and determining their parameters to achieve the best generalization performance for a specific data processing task. The parameters to be chosen are the centers $\mathbf{C}_k$ and the radial dilation factors, usually called *widths*. This problem is most often tackled by clustering the data points and using the cluster centers as the RBF centers [43]. Genetic evolution approaches for optimizing the center locations and widths have also been attempted [70].

The task of training a RBF network can be broken into two phases: selection of basis function parameters, followed by the determination of the output layer weights. In the case of the Gaussian kernels, the parameters are the centers and the variances. The network output layer adjusts its weights as it searches for the optimum contribution of the basis functions to the network output, so that the best match to the desired response is achieved.

4.2.1 EP estimation by Gaussian radial basis function network

EP responses are modelled by a finite number of Gaussian radial basis functions. The recorded j^{th} evoked response, X_j, may be vectorially denoted as,

$$X_j = S_j + V_j \tag{4.2}$$

where $S_j = [s_j(1) \ \cdots \ s_j(N)]$ and $V_j = [v_j(1) \ \cdots \ v_j(N)]$ denote the signal and noise content in the j^{th} sweep, with the time index ranging from 1 to N. Both the signal and the noise are assumed to be stationary random processes with Gaussian distribution and uncorrelated to each other. We have chosen *Gaussian function* as the radial basis function in designing a network with M hidden nodes to approximate the underlying dynamics of S_j in (4.2). The output of the GRBFNN may be written as,

$$Y_j = \hat{S}_j = \mathbf{w}^T\mathbf{H} \tag{4.3}$$

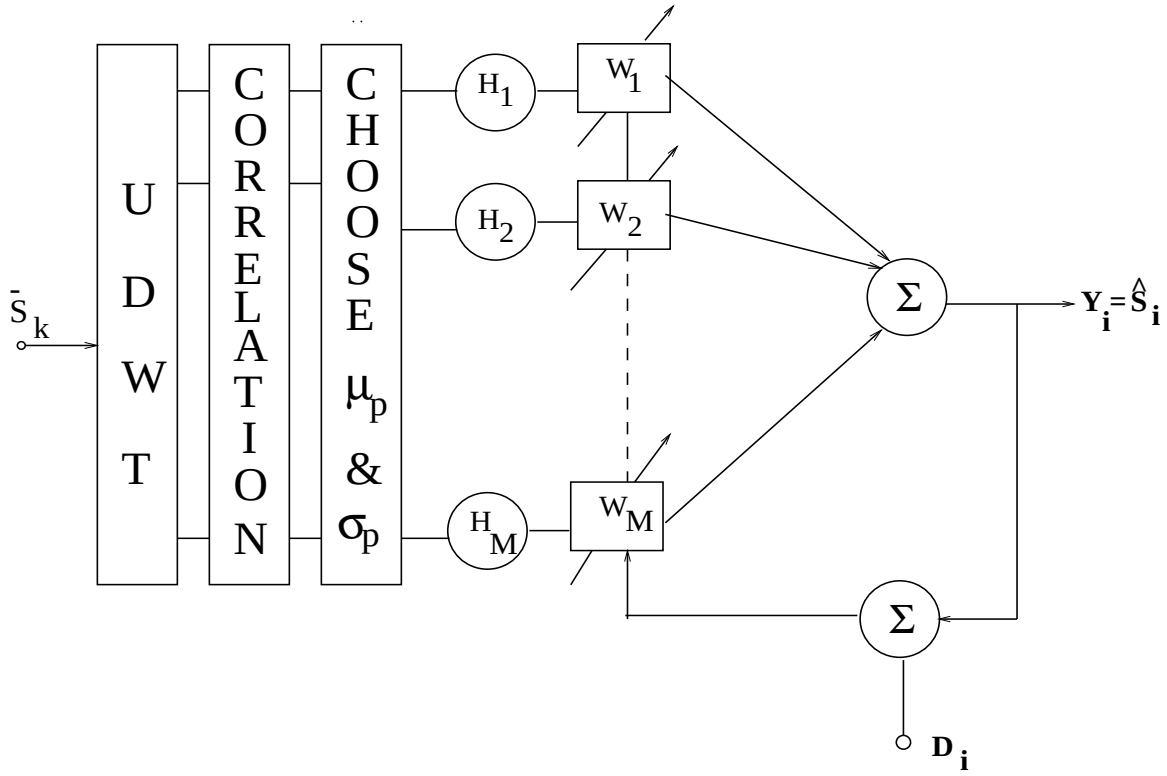

Figure 4.2: Schematic of the GRBF network for EP estimation

In the above equation, $\mathbf{H}^T = [H_1; H_2; \cdots H_M]$ is the hidden layer output matrix, and $H_p = [h_p(1)\ h_p(2)\ \cdots\ h_p(N)]$ represents the output of the p^{th} hidden node. The weights $\mathbf{w^T} = [w(1), \cdots, w(M)]$ can be determined using optimization methods such as gradient search algorithm by providing the input $\mathbf{X}_j$ and the corresponding desired output $\mathbf{Y}_j$ for few input-output measurements. A schematic of the GRBF network with M hidden nodes is shown in Fig. 4.2.

$$h_p(n) = exp\left(-\frac{(n-\mu_p)^2}{{\sigma_p}^2}\right) \tag{4.4}$$

where μ_p and σ_p are the Gaussian kernel parameters. The key problems to achieve the best performance are the placement of the centers μ_p and the determination of the variances σ_p. In the proposed method, the number of hidden nodes and the Gaussian kernel parameters are all obtained from the WT of the input signal.

4.3 Determination of the kernel parameters

In the wavelet domain, signal features are still well localized in space. Sharp transitions in the signal are preserved and depicted well. Wavelet transform modulus maxima capture the sharp

variations of a signal, and their evolution across the scales characterizes the local regulariy of the signal. By using undecimated wavelet transform, a signal edge is detected at a position where there are maxima at several adjacent scales [52]. The second order correlation between adjacent scales is used to identify the signal transition regions. A binary mask vector of length N corresponding to each scale is created in which the positions corresponding to each significant coefficient is equated to 1 (refer chapter2). For computing the correlation, we leave out the smallest scale. This is because noise dominates the smallest scale in low SNR signals and therefore, inclusion of the smallest scale for correlation based analysis of the input signal results in too many wrong edges being extracted [24]. The number of kernels used is the same as the number of edges detected in the wavelet domain. Their centers are determined as the mid-points of the regions in which the wavelet transform is highly correlated across scales. The width between two adjacent edges is taken as the variance of the kernel.

We decompose the EP signals into 4 scales using B_3- spline scaling function. A translation invariant and nonorthogonal decomposition using *à Trous* algorithm is used for the decomposition. As the technique is based on edges detected from the input signal in the wavelet domain, to obtain good results with less distortion, we summate the first l sweeps to initially improve the input SNR to a reasonable degree. This is carried out to avoid detection of noise edges which are likely to dominate at very low SNR. Subsequently, we use the current average of the sweeps as the desired signal in the GRBF network weight adaptation so that the model parameters converge faster. Fig. 4.3 shows a noisy BSAEP signal with a SNR of 1.5 dB, along with its decomposition into the 4 scales and the second order correlation vectors computed using scales 2,3 and 3,4. The binary mask obtained using the correlation vectors is also shown in the same figure. The mask indicates the most important signal edges and their widths. This technique of detecting edges in the wavelet domain is well explained in [27] and [35]. We used the number of edges detected in the space-scale domain as the number of GRBF kernels M to be used and their centers μ_p are determined as the mid points of the identified significant signal regions. The time interval between two adjacent edges is taken as the variance σ_p of the kernel.

4.4 Experimental results

The individual sweeps of AEPs have a low SNR. To obtain good results with less distortion, we summate the first 100 ensembles to initially improve the input signal SNR marginally. This

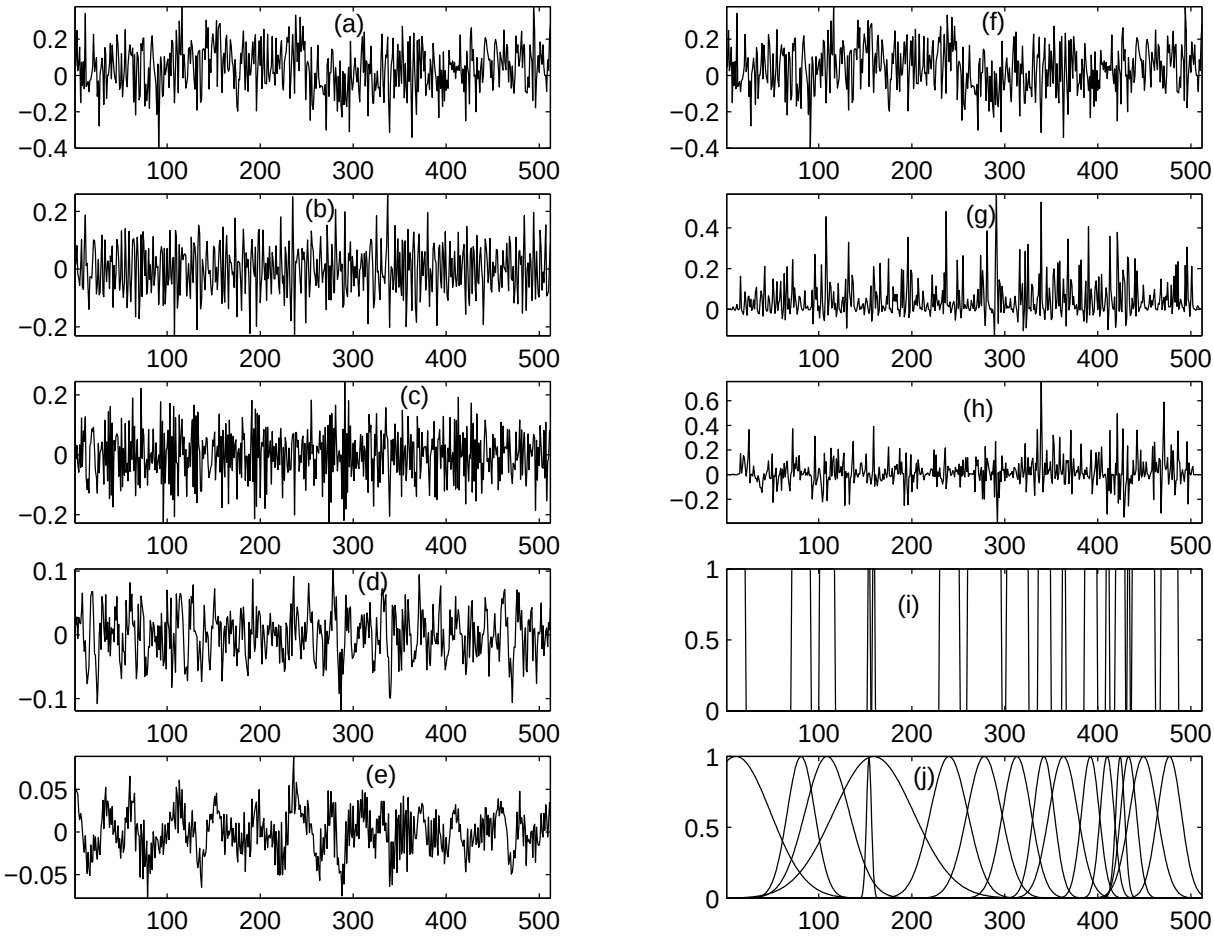

Figure 4.3: (a) and (f): Noisy BSAEP signal at SNR of 1.5 dB. (b), (c), (d), and (e): Its decomposition into scales 1, 2, 3, and 4, respectively. (g) and (h): 2nd order correlation between scales 2 - 3 and 3 - 4. (i) and (j): Binary and the corresponding Gaussian mask vectors.

is carried out to avoid detection of spurious noise edges which are likely to dominate in the wavelet domain at very low SNR. This enhanced signal with considerable remnant noise is used for wavelet decomposition and subsequent estimation of the EP signal. We use the instantaneous ensemble average upto the current sweep, called the current ensemble average (CEA), as the desired signal in the network weight adaptation. With every additional sweep, the SNR of the CEA improves as we assume a stationary EP signal across an ensemble of observations. Results obtained with the proposed technique (W-RBFN) are compared with those of the U-RBFN estimator. The comparison is carried out in quantitative terms using the correlation coefficient and the MSE of the estimated outputs, and also in terms of the measured latencies of the components, for different SNRs of the input signal. Results demonstrate the superiority of determination of network parameters based on signal knowledge rather than using uniformly spaced Gaussian kernels of fixed variance.

4.4.1 Results for simulated data

Figure 4.4 illustrates an EA of 100 BSAEP sweeps and the signal estimated from it using the proposed technique. Significant regions detected in the wavelet domain using the magnitude of inter-scale spatial correlation are shown as a binary vector in Fig. 4.4(b). In the wavelet domain, the number of significant regions detected is 22 and hence those many hidden nodes are used in the GRBF network. The corresponding Gaussian kernels used in the time domain are shown in Fig. 4.4 (c). The solid signal shown in Fig. 4.4(d) is the signal estimated using W-RBFN and the dotted line shows the signal estimated using U-RBFN. It can be seen from Fig. 4.4 that the component latencies are well preserved in the W-RBFN method whereas the U-RBFN method fails to estimate some of the significant components. A comparison of the latencies of the important components estimated by both the methods is presented in Table I, along with the true values. As mentioned in chapter 1, in BSAEP signals, wave III and V are the most important ones from the clinical angle. The failure of the U-RBFN in estimating some of the components may lead to misleading diagnosis. In comparison, the signal estimated using W-RBFN agrees closely with the original signal used in the simulation of BSAEP-Sim.

In Fig. 4.5, we present the signals estimated from the noisy CEA of different number of sweeps. In this figure, the first row shows the noisy CEA for different ensemble lengths. Second row shows the outputs of the U-RBFN estimator. The outputs of the W-RBFN estimator are

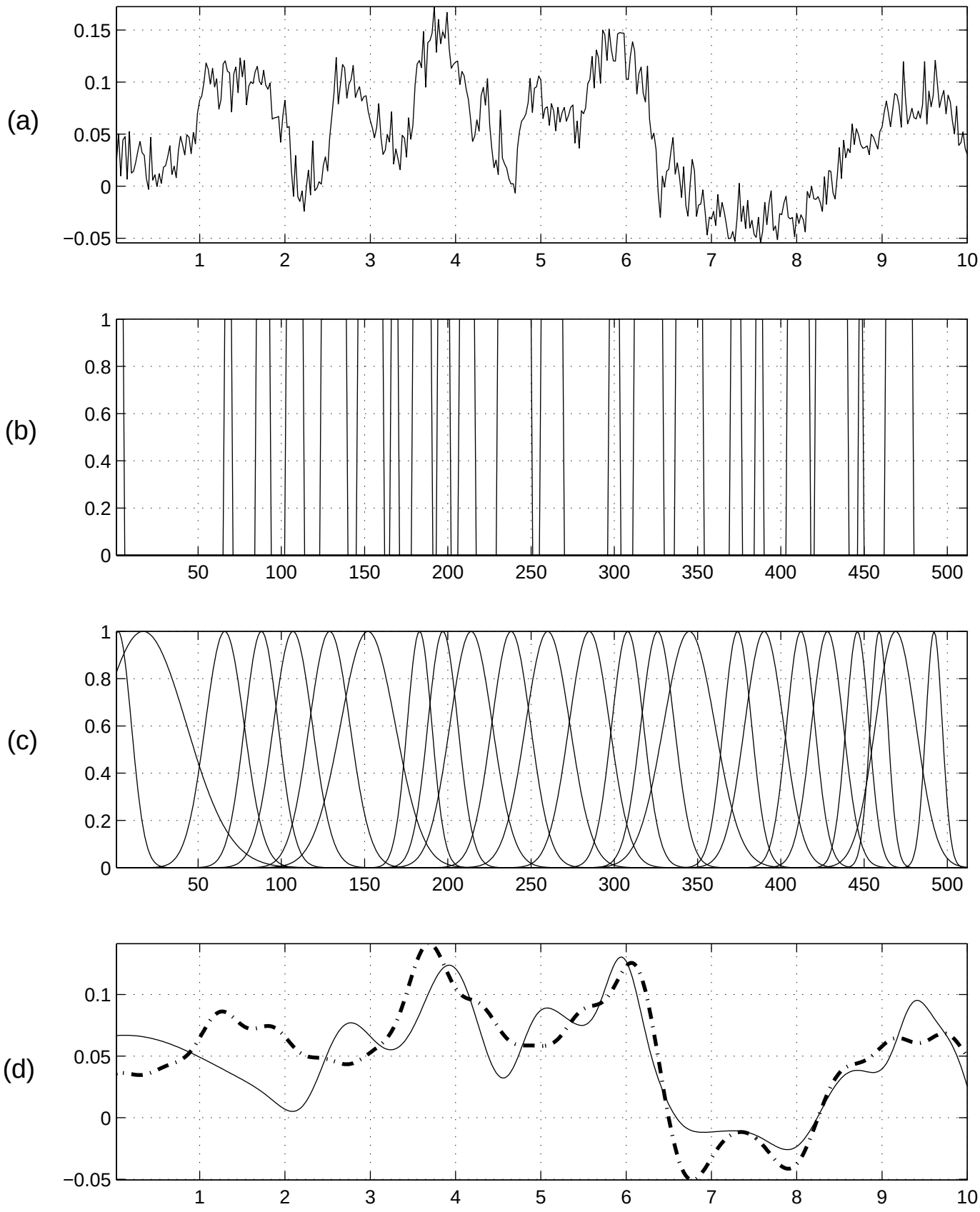

Figure 4.4: Signal estimation using GRBF network. (a) Simulated BSAEP signal (EA of 100 sweeps). (b) Binary mask vector in the wavelet domain. (c) The corresponding Gaussian kernels. (d) Signals estimated using W-RBFN (solid line) and U-RBFN (dashed line).

Table 4.1: **Comparison of estimated latencies (ms) for BSAEP-Sim1**

Peak component	I	II	III	IV	V
True latency	1.7	2.8	3.9	5.0	5.9
W-RBF estimate	1.65	2.75	3.81	4.98	5.95
U-RBF estimate	1.92	-	3.7	-	6.12

illustrated in the third row and in the fourth row, the original signal used for the simulations is presented for comparison. It can be seen that the W-RBFN is able to estimate the components well, whereas the U-RBFN is unable to estimate some of the components. This is because in an evoked potential signal, the component peaks are not equally spaced on the temporal scale, whereas the U-RBFN uses kernels with centers uniformly placed along the time axis and in the adaptation algorithm, only the weights of the basis functions are changed. It can be seen from the figure that although we use the same number of hidden nodes in both the methods, U-RBFN fails to estimate some of the components and their latencies correctly.

A comparison of the outputs of W-RBFN is also carried out with those of U-RBFN in terms of MSE and CC, and the values of these performance metrics are plotted against the number of sweeps. In Fig. 4.6(a), the values of MSE for different lengths of the ensemble are plotted and in Fig. 4.6(b), the values of the correlation coefficient are plotted. In both the figures, the solid line shows the respective performance index with the proposed method and the dashed line, that for U-RBFN method. The dotted line shows the values for the signals estimated using simple ensemble averaging. Both the quantities are computed with reference to the actual signal used in synthesizing BSAEP-Sim. It can be seen that the estimation using EA is inferior to both the methods because both methods attempt to remove the residual noise in the EA. The plots illustrate that for any given ensemble length, the GRBF performs an excellent approximation of the underlying signal from noisy observations and that wavelet preprocessing results in a more accurate approximation of the component peaks with fewer number of hidden nodes.

A similar study has been carried out for the case of MLR data too. These signals do not have as many components of importance as the BSAEP signals. Thus, the number of edges detected in the wavelet domain is 10. The signals estimated for different length EAs are shown in Fig. 4.7. In this figure too, the first row shows the noisy CEA and the second row shows the

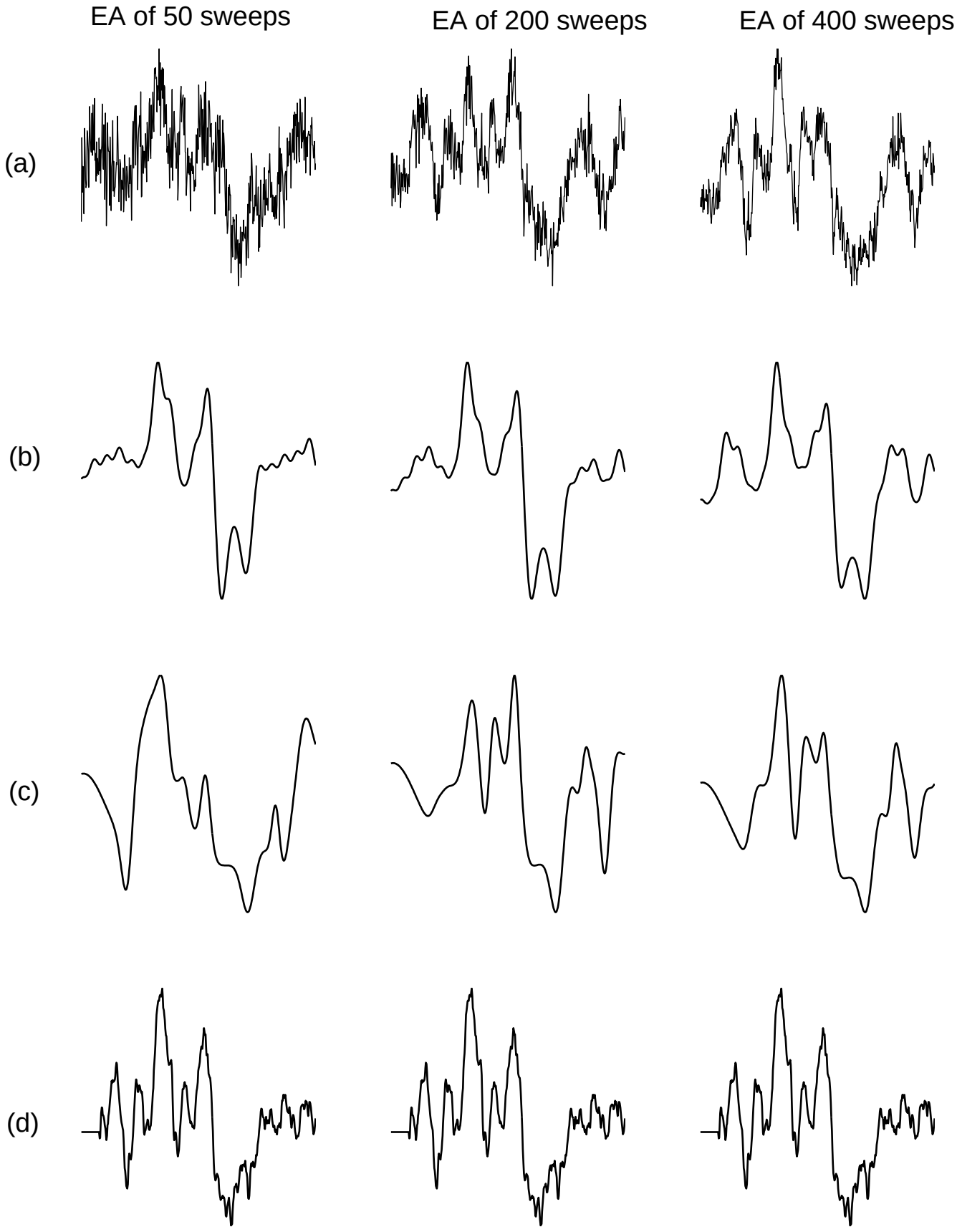

Figure 4.5: Signals estimated from BSAEP simulated with different lengths of the ensemble. Row(a): Current ensemble averages of 50, 200 and 400 sweeps, respectively. Row (b): Signals estimated using U-RBFN. Row (c): Signals estimated using W-RBFN. (d) Original signal.

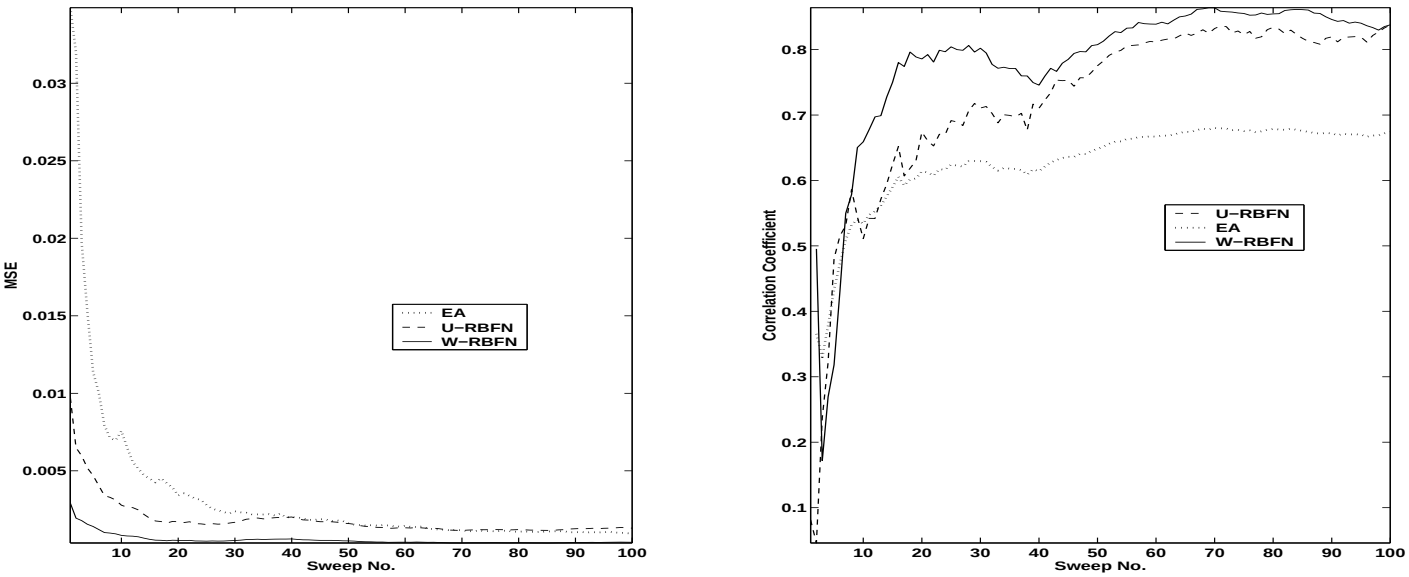

(a) (b)

Figure 4.6: Comparison of performance of U-RBF and W-RBF estimators on BSAEP-Sim signal. (a) MSE Vs. No. of sweeps. (b) Correlation coefficient Vs. No. of sweeps.

Table 4.2: **Comparison of estimated latencies (msec) of MLR-Sim1**

Peak Component	Na	Pa
True latency	18.5	33
U-RBFN estimate	22	30
W-RBFN estimate	19	33

signals estimated using U-RBFN and the third row shows the outputs of W-RBFN estimator. For comparison, the original signal used for the simulation is shown in the fourth row.

In Fig. 4.8, we compare the results of the two networks in terms of MSE and CC. Here too, both the methods outperform the EA estimator. Component latencies from the signals estimated using both the methods are listed in Table -II along with their true values from the original signal. It can be seen that in the case of MLR signals also, the latency estimation of components is better using W-RBFN.

4.4.2 Results for real data

The proposed technique has been tried on clinically recorded brainstem auditory evoked potentials. Figure 4.9(a) presents the average of 500 sweeps of a BSAEP signal and the signal

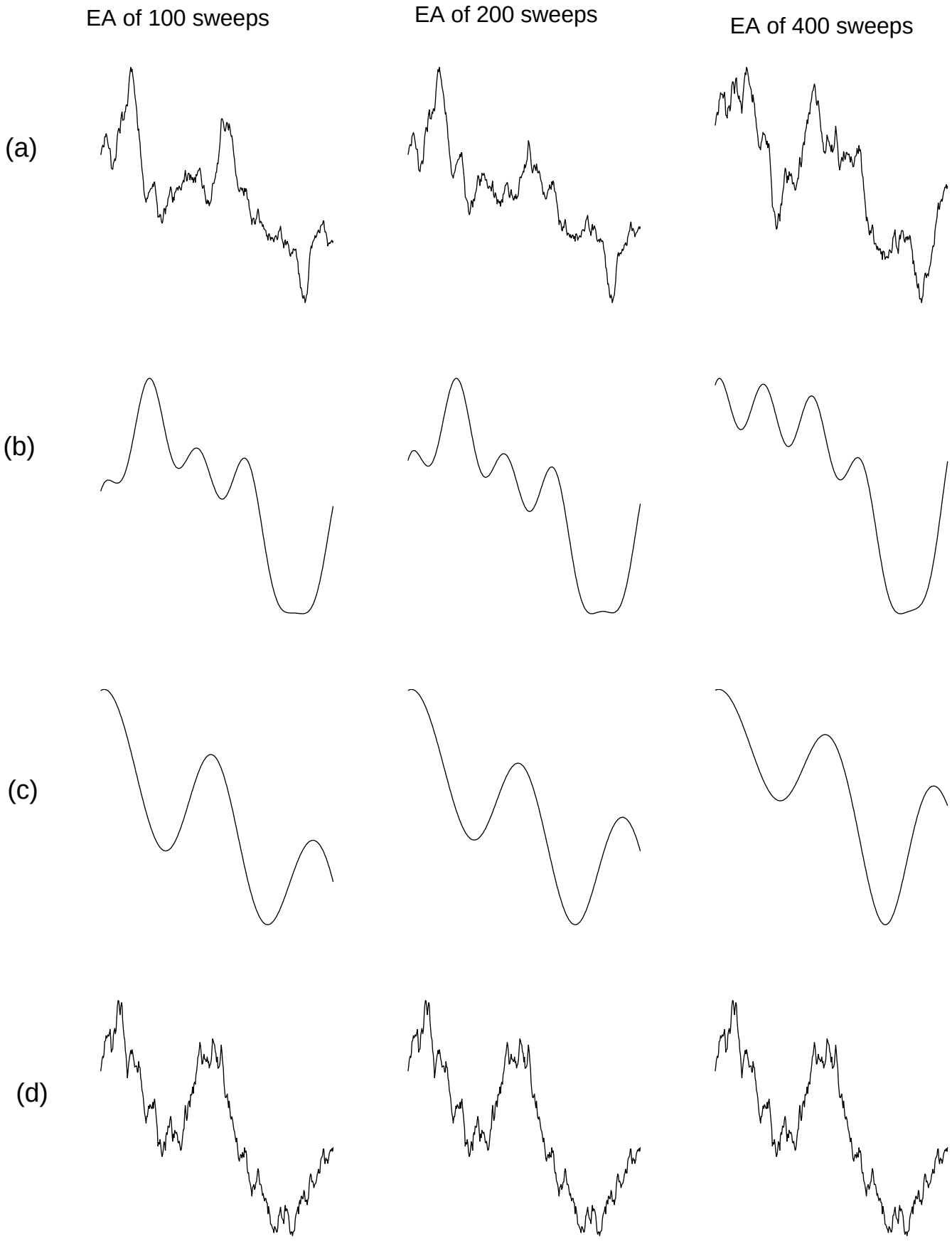

Figure 4.7: Signals estimated from MLR simulated with different lengths of ensemble. Row (a): Current ensemble averages. Row (b): Signals estimated using U-RBFN. Row (c): Signals estimated using W-RBFN. Row (d): Original signal.

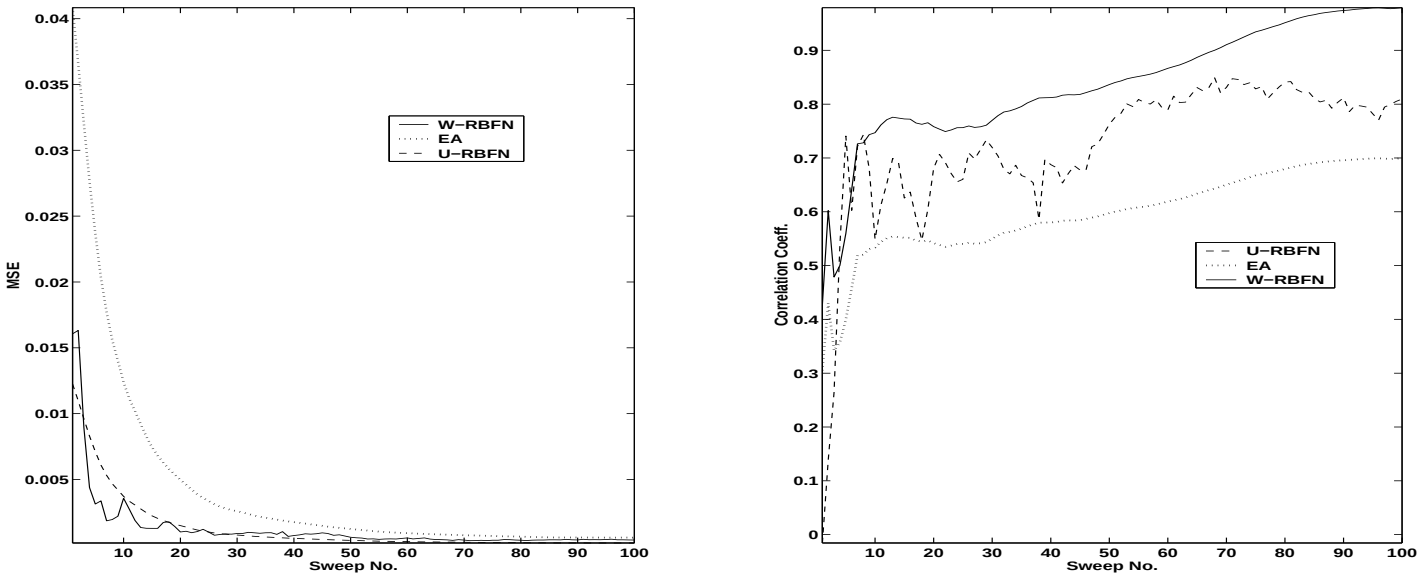

(a) (b)

Figure 4.8: Comparison of performance of U-RBFN and W-RBFN on simulated MLR signals. (a) MSE Vs. No. of sweeps. (b) Correlation coefficient Vs. No. of sweeps.

estimated using the proposed method from an ensemble average of 150 sweeps is shown in Fig. 4.9(b). It can be seen that the measurements such as the component latencies and their amplitudes can easily be made from the estimated signal, and this is not easily possible using the CEA of 500 sweeps shown in Fig. 4.9(a). The signal estimated using U-RBFN is shown in Fig. 4.9(c), wherein the components are not clearly visible.

The results for a real MLR input signal is shown in Fig. 4.10. This figure illustrates the estimation using both the methods for a specific EA. Figure 4.10(a) shows the CEA of 200 sweeps of MLR signal and in 4.10 (b & c), the signals estimated using W-RBFN and U-RBFN, respectively, are shown. Although both methods succeed in removing the residual noise in the EA, the U-RBFN estimator has a wavy appearance in comparison with the W-RBFN estimator, which shows well defined components. This is because, although both the methods use the same number of basis functions (10 in this case), the U-RBFN places them at equal distances over the analysis time. Hence, even though the network converges, it still has few additional peaks. Since the MLR signal is of low frequency, these additional components are visible. In the W-RBFN output shown in the third row of Fig. 4.10, the components are better defined, facilitating easy measurement of their latencies.

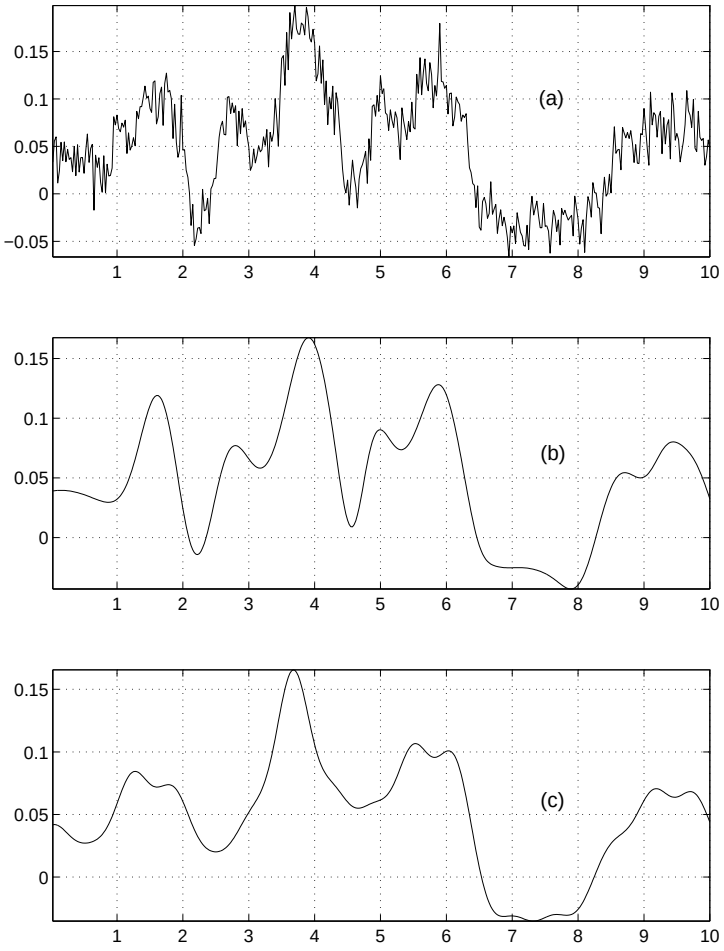

Figure 4.9: BSAEP signal estimated from real data. (a) EA of 500 sweeps. (b) Signal estimated using W-RBFN. (c) Signal estimated using U-RBFN.

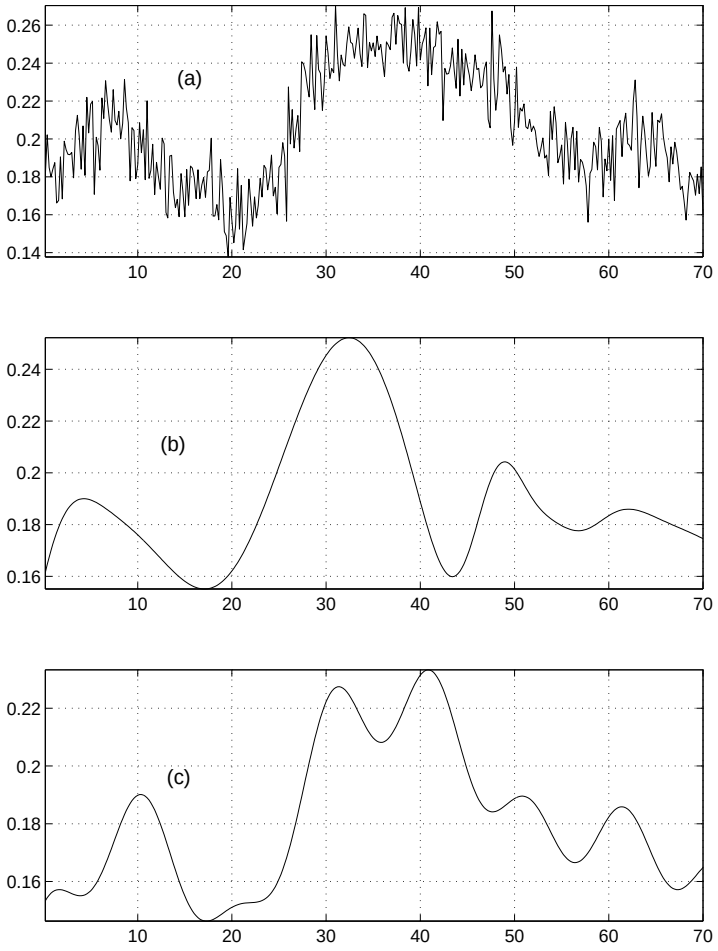

Figure 4.10: MLR signal estimated from real data. (a) EA of 200 sweeps. (b) Signal estimated using W-RBFN. (c) Signal estimated using U-RBFN.

4.5 Conclusion

The signal singularities are identified in a noisy background and then a signal is reconstructed that is better suited for the identification of the relevant peaks. The method uses the properties of the evolution of the wavelet transform maxima across scales and an RBF network in order to identify the signal singularities. The proposed method uses the correlation of wavelet coefficients across scales. The local characteristics of RBF training assure that the signal representation learned from the network approximates the interesting peaks well. The Inverse Discrete Wavelet Transform (IDWT) provides (at least theoretically) a signal that resembles more closely the original. The IDWT is computationally more effective than the training of an RBF network. However, the fact that the RBF network provides only the interesting peaks can be a significant advantage to the later processing tasks.

The powerful modeling capability of RBF networks is used to model the non-stationary characteristics of evoked potentials. The network with parameters derived from the signal itself entails a more accurate model and captures the essential features of the components of the EP. On the other hand, kernels with equally spaced centers and constant variance do not faithfully capture the underlying signal as the network cannot adapt to the individual components which convey diagnostically valuable information. Normally, the selection of the number of kernels is a difficult problem since a smaller number of basis functions results in poorer approximation and a larger number may cause overfitting of the data with a poorer generalization. In our case, using the characteristics of the edges detected in the wavelet domain for the RBF network design effectively solves the problem. The number of hidden nodes and the kernel parameters such as centers and widths are derived from the signal behaviour in the wavelet domain. The special treatment of the edges by the wavelet transform has been exploited in this. As the signal knowledge is incorporated into the network design, convergence becomes fast. A Gaussian function is chosen as the kernel as it is an universal approximator, bounded and therefore more stable in adaptive processing. Results obtained from simulated and real EP data demonstrate the estimator's ability to suppress the noise even at low SNR. The advantages of using signal dependent kernel parameters for the GRBFNN are in terms of model accuracy, and fewer nodes in hidden layer, and thus, in the speed of convergence of the network too. The proposed technique leads to enhanced signal components.

Chapter 5

Conclusion

There has been a recognized need to obtain evoked potentials with minimum number of stimulus repetitions. This need stems from the fact that use of fewer repetitions will allow tracking of physiological changes in the central nervous system, thereby providing useful information in neurosurgery, intensive care, anaesthesia monitoring, and other similar applications. In this thesis, we have proposed three different estimators based on wavelet transform. Any of these estimators can be incorporated into commercially available evoked potential equipment as a post processing module after ensemble averaging.

The wavelet domain Gaussian filter has edge and feature-sensitive selectivity in passing and scaling the wavelet coefficients. The filtering around the identified edges is smooth, thus enhancing the signal component regions, without introducing distortions like the ones caused by the binary masks. Temporally varying the threshold using local estimation of noise variance can handle slow transition regions better. The features with the same strength as the noise are distinguished by using the change in variance around the identified edges. By using this additional check, false detection of sharp noisy edges as signal featurs is avoided. Although the filter does not possess any optimality property, it is simple and efficient for the case of EPs. The proposed method is most suited as a post-processing tool for EP signal enhancement when the signal is non-stationary and a proper noise model is not available.

In our second approach, we propose a two level Wiener filtering scheme exploiting the inter-scale correlation in the wavelet domain. Enhancement of signal to noise ratio is obtained in the wavelet domain by comparing data at any scale to its correlation with the data at larger scales. Signal features are identified and retained because they are strongly correlated across

scales in the

transform domain. Noise is identified and removed since it is poorly correlated across scales in the wavelet domain. Signal features remain relatively undistorted because they are very well localized in space in the wavelet domain. The spurious fluctuations normally caused near the end points of the thresholding windows in hard thresholding schemes, and the smearing of the high frequency data due to Wiener filtering are both avoided by using a combination of these two approaches, resulting in an estimated signal superior to that obtainable by either of them alone.

In the third proposed technique, the powerful modeling capability of RBF networks is used to model the non-stationary characteristics of evoked potentials. The design of the network to achieve best generalization performance in a specific data processing task, involves the selection of the basis functions, their number, and determination of their parameters such as the centers and the radial dilation factors. We propose a method using which the GRBF network parameters are deduced from the wavelet transform of the noisy signal to enable the network to learn the functional form of the underlying EP signal more effectively. The GRBF network is determined using the characteristics of the significant signal features detected using the correlation in the wavelet domain. We show that this yields better results in terms of reduction in the order of the network and a more accurate signal model. The results are compared with a network whose kernel centers are evenly distributed over the entire length of the signal with equal spreads. We used the number of edges detected in the space-scale domain as the number of GRBF kernels to be used and their centers are determined as the mid points of the signal regions identified. The intervals between adjacent edges are taken as the variances of the kernels. Results demonstrate the superiority of determining the network parameters based on signal knowledge rather than using uniformly spaced Gaussian kernels of fixed variance.

This has ensured that the component latencies are well preserved in the W-RBFN method whereas the U-RBFN method fails to estimate some of the significant components. It can be seen that the W-RBFN is able to estimate the components. This is because in an evoked potential signal, the component peaks are not equally spaced on the temporal scale, whereas the U-RBFN uses kernels with centers uniformly placed along the time axis and in the adaptation algorithm, only the weights of the basis functions are changed. It is observed that although we use the same number of hidden nodes in both the methods, U-RBFN fails to estimate some of

the components and their latencies correctly.

5.1 Significant contributions of the thesis

- One of the chief contributions of the thesis lies in the exploitation of the persistence property of the wavelet coefficients to identify signal dominant regions in the time-scale domain. As per this property, large/small wavelet coefficients tend to propagate across scales. This motivated us to study the possibility of obtaining a cross-scale correlation based method for identifying signal features.

- *A new spatially selective Gaussian (SSG) filtering method which is better suited for the case of signals corrupted with colored noise.* In addition to the inter-scale correlation of the decomposed noisy signal in the wavelet domain, it also exploits the distribution of the wavelet coefficients in small localised regions. The proposed Gaussian filter in the wavelet domain possesses edge and feature-sensitive selectivity in passing and scaling the wavelet coefficients.

- We have proposed a combination of the principles of hard thresholding and Wiener filtering, resulting in an estimated signal superior to that obtainable individually by either of them. The spurious fluctuations normally caused near the end points of the thresholding windows in the hard thresholding schemes, and the smearing of the high frequency data due to Wiener filtering, are both minimized by using a judicious fusion of the two.

- The choice of the number of basis functions in the hidden layer and their parameters is a key problem in designing a radial basis function network. By deriving the kernel parameters from the signal, we have improved both the effectiveness of the model and tracking property of the network.

5.2 Directions for future research

All the methods proposed in this thesis assume that there is no major variation between sweeps in the morphological or temporal characteristics of the evoked potentials being recorded. One could explore the necessary modifications that may be necessary if one assumes dynamic modifications of one or more of the attributes of the signal during the session of recording. Such modifications

may be caused due to, say, surgery, innate jitter in the biological system, or pathology of the neural pathway such as fatigue due to conditions such as, myesthenia gravis.

The problem of single evoked potential estimation can be addressed.

Other methods of estimation, such as those based on neural networks, can be attempted for this problem.

Publications related to the thesis

1. G. Sita and A. G. Ramakrishnan, "Wavelet domain nonlinear filtering for evoked potential signal enhancement", Computers and Biomed. Res., 33, pp. 431-446, 2000.

2. G. Sita and A. G. Ramakrishnan, "Gaussian Radial Basis Function Network for evoked potential signal estimation", revised version under review, IEEE Trans. Biomed. Eng.

3. G. Sita and A. G. Ramakrishnan, "Evoked potential estimation using Gaussian Radial Basis Function Network", Proc. Intern. Conf. Neural Networks, Vienna, Austria, August 21-25, 2001.

4. G.Sita, R.V.S.Sastry and A.G.Ramakrishnan, "Time Varying Filters for Estimation of Evoked Potentials," Proc. I Reg. Intern. Conf. IEEE-EMBS, New Delhi, Feb.15-18, 1995, pp. 3.33-3.34.

5. G. Sita and A. G. Ramakrishnan, "Spatially selective Wiener filtering of EPs in the wavelet domain", submitted to Intern. Conf. Biomed. Engg. BioVision 2001, Bangalore, Dec. 21-24, 2001.

Bibliography

[1] F. Abramovich and T. Sapatinas. Bayesian approach to wavelet decomposition and shrinkage. In P. Muller and B Vidakovic, editors, *Lecture Notes in Statistics*. Springer-Verlag, New York, 1999.

[2] Hamid al Nashi. A maximum likelihood method for estimating EEG evoked potentia ls. *IEEE Trans. Biomed. Engg*, 33:1087–1095, Dec 1986.

[3] J. I. Aunon and C. D. McGillem. On the classification of single evoked potentials using quadratic classifier. *Comput. Progr. Biomed.,*, 14:29–40, 1982.

[4] J. I. Aunon, C. D. McGillem, and D. G. Childers. *Signal processing in evoked potential research: Applications of filtering and pattern recognition.* Critical reviews in bioengineering, Cleveland, OH:CRC, 1981.

[5] E. A. Bartnik and K. J. Blinowska. Wavelets-new method of evoked potential analysis. *Med. Biol. Eng., Comput.,*, 30:125–126, 1992.

[6] E. A. Bartnik, K. J. Blinowska, and P. J. Durka. Single evoked potential reconstruction by means of wavelet transform. *Biol. Cybernetics*, 67:175–181, 1992.

[7] H. Berger. On the electrocencephalogram of man. In S. W.Porges and M. G. H. Coles, editors, *psychophysiology*, pages 9–14. Dauson, Hutchinson and Ross Inc., Pennsylvania, 1967.

[8] Olivier Bertrand, Jorge Bohorquez, and J. Pernier. Time-Frequency digital filtering based on an invertible wavelet transform: An application to evoked potentials . *IEEE Trans. Biomed. Eng.,*, 41:77–88, 1994.

[9] G. Beylkin. On the representation of operation in bases of compactly supported wavelets. *SIAM J. Numer. Anal*, 29:1716–1740, 6 1992.

[10] J. R. Boston. Noise cancellation for brainstem auditory evoked potentials. *IEEE Trans. Biomed. Engg.,*, 32(12):1066–1070, Dec. 1985.

[11] J. S. Buchwald. Comparisons of sensory and cognitive brain potentials in the human and in an animal model. pages 242–257. Springer-Verlag, Berlin, 1989.

[12] F. H. Y. Chan, F. K. Lam, P. W. F. Poon, and W. Qiu. Detection of brainstem auditory evoked potential by adaptive filtering. *Medical and Biol. Engg. and Comp.*, 33:69–75, January 1995.

[13] K. H. Chiappa and A. H. Ropper. Evoked potentials in clinical medicine(1st part). *New Eng. Jl. Med.*, 306:1140–1150, 1982.

[14] D. G. Childers. Event-related potentials: A critical review of methods for single-trial detection. *CRC Critical Rev. Biomed. Eng.,*, 11:185–200, 1986.

[15] H. Chipman, E. Kolaczyk, and R. McCulloch. Adaptive Bayesian wavelet shrinkage. *J. Amer. Statist. Assoc.*, 92:1413–1421, 1997.

[16] Hyeokho Choi and Richard Baraniuk. Analysis of wavelet-domain wiener filters. 19.

[17] M. Clyde, G. Parmigiani, and B. Vidakovic. Multiple shrinkage and subset selection in wavelets. *Biometrika*, 85:391–401, 1998.

[18] Carlos E. Davila and Mohammad S. Mobin. Weighted averaging of evoked potentials. *IEEE Trans. Biomed. Eng.,*, 39:338–344, 1992.

[19] G. D. Dawson. Cerebral responses to electrical stimulation of peripheral nerve in man. *J. Neurol. Neurosurg. Psychiat.*, 10:134–140, 1947.

[20] G. D. Dawson. A summation technique for detecting small evoked potentials. *Electroencephalogr. Clin. Neurophysiol.*, 6:65–84, 1954.

[21] J. P. C. de Weerd. *A Posteriori* time-varying fltering of averaged evoked potentials, Parts I and II. *Biol. Cybern.*, 41:211–234, 1981.

[22] J. P. C. de Weerd and W. L. J. Martens. Theory and practice of *a posteriori 'Wiener' filtering of average evoked potentials. Biol. Cybern.*, 30:81–94, 1978.

[23] S. del Marco, J. Weiss, and K. Jager. Wavepacked-based transient signal detector using a translation invariant wavelet transform. In *Wavelet Applications in Signal and Image Processing*, volume 2242, pages 154–165. SPIE, San Diego, CA, July 1994.

[24] D. L. Donoho. Nonlinear methods for recovery of signals, densities, and spectra from indirect and noisy data. In *Proc. of Symposia in Applied Mathematics*, volume 00, pages 173–205. American Mathematical Society, 1993.

[25] D. L. Donoho and I. M. Johnstone. Adapting to unknown smoothness via wavelet shrinkage. *J. Am. Stat. Ass.*

[26] D. J. Doyle. Some comments on the use of Wiener filtering for the estimation of evoked potentials. *Electroenceph. Clin. Neurophysiol.*,, 38:533–534, 1975.

[27] Y. Xu et al. Wavelet transform domain filters: A spatially selective noise filtration technique. *IEEE Trans. Image Processing*, 3, 1994.

[28] K.S.M. Fung, F.H.Y. Chan, F.K. Lam, and P.W.F. Poon. A tracing evoked potential estimator. *Medical and Biological Engineering and Computing*, 37:218–227, 1999.

[29] MIRIAM FURST and AVI BLAU. Optimal *a posteriori* time domain filter for average evoked potentials . *IEEE Trans.Biomed. Eng.*, 38:827, 1991.

[30] J. G. Gallaire and A. M. Sayee. Wavelet-based empirical wiener filtering. In *IEEE Int'l Symp. on Time-Frequency and Time-Scale Analysis*, volume 2, pages 94–98, July 1998.

[31] I. Gath and A. B. Geva. Unsupervised optimal classification. *IEEE Trans. Pattern Anal. Machine Intell.*,, 7:773–781, 1989.

[32] A. S. Gevins and N. H. Morgan. Classifier-directed signal processing in brain research. *IEEE Trans. Biomed. Eng.*,, 33:1054–1068, 1986.

[33] S.P Ghael, A.M. Sayeed, and R. G. Baraniuk. Improved wavelet denoising via empirical wiener filtering. In *Proc. SPIE*, volume 3169, pages 389–399, San Diego, July 1997.

[34] Nason G.P. *Choice of the threshold parameter in wavelet function estimation.* Lecture notes in Statistics,Springer-Verlag, 1995.

[35] R.V.S.Sastry G.Sita and A.G.Ramakrishnan. Time Varying Filters for Estimation of Evoked Potentials. In *Proc. I Reg. Intern. Conf. IEEE-EMBS*, volume 3, pages 33–34, 1995.

[36] M. Hansson, Tomas Gansler, and Goran salomonsson. Estimation of single event related potentials ustilizing the Prony method. *IEEE Trans. Biomed. Engg.*, 43:973–981, 10 1996.

[37] H. J. Heinze and H. Kunkel. ARMA-Filtering of evoked potentials. *Meth. Inform. Med.*,, 23:29–36, 1984.

[38] M. Hoke, B. Ross, R E Wickesberg, and B. Lutkenhoner. Weighted averaging - theory and application of electric response audiometry. *Electroenceph. Clin. Neurophysiol*, 57:484–489, 1984.

[39] Daubechies I. *Ten lectures on wavelets.* SIAM, 1992.

[40] P. Ishwar, K. Ratakonda, P. Moulin, and N. Ahuja. Image denoising using multiple compaction domains. In *Proc. ICASSP*. IEEE, 1998.

[41] B. H. Jansen and W. K. Cheng. Structural EEG analysis: An exploratory study. *Int. J. Biomed. Comput.*,, 23:221–237, 1988.

[42] I. M. Johnstone and B. W. Silverman. *Empirical Bayes approaches to mixture problems and wavelet regression.* Technical report, Dept. of mathematics,Univ. Bristol, UK, 1998.

[43] Edson B. Moody Jr., Evangelia Micheli-Tzanakou, and S. Chokroverty. An adaptive approach to spectral analysis of pattern-reversal visual evoked potentials. *IEEE Trans. Biomed. Eng.*, 36:439–447, April 1989.

[44] M. Kaveh, S. Bruzzone, and F. Torres. A new method for the estimation of average evoked response. *IEEE Trans. Systems, Man and Cybernetics*, 8:414–417, May 1978.

[45] P. Laguna, O. Meste, P. W. Poon, P. Caminal, H. Rix, and N. Thakor. Adaptive filter for event-related bioelectric signals using an impulse correlated reference input: comparison with signal averaging techniques. *IEEE Trans. Biomed. Eng.*,, 39:1032–1044, 1992.

[46] M. Lang, H. Guo, J. Odegard, C. S. Burrus, and Jr. R.O. Wells. Noise reduction using an undecimated discrete wavelet transform. *IEEE Signal Processing Letters*, 3:10–12, 1 1995.

[47] M. Lang, H. Guo, J. Odegard, C. S. Burrus, and R.O. Wells. Nonlinear processing of a shift-invariant DWT for noise reduction. *SPIE conf. wavelet applications*, 2491, April 1995.

[48] J. Liang and T. W. Parks. A two-dimensional translation invariant wavelet representation and its applications. In *Proc. Int. Conf. Image Processing*, volume 1, pages 66–70, Austin, TX, November 1994. IEEE.

[49] J. Lu, D. M. Healey, and J. B. weaver. Signal recovery and wavelet reproducing kernels. *IEEE Trans. Signal Proc.*, 42:1845–1848, 7 1994.

[50] B. Lutkenhoner, M. Hoke, and Ch. Pantev. Possibilities and limitations of weighted avergaing. *Biological Cybernetics*, 52:409–416, August 1985.

[51] P. G. Madhavan. Minimal repetition evoked potentials by modifed adaptive line enhancement. *IEEE Trans. BME*, 39, 7 1992.

[52] S. Mallat. Zero-crossings of a wavelet transform. *IEEE Trans. Inform Theory*, 37(4), July 1991.

[53] S. Mallat. *A wavelet tour of signal processing.* Academic Press, San Diego, CA, 1998.

[54] S. Mallat and S. Zhong. Characterization of signals from multiscale edges. *IEEE Trans. on PAMI*, 14(7):725–733, July 1992.

[55] C. D. Mcgillem and J. I. Aunon. Measurements of signal components of single visually evoked brain potentials. *IEEE Trans. Biomed. Eng.,*, 24:232–241, 3 1977.

[56] Quan Pan, Lei Zhang, Guanzhong Dai, and Hongcai Zhang. Two denoising methods by wavelet transform. *IEEE Trans. Signal Proc.,*, 5:3401, 1999.

[57] Vijay Parsa and Philip A. Parker. Multireference adaptive noise cancellation applied to somatosensory evoked potentials. *IEEE Trans. Biomed. Eng.,*, 41:792–800, 8 1994.

[58] V.J. Samar, K. P. Swartz, and M. S. Raghuveer. Multiresolution analysis of event-related potentials by wavelet decomposition. *Brain and cognition*, 27:298–338, 3 1995.

[59] J. M. Shapiro. Embedded image coding using zerotrees of wavelet coefficients. *IEEE Trans. Signal processing*, 41:3445–3462, 12 1993.

[60] M. J. Shensa. The discrete wavelet transform: Wedding the a' trous and Mallat algorithms. *IEEE Trans. Inform. Theory*, 40:2464–2482, 1992.

[61] M. V. Spreckelsen and B. Bromm. Estimation of single-evoked cerebral potentials by means of parametric modeling and Kalman filtering. *IEEE Trans. Biomed. Engg.*, 35:691–700, 1988.

[62] A. Starr and K. Squires. Distribution of auditory brainstem potentials covering the scalp and nasophorynx in humans. *Ann. N.Y. Acad. Sci.*, 388:427–442, 1982.

[63] G. Strang and T. Nguyen. *Wavelets and filter banks.* Wellesley, Cambridge Press, 1996.

[64] Vasily Strela. Denoising via block wiener filtering in wavelet domain. 19.

[65] N. V. Thakor. Adaptive filtering of evoked potentials. *IEEE Trans. Biomed. Engg*, 34:6–12, 1987.

[66] N. V. Thakor, Guo Xin-rong, Sun Yi-Chun, and Daniel F. Hanley. Multiresolution wavelet analysis of evoked potentials. *IEEE Trans. Biomed. Eng.,*, 40:1085–1093, 11 1993.

[67] P. Ungan and E. Basar. Comparison of Wiener filtering and selective averaging of evoked potentials. *Electroencephalogr. Clin. Neurophysiol.,*, 40:516–520, 1976.

[68] C.A. Vaz and N. V. Thakor. Adaptive Fourier estimation of time-varying evoked potentials. *IEEE Trans. Biomed. Engg.,*, 36:448–455, 1989.

[69] D. O. Walter. A posteriori Wiener filtering of average evoked responses. *Electroencephalogr. Clin. Neurophysiol.,*, 27:61–70, 1969.

[70] B.A. Whitehead and T.D. Choate. Cooperative-Competitive Genetic Evolution of Radial Basis Function Centers and Widths for Time series p rediction. *IEEE Trans. Neural Networks*, 7:869–880, April 1996.

[71] A. Witkin. Scale space filtering. In *Proc. 8th Internat. Joint Conf. on Artificial Intell.,*, pages 1019–1022, Karlsruhe, Germany,, 1983.

[72] A.P. Witkin. Scale space filtering: a new approach to multi scale description. In *Image Understanding*, pages 79–95, Norwood, NJ, 1984. S. Ullman and W. Richards, Eds.

[73] K. B. Yu and C. D. McGillem. Optimum filters for estimating evoked potential waveforms. *IEEE Trans. Biomed. Eng.,*, 30:730–737, 5 1983.

[74] Xiao-Hu Yu, Zhen-Ya He, and Yi-Sheng Zhang. Time-varying adaptive filters for evoked potential estimation. *IEEE Trans. Biomed. Engg.*, 41:1062–1071, 1994.

[75] D.B.T. Yuanjin Zheng and L.Li. Signal extraction and power spectrum estimation using wavelet transform scale space filtering and Bayes shrinkage. *Signal Processing*, 80:1535–1549, 8 2000.

[76] George Zouridakis, B. H. Jansen, and N. N. Boutros. A fuzzy clustering approach to EP estimation. *IEEE Tran Biomed. Eng.*, 44:673–680, 8 1997.